TAMPEREEN TEKNILLINEN YLIOPISTO
TAMPERE UNIVERSITY OF TECHNOLOGY

EEVA HYKKÖ

MANUFACTURING AND CHARACTERIZATION OF NANOFILLED EPOXY

Master of Science Thesis

Examiners: Professor Pentti Järvelä
And Docent Mikael Skrifvars
Examiners and Topic Approved in The Automation, Mechanical and Materials Council Meeting on 6th of June 2012

ABSTRACT

TAMPERE UNIVERSITY OF TECHNOLOGY
Master's Degree Programme in Materials Science
HYKKÖ, EEVA: Manufacturing and characterization of nanofilled epoxy
Master of Science Thesis, 71 pages, 7 appended pages
May 2013
Major subject: Polymeric materials
Examiners: Professor Pentti Järvelä and Docent Mikael Skrifvars
Key words: nanocomposites, epoxy, nano-SiO_2, silicon dioxide, nanoclay, multi-walled carbon nanotubes

Nanocomposites are a new field in the polymer industry offering improved mechanical, thermal, electrical and optical properties with low filler content. Nanocomposites have a huge potential in many applications, but the preparation methods are still under investigation. This is due to the tendency of nanoparticles to form large clusters during manufacturing due to their small size and high surface energy. Improved properties in composites cannot be achieved if the nanofiller dispersion is poor.

The scope of this study was to successfully manufacture epoxy composites with uniform nanofiller dispersion. Furthermore, the mechanical, thermal and rheological properties of the prepared samples were examined. Nanosized silicon dioxide (SiO_2), organoclay and multi-walled carbon nanotubes (MWCNT) were incorporated into the epoxy resin by high shear mixing. Samples were prepared by moulding and the curing with a hardener was performed at elevated temperature.

Some difficulties were observed during manufacturing. A notable amount of air bubbles was formed on the resin during the mixing of the nanofillers and their removal slowed down the manufacturing process. Furthermore, viscosity of the nanofilled resin was strongly affected by the nanoparticles limiting the preparation of higher filler loadings. Small amounts (0.5 wt.%) of MWCNTs increased the viscosity of the resin significantly. In case of nano-SiO_2 and nanoclay, concentration of 2 wt.% increased the viscosity so that the air bubble removal was extremely slow. Furthermore, the mixing of sample with 4 wt.% of nano-SiO_2 was not possible anymore with the high shear mixer due to the markedly increased viscosity.

Improved properties in mechanical and thermal tests were not totally achieved. Scanning electron microscope (SEM) and field emission scanning electron microscope (FESEM) images indicated that the samples contained agglomerated nanoparticles indicating that the mixing may not have been effective enough.

Difficulties during manufacturing and the poor dispersion in the final composites require further research in terms of more effective preparation methods and matrix/filler compatibility. Other processing methods (such as ultrasonication or using solvents) in addition to high shear mixing are needed to achieve proper dispersion.

TIIVISTELMÄ

TAMPEREEN TEKNILLINEN YLIOPISTO
Materiaalitekniikan koulutusohjelma
HYKKÖ, EEVA: Nanoseostetun epoksin valmistus ja karakterisointi
Diplomityö, 71 sivua, 7 liitesivua
Toukokuu 2013
Pääaine: Tekniset polymeerimateriaalit
Tarkastajat: Professori Pentti Järvelä and Dosentti Mikael Skrifvars
Avainsanat: Nanokomposiitti, epoksi, nano-SiO_2, nanosavi, moniseinämäinen hiilinanoputki

Nanokomposiitit ovat yksi uusimpia materiaaleja polymeeriteollisuudessa, joilla voidaan saavuttaa parannuksia mekaanisissa, termisissä, sähköisissä ja optisissa ominaisuuksissa varsin pienillä täyteainepitoisuuksilla. Nanokomposiittien valmistus on kuitenkin edelleen hyvin haasteellista, sillä nanokokoiset partikkelit muodostavat erittäin helposti agglomeraatteja. Jotta nanokomposiittien hyvät ominaisuudet voidaan saavuttaa, täytyy nanotäyteaineen olla tasaisesti dispergoitunut matriisiin.

Tämän työn tavoitteena oli valmistaa epoksinanokomposiitteja käyttäen eri nanotäyteaineita ja testata lopullisten nanokomposiittien mekaanisia, termisiä ja reologisia ominaisuuksia. Nanokokoista silikaa (SiO_2), nanosavea ja moniseinämäisiä hiilinanoputkia (MWCNT) sekoitettiin epoksimatriisiin korkealla leikkausnopeudella. Näytteet valmistettiin valamalla sekoitettu hartsi ja kovettaja muotteihin ja kovettamalla ne korotetussa lämpötilassa.

Nanokomposiittien valmistuksen aikana ilmeni joitakin hankaluuksia. Sekoituksen aikana hartsiin muodostui ilmakuplia, joiden poistaminen hidasti merkittävästi valmistusprosessia. Lisäksi nanotäyteaineet kasvattivat selvästi hartsin viskositeettia, mikä rajoitti korkeampien täyteainepitoisuuksien valmistusta. Puolen painoprosentin MWCNT-pitoisuus kasvatti viskositeettia huomattavasti enemmän kuin muut nanotäyteaineet. Viskositeetin nousu näytteissä joissa oli kaksi painoprosenttia nano-SiO_2:a tai nanosavea hidasti merkittävästi ilmakuplien poistoa. Neljä painoprosenttia nano-SiO_2:a nosti viskositeettia niin paljon että mekaaninen sekoitus ei enää ollut mahdollista.

Parannuksia mekaanisissa ja termisissä ominaisuuksissa ei täysin saavutettu. Elektronimikroskooppikuvat paljastivat, että näytteet sisälsivät agglomeroituneita nanopartikkeleita osoittaen, että nanotäyteaineiden dispersio ei ollut riittävä toivottujen ominaisuuksien saavuttamiseksi.

Haasteet valmistusvaiheessa ja nanotäyteaineiden heikko dispersio osoittavat, että lisätutkimukselle on tarvetta nanokomposiittien valmistusmenetelmien ja raaka-aineiden yhteensopivuuden parantamiseksi. Muita prosessointimenetelmiä (kuten ultraäänisekoitusta tai liuottimen käyttöä) on tarpeen yhdistää korkean leikkausnopeuden sekoittamiseen tarvittavan dispersion aikaansaamiseksi.

PREFACE

This thesis was done at Tampere University of Technology for the Plastics and Elastomers Department from April 2012 to May 2013.

I would like to specially thank my supervisors Professor Pentti Järvelä and Docent Mikael Skrifvars for giving me this opportunity, for their advices and guidance throughout the work and for evaluating my thesis. I would also like to thank Egidija Rainosalo for her advices and help.

I am very grateful for Reija Suihkonen for the invaluable guidance with the nanocomposite preparation and for her assistance with the writing work.

I would also like to thank Professor Jyrki Vuorinen for providing me the facilities and work safety to work with the nanoparticles, Olli Orell for the help in the tensile and fracture toughness tests, Seppo Syrjälä for the rheology measurements, Sinikka Pohjonen for the thermal analysis tests and the SEM-imaging, Kosti Rämö for the thermal analysis tests and help with the laboratory work, Merja Ritola also for the SEM-imaging, Jarmo Laakso and the Material's department for the FESEM imaging, and everyone else who gave me advice, and the whole Plastics and Elastomers department for the inspiring environment.

I also want to thank my family and friends for the support during my studying, and especially my parents for the encouragement during the intense work period with the thesis.

Tampere 10.5.2013

Eeva Hykkö

CONTENTS

ABBREVIATIONS AND NOTATIONS

Ø	Diameter
ε	Strain
σ	Stress
Ω	ohm
a	Crack length
A	Area
Ag	Silver
Au	Gold
B	Thickness
CNT	Carbon nanotube
CVD	Catalytic chemical vapour deposition
d	Diameter
DMA	Dynamic mechanical analysis
DSC	Differential scanning calorimetry
E	Young's modulus
E'	Storage modulus
E''	Loss modulus
EP	Epoxy
EPDM	Ethylene propylene diene monomer
EVA	Ethylene vinyl acetate
F	Force
Fe_3O_4	Iron oxide
FESEM	Field emission scanning electron microscopy
I	Current
K_{ic}	Critical stress intensity factor
MWCNT	Multi-walled carbon nanotubes
min	minutes
n	rotating speed
N_2	Nitrogen
NBR	Nitrile butadiene rubber
NR	Natural rubber
nm	Nanometer
O_2	Oxygen
Pa	Pascal
PA	Polyamide
PC	Polycarbonate
PE-HD	High-density polyethylene
PEI	Polyetherimide
PET	Poly(ethylene terephthalate)

PP	Polypropylene
P_Q	Critical load for crack propagation
PS	Polystyrene
PU	Polyurethane
PVC	Polyvinyl chloride
R_s	Surface resistivity
R_v	Volume resistivity
rpm	Revolution per minute
SBR	Styrene-butadiene rubber
SEM	Scanning electron microscopy
SiO_2	Silicon dioxide, silica
t	Thickness of the sample
TEM	Transmission electron microscopy
T_g	Glass transition temperature
TGA	Thermogravimetric analysis
TiO_2	Titanium dioxide
TPO	Thermoplastic olefin
U	Voltage
v	Circumference velocity
W	Width
wt.%	Weight percent

1 INTRODUCTION

Nanoparticles, having one dimension less than 100 nm [1], have gained increased interest during the past few years. This is due to their novel properties and high potential for many applications, such as in biology, medicine, electronics, chemical processes and high-strength materials. [2] Polymeric nanocomposites are one of the newest polymeric materials that are discovered and developed. [3] Nanocomposites offer improved mechanical, thermal, electrical and optical properties compared to conventional composites. [1] This is due to the large aspect ratio and high specific surface area of the nanoparticles, which enable greater interaction between the fillers and the matrix. [4] Applications of the nanocomposites include aerospace, coatings, electronics, sports goods and automotive industries. [5]

Polymer nanocomposites consist of polymer matrix and nanofillers. Studies have been made widely in thermoplastics, for example PA, PP, PS, PVC [6], PE-HD [7], EVA [8], PET [9], PC, TPOs, and PEI [10]. Also thermosets, such as epoxy [1], vinyl ester [5], phenol [11], cyanate ester [12], unsaturated polyester and polyimide [13] and elastomers, for example NR, SBR, PU, silicone [14], EPDM and NBR [15] have been studied.

Mixing of the nanosized fillers on the polymer can improve its mechanical properties due to the high specific surface area of the particles that can enhance the stress transfer from matrix to the nanoparticles. Other properties like dimensional stability, flame retardancy, gas barrier properties and corrosion resistance can also be improved. The filler-matrix interface determines the degree of interaction between the filler and the matrix and therefore proper dispersion and the interfacial interactions are needed for achieving the desired properties. [16]

Because of the very small particle size, the manufacturing process and the final properties of the nanocomposite are very difficult to control. [1] Nanoparticles have a high tendency to form agglomerates, where the particles are stuck together by adhesive forces. [4] In addition to the large surface area, adhesive forces tend to increase when the particle size decreases. [17] The stacked fillers are not in nanoscale anymore and will behave like conventional fillers losing the advantages of the small particle size. [4] Therefore, preparation of the true nanocomposite is crucial and it has become a technological challenge in materials science. [1] The right preparation methods for the nanoparticles and the proper dispersion techniques are still under research. Furthermore, high cost of some nanofillers, especially carbon nanotubes, has also restricted the usage of nanofillers in a large scale. When the nanocomposite technologies develop, the nanofiller market will increase and the costs will reduce. [4]

In this work, nanocomposites with different nanoparticles were prepared and the samples were characterized with different methods. Three different nanofillers were used to prepare epoxy nanocomposites with epoxy resin: 1 and 2 wt.% of nano-SiO_2, 1 and 2 wt.% of nanoclay and 0.5 wt.% of MWCNTs. High shear mixing was used to disperse the nanoparticles into the matrix. Interaction between the fillers and the matrix and the level of dispersion were analyzed by the test results that included viscosity measurements, tensile tests, fracture toughness tests and thermal analysis methods. The samples were also investigated by scanning electron microscopes.

The main goal of this work was to investigate the behaviour of the nanofillers with the epoxy resin and to examine the potential of the high shear mixing as an option for the nanocomposite preparation. These results will give more information about thermoset nanocomposite preparation and lay the groundwork for further research.

2 POLYMER NANOCOMPOSITES

2.1 General

Polymer nanocomposite is a structure that consists of two interacting phases, a polymer matrix and a filler phase of nanosized particles. [1] Nanofillers that are the most often used in polymer matrices are natural and synthetic clays (layered silicates), nanosized silica (SiO_2), nanoceramics, nanocalcium carbonates and carbon nanotubes. Matrix material can vary from thermosets and thermoplastics to elastomers. [18]

Nanocomposites are a quite new discovery. First nanocomposites were developed in the late 1980s. The first company that produced commercial nanocomposites was Toyota in collaboration with Ube in 1991. [1] [19] They discovered that a very small nanofiller amount had a considerable improvement in thermal and mechanical properties. [20] Layered silicate based nanocomposites were used as timing belt covers for the Toyota cars. [19] Nanosized fillers, however, have already been used in rubber compounding in 1860s. Carbon black was used in tires to enhance the mechanical properties of vulcanized rubber. Also other nanoscale fillers, fumed silica and precipitated calcium carbonate, were also used for reinforcing in the early twentieth century. [10]

Definition of a nanoparticle is that at least one of its dimensions is less than 100 nm. One nanometer is a billionth of a meter (10^{-9}m) and it is approximately the length of seven carbon atoms side by side (diameter of a carbon atom is about 140 picometers = 0.14 nanometers). [10] Nanoparticles can be divided into spherical, fibrous and platelet-shaped fillers (Figure 2.1). Spherical nanoparticles are called isodimensional, because they have all three dimensions in nanoscale. Typical spherical nanoparticles are nanosilica and titanium dioxide. Fibrous nanofillers are two-dimensional particles, because the diameter of the fibre is in nanoscale, but the length can be in microscale. Typical fibrous nanoparticles are carbon nanotubes and cellulose whiskers. Platelet shaped nanoparticles, typical being layered silicates, have only the thickness in nanoscale, the particle diameter can be in microscale. Fibrous and platelet shaped particles have a very high aspect ratio. [21]

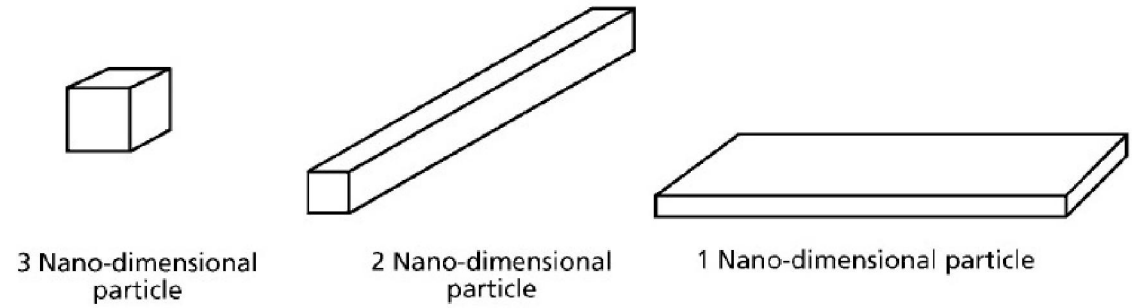

Figure 2.1. Different types of nanoparticles [22]

In addition to the excellent reinforcement, nanocomposites can also reduce the shrinkage during curing, improve the thermal stability, flame retardancy and abrasion resistance, as well as barrier, electrical, electronic and optical properties. [18] [17] Nanoparticles are used with very low filler content, usually 1-5 wt.%. Combined with low density of the nanoparticles, the final material will have significantly lower weight than conventional composites. Also the optical properties are similar to that of the matrix polymer because nanofillers have much smaller wavelength than the visible light. [1] Optimum formulation of the nanofiller has to be established for the desired properties. This can be done by manufacturing different filler contents and comparing the test results. [17] The interaction between the matrix and the fillers can be enhanced with organic modifiers, which can be bonded ionically or chemically on the nanoparticle surface. [1]

2.2 Nanocomposite structure

The special feature of the nanoparticles is their very high specific surface area compared to conventional fillers. The surface area per unit volume is inversely proportional to the particles diameter. [20] As demonstrated in Figure 2.2, the specific surface area increases when the particle size gets smaller. For an example, titanium dioxide with particle size of 300 nm has a specific surface area of 5 m^2/g. When the particle size is reduced to 21 nm, the specific surface area increases to 50 m^2/g. [17]. The total surface area of the filler phase with nanoparticles can be higher than with microsized fillers, even though the nanofillers are used with significantly lower volume fractions than conventional sized fillers. [22]

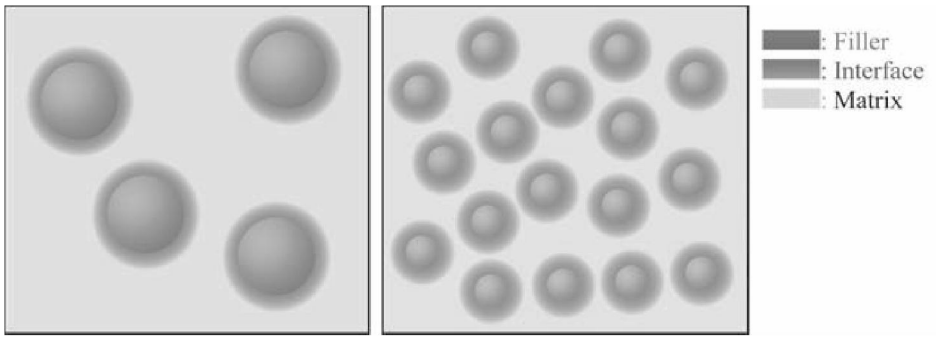

Figure 2.2. The effect of particle size on the interface [23]

Interaction between the fillers and the matrix is crucial for the properties of the nanocomposite since good interaction is a prerequisite for an efficient reinforcement. When a load is applied on a composite, the main function of the matrix is to transmit the load on the fillers. [24] If the filler-matrix interaction is poor, the filler particles cannot support the external load. [17] The lack of contact makes the interface act like a crack, which makes the material more brittle. [24]

An efficient interaction requires that the nanofillers are dispersed as individual particles into the matrix. Nanoparticles have a high tendency to agglomerate due to their high specific surface area, high aspect ratio and the adhesive forces that tend to increase with decreasing particle size. With a small particle size the amount of particles is very high and they have a small distance to each other. This is demonstrated in Figure 2.3., where the volume-content of the filler phase is the same (3 volume-%), but the number of particles increases enormously when the particle size is in nanometers. [17]

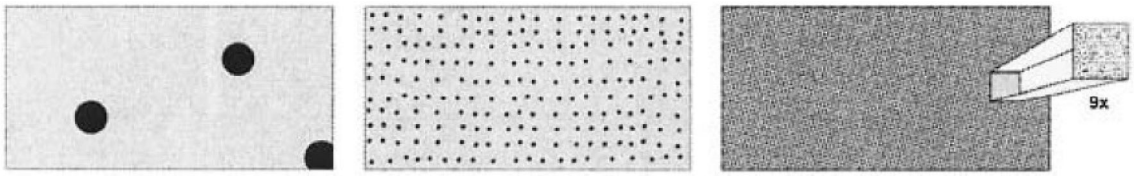

Figure 2.3. Constant filler content of 3 volume-%: Left: d = 10 µm, n ~ 2.8, Middle: d = 1 µm, n = 2860, Right: d = 100 nm, n = 2 860 000 [17]

If the particles are stuck together as agglomerates, the particles are not in nanoscale anymore and therefore the final product cannot be called a nanostructured composite. In that case, the clustered nanoparticles will act as conventional fillers. [4] The nanofillers have to be dispersed as individual particles and distributed evenly into the matrix to get the desired properties for the nanocomposite. The mixing phases are demonstrated in the Figure 2.4., where the dispersive mixing describes the level of agglomeration, and distributive mixing describes the homogeneity of the mixture.

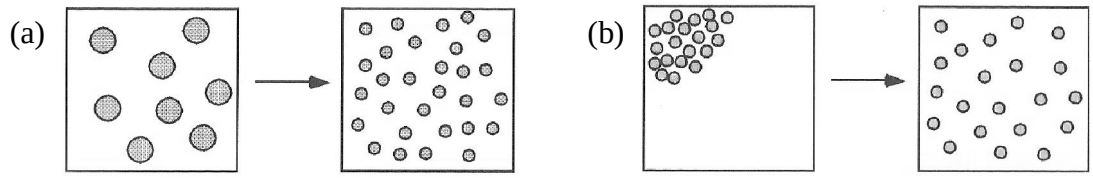

Figure 2.4. States of mixing: (a) Dispersive mixing (b) Distributive mixing [25]

The level of dispersion can be examined with scanning electron microscopy (SEM) from the sample surface. The dispersion of titanium dioxide nanoparticles (Ø 300 nm) has been inspected from the epoxy fracture surface using SEM (Figure 2.5.). The nanoparticle agglomerates can be clearly seen in the Figure 2.5.a as compared to evenly distributed particles in the Figure 2.5.b. [1]

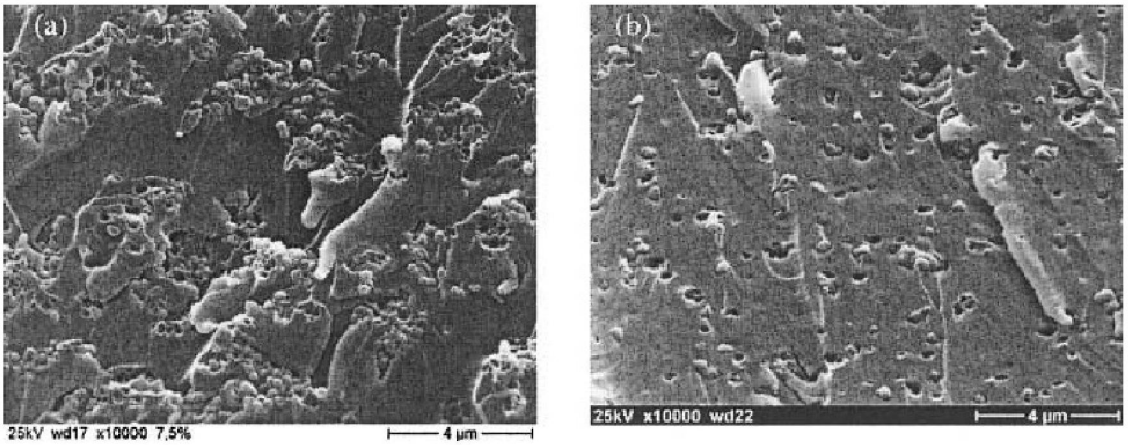

Figure 2.5. Fracture surface of epoxy resin with (a) undispersed (b) well dispersed titanium dioxide nanoparticles [17]

2.3 Manufacturing

There are several different methods for incorporating the nanoparticles into the matrix: in situ polymerization, direct mixing and solvent mixing. In situ polymerization method incorporates the nanoparticles directly to the polymer chains by chemical methods. [17] It is suitable for raw polymer manufacturers. [19] Solvent mixing uses solvent, for example acetone or ethanol, to help breaking the agglomerates. Solvent must be removed before adding the hardener. [4] [26] Direct mixing is the most compatible method to use at the industrial level, because it allows production of nanocomposites with lower costs. [27] It is also environmentally safe without the solvents and contaminants that are used in solution method and in situ polymerization. [28] In direct mixing, the nanoparticles are added into the resin using, for example, high shear or sonication. High shear mixing can be done with rotating disc (Figure 2.6.), which breaks the agglomerates and distributes the particles evenly into the matrix polymer. Grinding by ceramic balls can also be used. [4] [17] Sonication is used only for small scale production, because the vibration energy works well only between small

distances. [29] In addition to processing methods described above, other techniques have been also developed including solid intercalation, covulcanization, and sol-gel method. Some of these are still being developed and not yet used widely. [19] High shear mixing is used in this work to manufacture epoxy nanocomposites and therefore it is elaborated further in the following chapter.

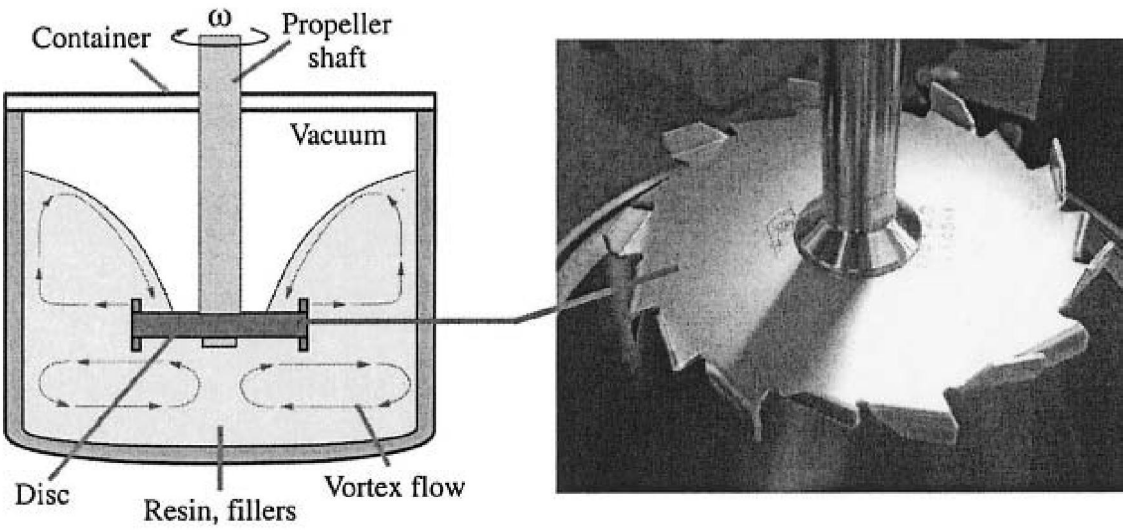

Figure 2.6. High shear mixing with a rotating disc [17]

High shear mixing is especially used for incorporating extremely fine filler particles into fluids, such as thermosetting resins. The high shear will first wet the particles surfaces by the fluid and then break down the particle agglomerates to smaller particles and distribute them evenly into the fluid. The shear is most effective at the tip of the dissolver disc, where the speed through the fluid is the highest. The circumference velocity can be calculated by the equation 1, where d is the dissolver disc diameter in meters and n is the rotating speed in rpm.

$$v = \frac{\pi \cdot d \cdot n}{60} \qquad (1)$$

With a dissolver disc of Ø 50 mm and rotating speed of 4000 rpm (both used in this work) the circumference velocity is 10.5 m/s.

The mixing efficiency is affected by the geometry of the dispersion container, the diameter of the dissolver disc and its height in the container, the peripheral velocity and the rheological properties of the fluid. Usually the smaller distance between the disc and the container gives higher shear rates within the gap. During the high shear mixing the fluid should form a doughnut-like flow pattern (Figure 2.7.). It is a sign that the maximum mechanical power possible is being applied on the fluid and eventually all the fillers will reach the dissolver disc. The doughnut effect is affected by the viscosity of the fluid. With too low viscosity the fluid will splash and generate bubbles during mixing, and with too high viscosity the doughnut effect cannot be achieved. The

rotational speed used should be the highest possible to obtain the greatest peripheral velocity but not too high to be able to maintain the doughnut flow pattern. [30]

Figure 2.7. Doughnut effect [31]

In addition to the mixing method used, the dispersion of the fillers is also affected by the shape, size and specific surface area of the particles, total volume content of the fillers, mixing conditions [17], polarity of the matrix resin, surface treatment of the particles and the curing temperature of the resin. [4] Even if the dispersion during mixing has been successful, maintaining the stable dispersion until the materials has cured may become a problem due to the secondary agglomeration, which may occur after mixing. Elevated temperature may enhance the reagglomeration because the viscosity of the resin decreases in the very beginning of the curing process. Reagglomeration occurs more easily when the filler content is higher, because the distances between the particles are shorter. [23]

2.4 Matrix materials

Polymers can be divided into thermoplastics and thermosets, according to their behaviour under temperature rise. Thermoplastics become softer when they are heated and harden back when they are cooled. This is a reversible process. When thermosets are heated, they become permanently hard. [32] This behaviour is based on the chemical reactions during curing. Thermoplastics have only physical changes where the polymer chains are entangling with each other. This makes it possible to repeat the softening and hardening cycles. [33] Both thermoplastics and thermosets can be used to make nanocomposites, and also elastomers are widely used. [18] [14]

Thermosets form a crosslinked network during curing, where covalent bonds are formed between the polymer chains. These bonds cannot be broken with re-heating. They resist the vibrational and rotational movements of the cured structure, which prevents the material to soften during temperature rise. [32]

When cured thermoset is heated above a certain temperature, they go through glass transition (T_g) temperature. Below T_g the material is glassy and hard, but after glass

transition temperature it changes into soft and flexible and loses its dimensional stability. Properties, such as tensile modulus, drop significantly. This is a reversible process, the polymer becomes glassy again after cooling back below T_g. [33] [34] When the temperature is elevated further after T_g, the material will reach the degradation temperature. [33]

Most thermosets need an extra component to be able to cure, which is often called hardener or curing agent. [35] The ratio of resin and hardener varies depending on the thermoset system. The right ratio is important, because small deviations may change the curing behaviour and mechanical properties of the final material. Mixing of the resin and hardener is done at room temperature or at elevated temperatures. The viscosity has to be low enough to achieve a homogeneous blend, which can be enhanced by heating the resin. However, the heating should be moderate in order to avoid the accelerated curing reaction, which can make the mixing and moulding difficult. [36] An example of the crosslinking is presented in Figure 2.8., where epoxy is cured with amine hardener.

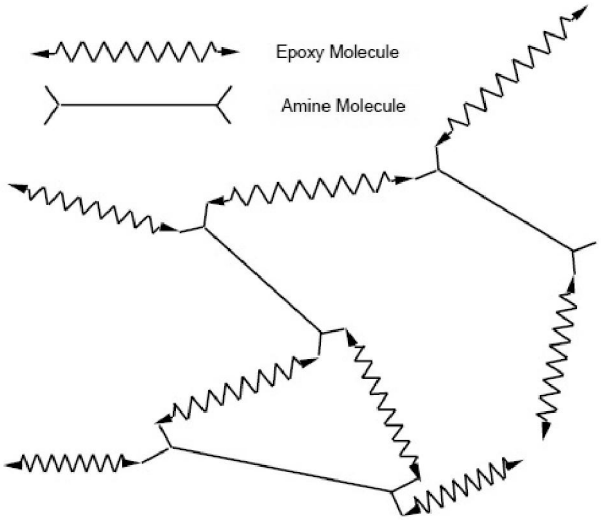

Figure 2.8. Crosslinking network of epoxy resin with amine hardener [34]

When the thermoset is cured at elevated temperatures, the viscosity of the thermoset mixture (thermoset + hardener) decreases at the beginning of the temperature rise. As the curing is continued, molecular weight increases, which also causes the viscosity to increase. As the curing is continued further, the mixture starts to behave like a gel. [36] This phenomenon is called gelation. The gel point is the point in polymerization when the network structure first starts to occur. [33] As the structure develops, the network will stiffen and the glass transition temperature of the material will increase. [37] The gel point is also the time limit for the processing conditions when the moulding of the mixture is not possible anymore due to the extreme increase of the viscosity. This is why the shaping of the thermoset in the mould has to be done before the gel point. [36]

A common method to manufacture thermoset products is moulding. After the resin and hardener is mixed, the mixture is usually held under vacuum to remove the air bubbles that are usually formed during stirring. After that, the resin mixture can be

poured into the mould. The liquid resin fills the mould evenly and during curing it takes the shape of the mould. Curing is then performed for suitable time and temperature for the specific resin system. The sample can be removed from the mould after the curing is finished and the sample and the mould have cooled. [33]

The cured thermosets have many good properties, including solvent resistance, heat resistance, fatigue strength and excellent adhesion. [38] Thermosets have low viscosity in the beginning of processing, which enables less pressure and lower temperature during manufacturing than thermoplastics. [36] However, manufacturing of thermoplastic products takes generally less time than with thermosets, which is why they are better for high volume applications. [35] Thermosets are commonly used as the polymer matrix material in nanocomposites. [3] With thermoset resins the nanoparticles are used to reduce thermal shrinkage and brittleness, and to increase hardness, toughness and abrasion resistance. [1]

The most common thermoset resins are divided into polyester, vinyl ester and epoxy resins. Also phenolic and urethane resins are used. [38] Epoxy is a widely used thermoset resin in aircraft components and boat structures due to the good mechanical and adhesive properties and resistance to environmental degradation. Epoxy is also easy to process due to its low viscosity and relatively short curing time. [34] Epoxy is, however, more expensive than other thermoset resins like vinyl ester.

Epoxy has a long-chain structure that forms a three-dimensional network during curing. Epoxy groups form reactive sites in the chains that connect with the hardener. The epoxy group, circled in Figure 2.9., is a three-member ring, where two bonded carbon atoms are bound to one oxygen atom. Figure 2.9. shows also a typical structure of epoxy containing a monomer called diglycidyl ether of bisphenol A. The molecule contains two ring groups in the centre. They are able to absorb mechanical and thermal stresses, which offers good stiffness, toughness and heat resistance properties for the resin. [34]

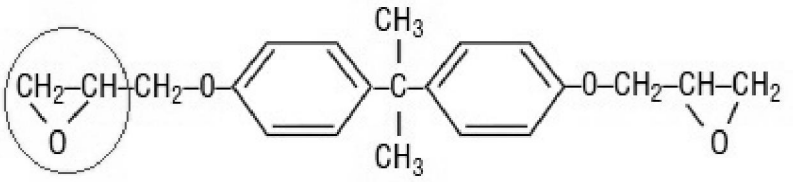

Figure 2.9. Chemical structure of an epoxy group [34]

Curing agent for the resin is chosen by the curing conditions and the final application of the epoxy material. [33] Amines are widely used for curing because they have a good reactivity with epoxy and they are provided in wide variety. [39] Amines can be divided into aliphatics, cycloaliphatics and aromatics. Other curing agents include thiols and alcohols. Accelerators can also be used if the reaction is too slow for the application. [33]

Figure 2.10. shows curing of the epoxy with amine curing agents. In the first step the primary amine is added to the epoxy group. This is followed by the addition of the

secondary amine to add to another epoxy group. Hydroxyl groups accelerate the reaction by opening the epoxy ring. [39]

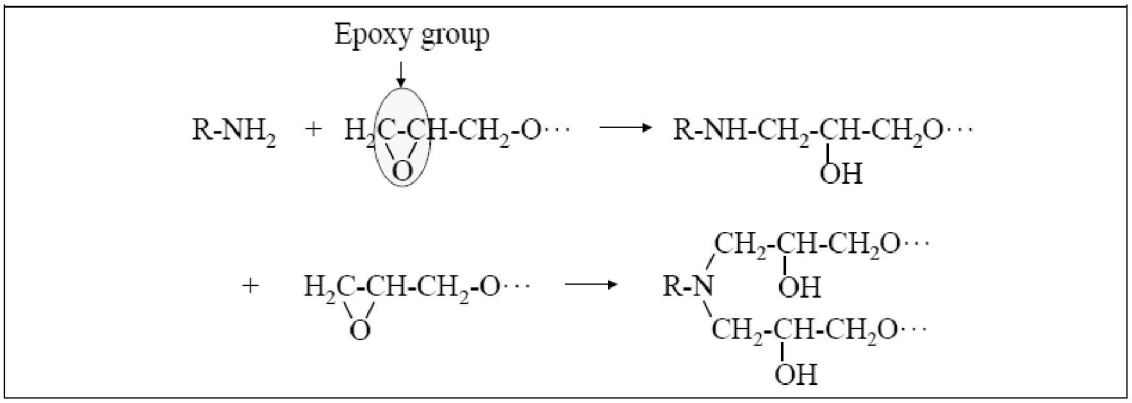

Figure 2.10. Curing steps of the epoxy with amine curing agent [39]

The curing treatment determines the properties, such as strength, stiffness and glass transition temperature, of the final material. Depending on the epoxy and the hardener, curing temperature can be somewhere between 5ºC and 150ºC. Usually the higher temperature gives better properties for the system. [34] [40]

Epoxy resins have a wide range of applications, including construction materials, automobile and aerospace applications, and as adhesives, coatings and electronic circuit board laminates. [41] The advantages of epoxy include excellent rigidity, high strength, low viscosity, low shrinkage during cure, chemical and thermal resistance, low creep and good adhesion to many substrates. [42] [1] Advantages compared to other thermosets include also low residual stresses in cured resin and minimum pressure that is needed during fabrication. Epoxy resin is available in many different viscosities, and the curing agents give many alternatives for different curing temperatures. [33] The disadvantages of epoxy are its brittleness in the cured state and poor resistance to crack growth. [1] Different nanoparticles can be used to improve the toughness of the epoxy, without degrading the properties of the epoxy resin. [42]

2.5 Nanoparticles

Inorganic nanoparticles can be divided into nanotubes (e.g. carbon nanotubes), layered silicates (e.g. montmorillonite), metals (e.g. Au, Ag) and metal oxides (e.g. Fe_3O_4, TiO_2). [43] There are also other carbon based nanomaterials like fullerenes [6], and also nanofibers like cellulose whiskers [39]. The nanoparticles used in this work are presented in detail in the following chapters.

2.5.1 Layered silicates / Nanoclay / Montmorillonite

Layered silicates are clay minerals that can be either natural or synthetic. Natural clay called montmorillonite, belonging to the smectite family, is the most widely used clay as nanofiller. Synthetic clays like magadiite, mica, laponite and fluorohectorite are also widely used in nanocomposites. [39]

Montmorillonite clay was first found in Montmorillon, France in 1847. Nowadays it can be found in numerous places around the world. Montmorillonite is usually produced by weathering of eruptive rock material like volcanic ash or tuffs. Purification of other volcanic rock minerals like crystobalite and quartz is needed before usage. [39]

One layer of the montmorillonite clay is about 1 nm thick and the diameter can be from tens of nanometres to even microscale. The structure belongs to the class of 2:1 phyllosilicates. [44] They consist of two tetrahedral sheets of silica with an octahedral sheet of aluminium or magnesium hydroxide in the middle, as illustrated in the Figure 2.11. [39] Oxygen ions of the octahedral sheet are shared by the tetrahedral sheets. These 2:1 structures form stacks (about 8-10 nm thick [39]) of several layers that are held together by van der Waals forces. These forces are relatively weak, which enables an intercalation of small molecules (like polymer) between the layers. [44] Isomorphous substitution, where Si^{4+} can be replaced by Al^{3+} in the tetrahedral sheet or Al^{3+} by Mg^{2+} in the octahedral sheet, creates negative charges between the layers. [39] Those are counterbalanced by alkali or alkaline earth cations. [44] There are usually also water molecules present between the layers, because clay is very hydrophilic. [39] This is due to the hydration of exchangeable cations and the polar nature of the Si-O groups. [18] Clay particles can be modified to be more compatible with hydrophobic polymers. [39] The cations of the interlayer can also be exchanged with cationic surfactants, like alkylammonium or alkylphosphonium, to lower the surface energy between the layers and making it easier for the polymer molecules to intercalate into the galleries. [44]

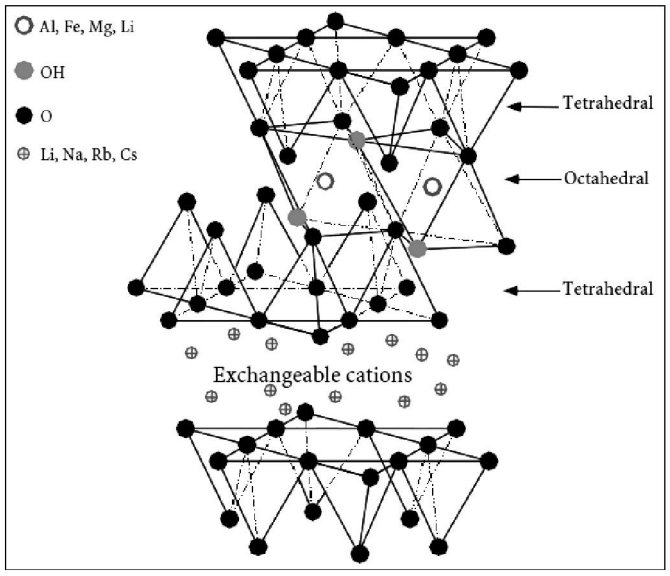

Figure 2.11. The 2:1 structure of Montmorillonite [18]

The chemical formula of the montmorillonite is $M_x(Al_{4-x}Mg_x)Si_8O_{20}(OH)_4$. M is a monovalent cation, for example sodium ion, and x is the degree of isomorphic substitution (between 0.5 and 1.3). [45]

Mixing of the layered silicates is a complex process. In addition to the good dispersion of the particles, exfoliation of the layered platelets is also required to get the desired properties. According to the organizing of the clay particles in the matrix, the clay-nanocomposites can be divided into three types: phase separated microcomposite, intercalated nanocomposite and delaminated nanocomposite. These are presented in Figure 2.12. [44] In the phase separated microcomposite, the clay particles act as normal microscale fillers, because the polymer has not been intercalated between the clay layers. [39] [44] In the intercalated nanocomposite, the clay layers have moved slightly apart [40] and the polymer molecules have been moved between the layers. In the delaminated (also called exfoliated) nanocomposite, the clay layers have totally separated from each other [39] and dispersed as individual particles into the matrix. [22] This increases the number of reinforcing components [19] and the total surface area of the filler phase. [18] The entire surface of the clay layer is available for the polymer. [39] The platelets can be aligned or in random state. [22] The delaminated structure forms the "true" nanocomposite. [40], giving the maximum reinforcement for the composite. [18] However, the fully delaminated structure is very difficult to achieve. Conventional processing methods usually give a mixture of the three above mentioned structures. [22]

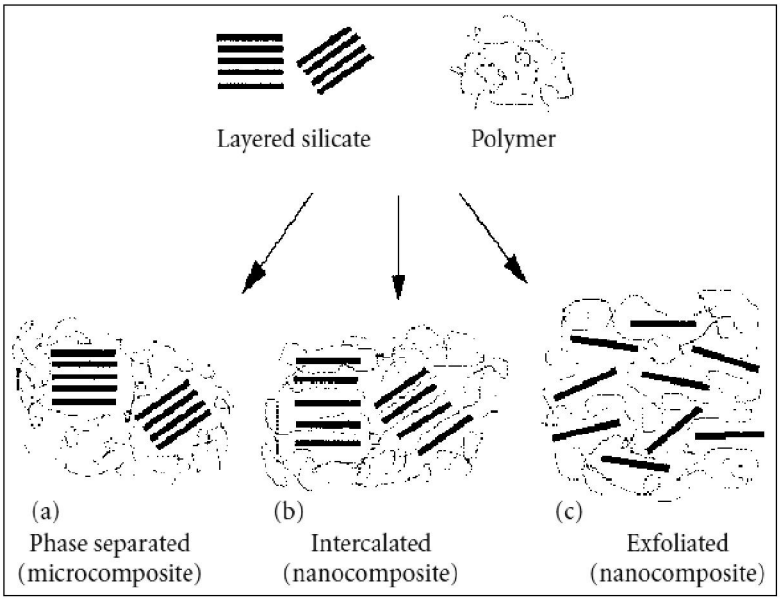

Figure 2.12. Different forms of clay-nanocomposite structures. [18]

Manufacturing of the clay-nanocomposites is usually done using *in situ* polymerisation, melt intercalation or solution induced intercalation. *In situ* polymerisation inserts polymer precursors between the clay layers to expand the

galleries and dispersing the individual layers into the matrix by polymerisation. This method can produce well-exfoliated nanocomposites. It is suitable for raw polymer manufacturers to use in polymer synthetic processes. Melt intercalation combines the clay and polymer during melt processing. Even though it may not be as efficient as the *in situ* method, melt processing has increased the commercial production of clay-nanocomposites. Solution induced intercalation uses solvents for swelling and dispersing the clay layers into the matrix. [19] Solvent method may not be the best option for commercial production since solvent has to be removed before adding the curing agent, and the solvents may be expensive. [4] [19]

Layered silicates are used as nanocomposite fillers to improve the mechanical properties, barrier properties, thermal resistance and fire resistance. [39] Barrier properties require the alignment of the clay plates, which creates a tortuous diffusion path. [22] Optical clarity occurs in exfoliated structure, because the nanometer-thick layer is much smaller than the wavelength of the visible light. [19] Nanoclays are also relatively cheap. [18] In epoxy, nanoclay is often used to improve thermal and mechanical properties in integrated circuit packaging and printed circuit boards, and also in coatings, automotive and aerospace industries. [46]

2.5.2 Carbon nanotubes (CNTs)

Carbon nanotubes are long chain-like structures that consist entirely of carbon. Other forms of pure carbon include fullerenes, and the more commonly known graphite, diamond and fullerenes. These different forms of carbon are presented in Figure 2.13. Graphite has a two-dimensional structure that consists of large planar sheets of aromatic rings with alternating single and double bonds (Figure 2.13.a). Diamond, on the other hand, has a three-dimensional structure that consists entirely of single carbon-carbon bonds in traditional 109° angles (Figure 2.13.b). [3] Properties of these two carbon allotropes are highly different from each other: diamond is transparent and one of the hardest materials known where graphite is black in colour and so soft that it can leave a mark on paper. [23] Fullerenes and carbon nanotubes are nanoscale structures. Fullerenes (Figure 2.13.c) consist of hollow spherical clusters where sixty carbon atoms are face-centered. Carbon nanotubes consist of graphite sheets rolled on a tube (Figure 2.13.d). [32] The ends of the tubes are usually closed with a structure of a half fullerene. [23] Carbon nanotubes and fullerenes can both be made as highly conductive or semiconductive. [32]

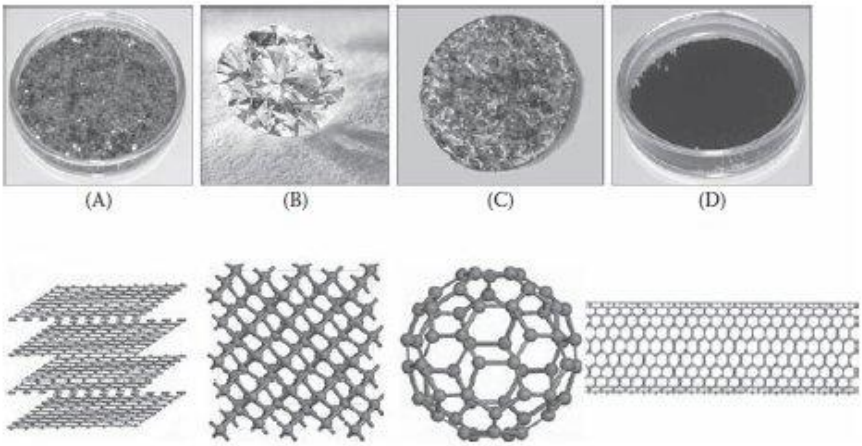

Figure 2.13. Allotropes of carbon: (a) graphite, (b) diamond, (c) fullerene, (d) carbon nanotube [23]

Carbon nanotubes are a quite new discovery. Fullerenes were discovered first, by Robert F. Curl, Harold W. Kroto and R. E. Smalley in 1985. Their finding was later awarded by the Nobel Prize. [3] In 1991 Japanese scientist Sumio Iijima observed carbon nanotubes as a result of electric arc discharge technique. [23] The first discovered tubes were multi-walled, and single-walled tubes were found shortly after that. [47] Since then the carbon nanotubes have been under considerable research. [48]

The walls of the carbon nanotubes consist of the same structure as graphite sheets (Figure 2.14.a): hexagonally structured carbon atoms where each hexagon is a six-membered aromatic ring. [3] Carbon nanotubes can exist as single-walled or multi-walled tubes. A single-walled tube, as in Figure 2.14.b, consists of one wall, while multi-walled tube, as in Figure 2.14.c, consists of several coaxial tubes. [40] Van der Waals forces between the tubes are keeping them together. [48]

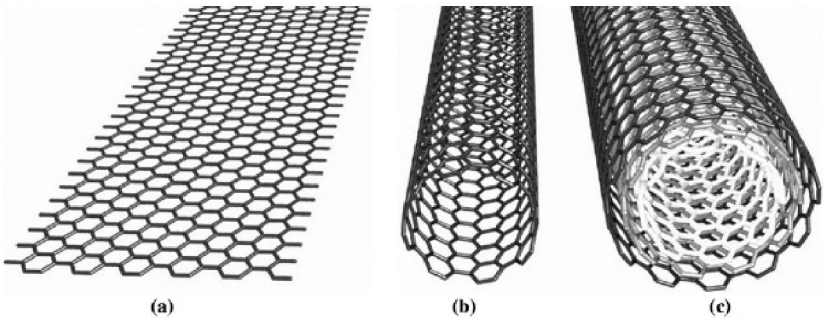

Figure 2.14. (a) Graphite sheet, (b) single-walled carbon nanotube, and (c) multi-walled carbon nanotube [49]

When the tube is thought of as rolled graphite sheet, the atomic arrangement of the hexagonal wall structure is defined by the rolling angle of the sheet. The structure has an effect on the transport properties, which defines the electrical and thermal conductivity of the tube. The atomic structure can be described by chirality, which is determined by the chiral vector C_h and chiral angle θ. The atomic arrangements are

categorized as ‘zig zag’, ‘armchair’ and ‘chiral’ (Figure 2.15.). They are described by the chiral vector $C_h = na_1 + ma_2$, where the integers n and m present the number of steps through the carbon bonds along the unit vectors a_1 and a_2. The chiral angle determines the amount of ‘twist’ of the tube. In multi-walled carbon nanotubes each tube can have a different structure. [23] [40] [48]

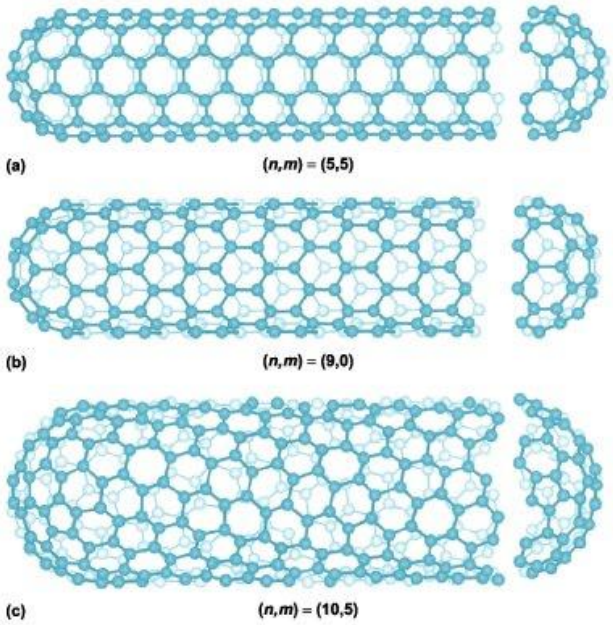

Figure 2.15. Different carbon nanotube structures: (a) armchair, (b) zig zag, (c) chiral [47]

Density of the carbon nanotubes is estimated to for the SWCNTs to be only 0.6 g/cm^3 and for the MWCNTs between 1 and 2 g/cm^3. [50] The diameter, being between 1-100 nm [51], depends on the number of aromatic rings that form the circumference of the tube. [3] The length of the tube can be up to millimetres. [51] This creates a very high aspect ratio [23], and the specific surface area of a single tube can be as high as 10-20 m^2/g. [52] However, many processing methods reduce the tube length to about 100 nm for the final products. [3]

Carbon nanotubes have exceptional mechanical, thermal and electrical properties. Young’s modulus can be greater than 1 TPa [51], and strength can be even 100 times higher (about 150 GPa) than high strength steel. [53] Comparing single-walled and multi-walled tubes, the multi-walled tubes are stiffer than the single-wall tubes. [2] Carbon nanotubes are thermally stable up to 2800ºC in vacuum, and its thermal conductivity is higher than the one with diamond. Also, carrying capacity of electric current is 1000 times higher than in copper wires. [48] Therefore, CNT-composites are suitable for light-weight applications combined with high strength and electrical conductivity. [54] However, in order to have composite with such properties, nanotubes have to be evenly dispersed into the matrix. Due to their long and flexible structure combined with strong van der Waals forces between them, carbon nanotubes have an

extremely high tendency to agglomerate. [55] The commercial CNTs are usually supplied already as heavily entangled bundles [23], as in Figure 2.16., and their separation is very challenging. [55] Carbon nanotubes are used with very low filler contents.

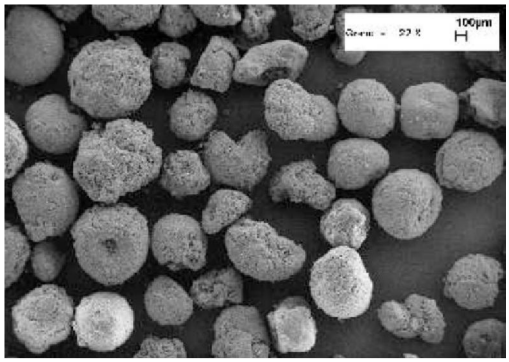

Figure 2.16. Scanning electron microscope image of MWCNT bundles [56]

Single- and multi-walled carbon nanotubes can be produced with several different methods: arc-discharge, laser ablation, gas-phase catalytic growth from carbon monoxide, and chemical vapour deposition (CVD) from hydrocarbons. [48] Arc-discharge method is based on a direct current going through two high-purity graphite electrodes under helium atmosphere. High volumes of single-walled and multi-walled tubes can be produced. [40] Laser ablation method was earlier used for the initial synthesis of fullerenes, but it is now developed to produce single-walled carbon nanotubes. Laser ablation is based on laser associated vaporization of graphite and its condensation on a water-cooled target. Both arc-discharge and laser-ablation methods are limited by the low volume production and the necessary of purification from the undesired by-products. Chemical vapour deposition (CVD) is a gas-phase technique where the decomposition of carbon-containing gas forms carbon nanotubes. A direct current between two electrodes produces plasma where carbon is vaporized from the anode and reorganized at the cathode. This forms a cylindrical deposit of un-aligned graphite planes, where multi-walled tubes are forming. [17] This is a continuous process that enables high yield of the tubes. CVD is able to control the diameter and length of the tubes, and purification is less needed. [48]

Carbon nanotubes are used with polymers to increase mechanical, thermal and electrical properties. [57] Carbon nanotubes have a great potential for reinforcement, because they are the stiffest fiber known. They could be used to replace glass and carbon fibers in polymer composites [58], but the challenges with the production techniques and the raw material price has to be overcome before they can be used to produce cost-effective composites. [48] Potential applications for CNT-filled nanocomposites are coatings, sensors, probes, energy storage devices, field emission displays, lightweight vehicles, aircrafts, civil constructions, sports equipments, marine, and military hardware. [57]

2.5.3 Silicon dioxide (SiO_2)

Silica (SiO_2), or silicon dioxide, belongs to the silicate materials, which are primarily composed of silicon and oxygen. Silicate materials include the bulk of soils, rocks, clays and sand. Structure of silicate materials consist of SiO_4^{4-}-tetrahedrons, with one silicon atom in the middle and four oxygen atoms at the corners. Different silicate materials consist of different arrangements of the tetrahedron. Silica is the most simple silicate structure. It is a three-dimensional network, where every corner oxygen atom of each SiO_4^{4-}-tetrahedron is shared by the neighbouring tetrahedron (Figure 2.17.). Bonds between the silicon and oxygen atoms are strong, which results in high melting temperature (1710°C). [32]

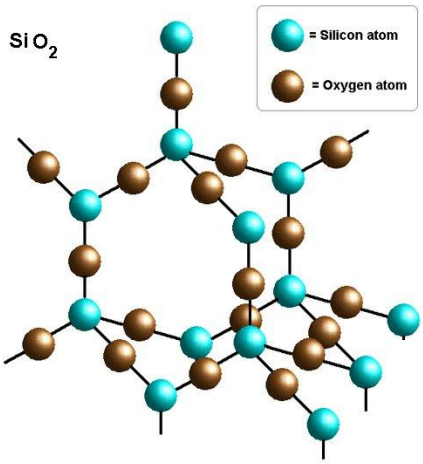

Figure 2.17. Chemical structure of silicon dioxide (SiO_2) [59]

Silica can exist in crystalline or amorphous form. [60] The primary forms of crystalline silica are quartz, trydimite and cristobalite. [32] Natural quartz constitutes 12,5% of the Earth's crust. [21] Amorphous silica and the part of the crystalline silica forms can be divided into natural and synthetic products. [60] Generally the different forms of silica include fused quartz, crystal, fumed and colloidal silica, silica gel and aerogel. Applications of silica include electronics, ceramics, polymer industry and concretes in construction industry. [61]

Nanosized silica has a density of 1.09-1.3 g/cm^3 and diameter of the spherical particle can be only 4 nanometers. [21] Nano-SiO_2 can be produced with several methods, including sol-gel process, vapour-phase and thermal decomposition technique. [61] Commercial nano-SiO_2 powder is usually fine and white amorphous powder produced by a fuming method. It is a high-temperature vapour process where $SiCl_4$ is hydrolyzed in an oxygen-hydrogen flame according to the reaction

$$SiCl_4 + 2H_2 + O_2 \rightarrow SiO_2 + 4HCl \qquad (2)$$

Silica has a hydrophilic nature because of the silanol and siloxane groups that are formed on the silica surface. [43] Mixing of the hydrophilic silica with hydrophobic epoxy resin can be challenging due to their different polarities. [62] Furthermore, the silanol groups (Si-OH) on the adjacent particles (Figure 2.18.) form hydrogen bonds that hold the individual silica particles together creating agglomerates, which can be difficult to break. [43]

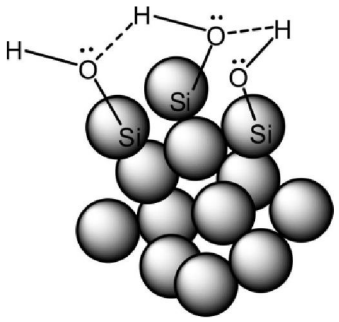

Figure 2.18. Hydrogen bonding among the silanol groups between silica particles [43]

Nano-SiO_2 is widely used in different kind of industries including cosmetics, drugs, printer toners, varnishes and biotechnological applications such as cancer therapy and drug delivery. [60] Technological applications include thixotropic agents, thermal insulators and composite fillers. [61] Nano-SiO_2 has been used with thermoset resins to increase the fracture toughness, impact strength, tensile modulus, durability and abrasion resistance, and to improve dielectric properties, heat distortion and chemical resistance. [17]

3 EXPERIMENTAL

3.1 Materials used in this study

3.1.1 Resin

Epoxy resin and curing agent used in this study were PRIME^{TM} 20LV and PRIME^{TM} Slow hardener, respectively. PRIME^{TM} 20LV is a bisphenol A based epoxy resin and PRIME^{TM} Slow hardener is an amine based hardener. Slow hardener gives a working time of one hour at room temperature for pure resin. The mixing ratio of the resin and the hardener was 100:26 by weight and the curing was done in oven at 65°C for 7 hours.

Table 3.1. Properties of the epoxy resin and hardener [63]

	PRIME^{TM} 20LV resin	**PRIME^{TM} Slow hardener**
Supplier	Gurit	Gurit
Density (g/cm^3)	1.123	0.936
Mixing ratio (by weight)	100	26
Viscosity at 20°C (cP)	1010-1070	22-24
Viscosity at 25°C (cP)	600-640	15-17
Viscosity at 30°C (cP)	390-410	12-14

3.1.2 Nanofillers

Three different nanofillers were tested in this study: nano-SiO_2 (nanosilica), nanoclay and carbon nanotubes (Table 3.2. and Figure 3.1.). Multi-walled carbon nanotubes and nano-SiO_2 were both purchased from Sigma-Aldrich while nanoclay (trade name Cloisite 11) was from Rockwood Clay Additives. Carbon nanotubes have outer diameter of 6-9 nm, length of 5 µm and the number of walls between 3 and 6 and they are produced by catalytic chemical vapour deposition (CVD) method. [64] Spherical nano-SiO_2 particles have diameter of 12 nm and they do not have any surface treatment according to the manufacturer. [65] Cloisite 11 is based on natural bentonite (consists mostly of montmorillonite) and the surface treatment is based on a quaternary ammonium salt. The diameter of the clay platelets is under 40 µm. [66] The prepared samples for tensile tests are presented in Figure 3.2. Filler contents by weight and volume are presented in Tables 3.3 and 3.4.

Table 3.2. Commercial nanofillers used in the work

Trade name	Supplier	Density [g/cm^3]
Multi-walled carbon nanotubes	Sigma-Aldrich	1.7 *
Silica nanopowder	Sigma-Aldrich	1.1 **
Cloisite 11	Rockwood Clay Additives	1.6 ***

* [67], ** [21], *** [68]

Figure 3.1. Pure powder of nanoparticles: (a) nano-SiO_2, (b) nanoclay, (c) MWCNT

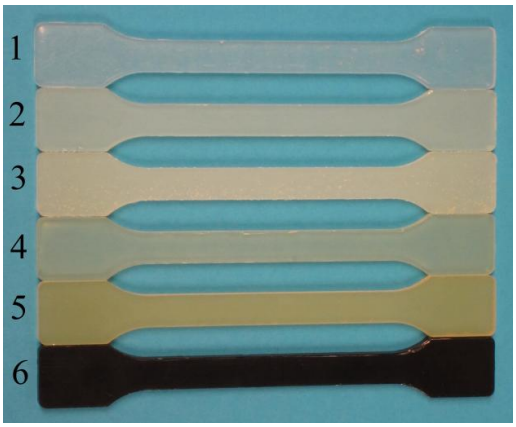

ID	Sample
1	EP
2	EP / 1 wt.% nano-SiO_2
3	EP / 2 wt.% nano-SiO_2
4	EP / 1 wt.% nanoclay
5	EP / 2 wt.% nanoclay
6	EP / 0.5 wt.% MWCNT

Figure 3.2. Tensile test samples and sample concentrations

Table 3.3. Filler contents in manufactured samples (by weight)

Sample	Filler [Weight-%]	Resin [Weight-%]	Hardener [Weight-%]
EP	0.0	79.4	20.6
EP / 1 wt.% nano-SiO_2	1.0	78.6	20.4
EP / 2 wt.% nano-SiO_2	2.0	77.8	20.2
EP / 1 wt.% nanoclay	1.0	78.6	20.4
EP / 2 wt.% nanoclay	2.0	77.8	20.2
EP / 0.5 wt.% MWCNT	0.5	79.0	20.5

Table 3.4. Filler contents in manufactured samples (by volume)

Sample	**Filler [Volume-%]**	**Resin [Volume-%]**	**Hardener [Volume-%]**
EP	0.0	76.2	23.8
EP / 1 wt.% nano-SiO_2	1.0	75.5	23.6
EP / 2 wt.% nano-SiO_2	2.0	74.7	23.3
EP / 1 wt.% nanoclay	0.7	75.7	23.6
EP / 2 wt.% nanoclay	1.4	75.2	23.5
EP / 0.5 wt.% MWCNT	0.3	76.0	23.7

3.2 Sample preparation

Before mixing, the nanofillers were dried overnight in an oven at 80ºC to remove the absorbed moisture from the structure. Manufacturing process was started by pre-heating the resin in an oven at 40°C to reduce the viscosity. The mixing chamber was also heated with a water circulation to 40°C. Mixing of the hardener was done at room temperature, but the resin was usually still a little warm, about 30°C. Mixing was performed with high shear mixer Dispermat CA-40 (Figure 3.3.a) and a cogged mixing head with a diameter of 50 mm (Figure 3.3.b). Mixing of the nanofillers was done under vacuum (0.7-0.75 bar) for 60 minutes with a rotating speed of 4000 rpm. During mixing, the temperature of the mixture was raised to 45-56°C (MWCNT-filled mixtures increased more than others) due to friction. After the nanofiller mixing, the hardener was mixed to the nanofiller doped resin under vacuum (0.7-0.75 bar) with a rotating speed of 500 rpm for 2 minutes. The maximum amount of material that can be mixed at a time under vacuum is 200 ml.

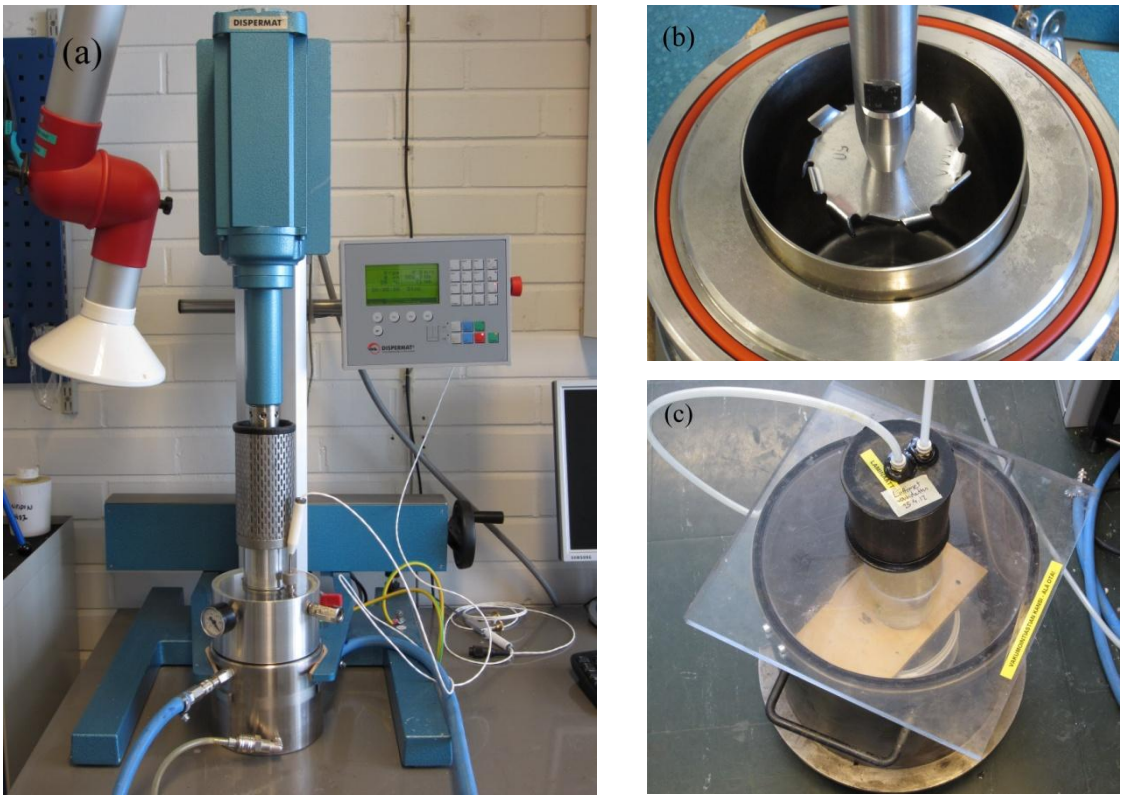

Figure 3.3. (a) Dispermat CA-40 high shear mixer, (b) mixing head and (c) vacuum chamber

Temperature rise during the nanofiller mixing can be seen from the mixing data collected during mixing of the sample EP/1 wt.% of nano-SiO_2 in Figure 3.4. As the temperature rises, the torque decreases, which is indicative of viscosity decrease due to the higher temperature.

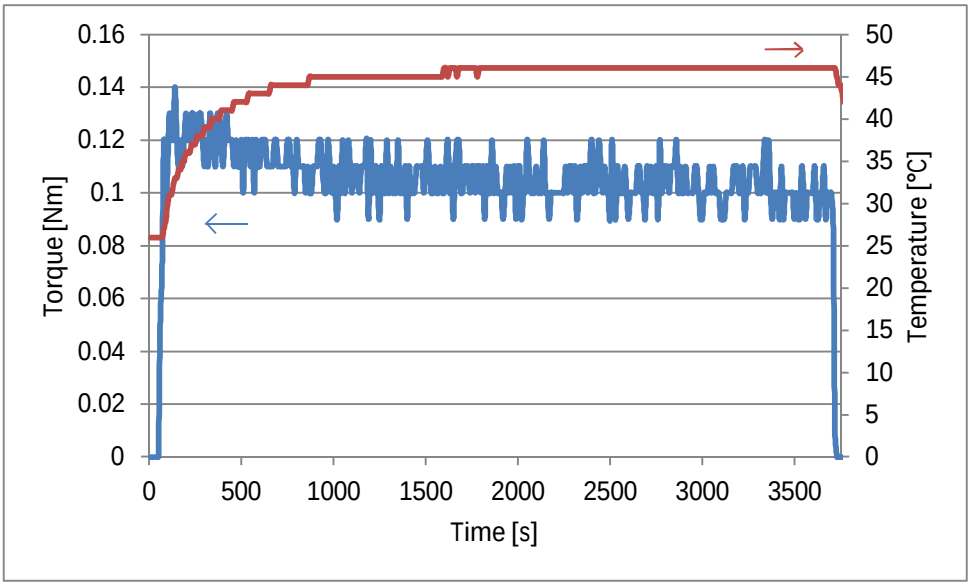

Figure 3.4. Mixing data of the sample EP/1 wt.% nano-SiO_2

Air bubbles were formed into the resin during the high shear mixing of nanofillers and they were removed before the addition of hardener in a separate vacuum chamber (0.7-0.8 bar), presented in Figure 3.3.c. During vacuuming the mixture cooled down, which made it necessary to heat the resin in an oven (40°C) between the vacuum cycles to lower the viscosity. Lower viscosity of the nanofilled resin made the removal of the bubbles more efficient. Vacuum cycles were repeated for necessary times, depending on the amount of air bubbles in the structure.

Mixing of the hardener was done at room temperature to avoid a catalytic reaction caused by the nanofillers and their surface treatment. This catalytic effect decreased the working time of epoxy significantly and it was noticed especially when using nanoclay. This may indicate that the nanoclay was not compatible with the epoxy resin. The hardener was mixed with lower speed and shorter time to reduce the formation of new bubbles. If a notable amount of bubbles formed, the mixture was held under vacuum for a maximum of 30 minutes after adding the hardener. The manufacturing procedure is presented also in Figure 3.5.

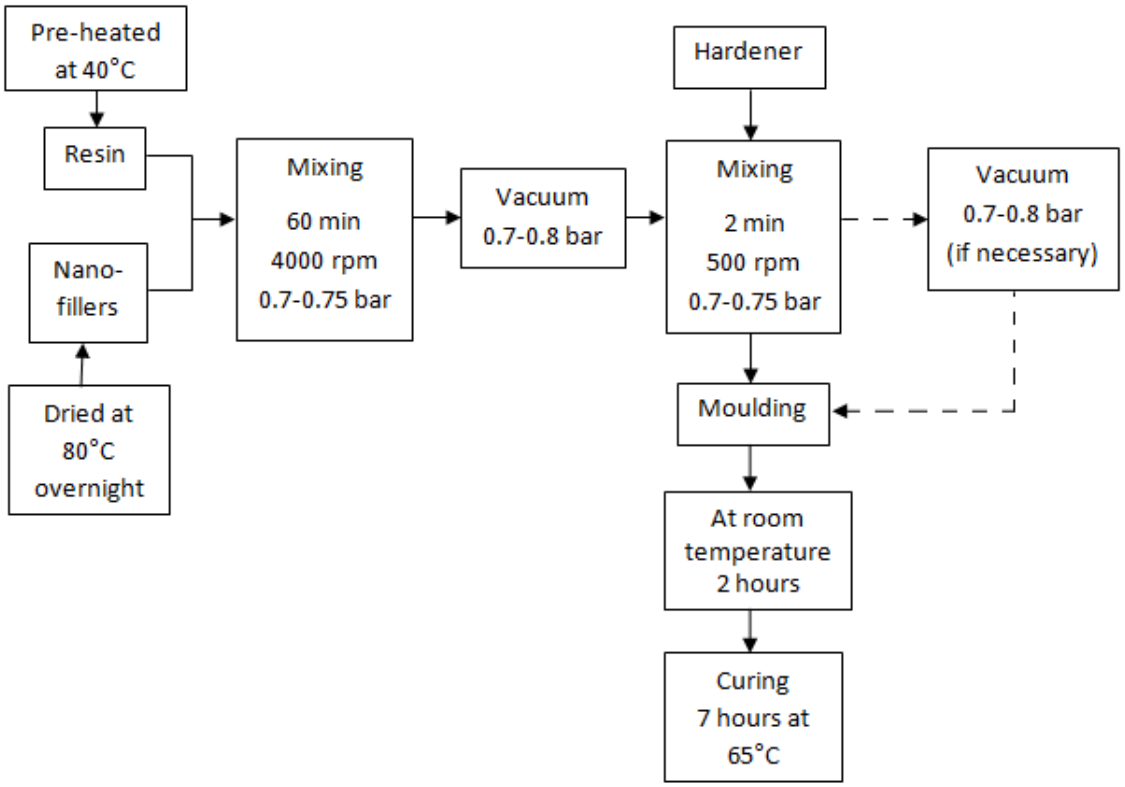

Figure 3.5. The thermoset nanocomposite sample preparation process

Metal frames (Figure 3.6.) were used for moulding the samples. They were placed on top of steel plate (thickness 10 mm), which was covered with a PTFE sheet. In addition, the frames were treated with a mould release agent (Chemlease 75) before moulding. Bone-shaped frames were used to manufacture tensile test samples (type 1A test bar according to standard SFS-EN ISO 527-2). Furthermore, fracture toughness samples were cut from the square samples (size 8 mm x 35 mm). Six tensile test samples (thickness 4 mm) and 2 square samples (thickness 4 mm) were manufactured from each material. The filled moulds were kept at room temperature for two hours to allow the air bubbles to come on the surface. Curing was done at 65°C for seven hours.

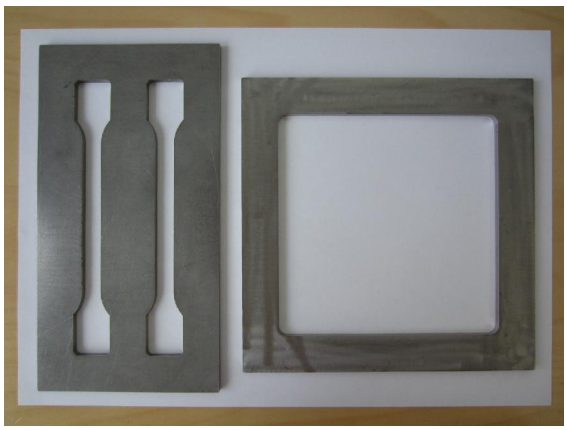

Figure 3.6. Moulding frames (placed on an A4-sized paper sheet)

3.3 Characterization

3.3.1 Viscosity

Viscosity measurements were used to examine the flow properties of the nanofilled resins. Viscosity can be used to analyse the dispersion of the nanoparticles and the interaction between resin and the fillers. [1]

Viscosity measurements were done with Anton Paar's rotational rheometer Physica MCR 301 (Figure 3.7.a). Plate-plate configuration (Figure 3.7.b) was used with a 1 mm gap. Viscosity was measured as a function of temperature between 23°C and 65°C with a shear-rate of 10 1/s, and as a function of shear rate between 0.1 and 100 1/s at room temperature (Table 3.5.). Oscillating measurement was also done for samples with nano-SiO_2 contents of 2 and 4 wt.%. Different gap distances were experimented with 4 weight-% of nano-SiO_2. All the measurements were performed to the nanofilled resin without the hardener, so the filler amount was somewhat higher than in the final samples.

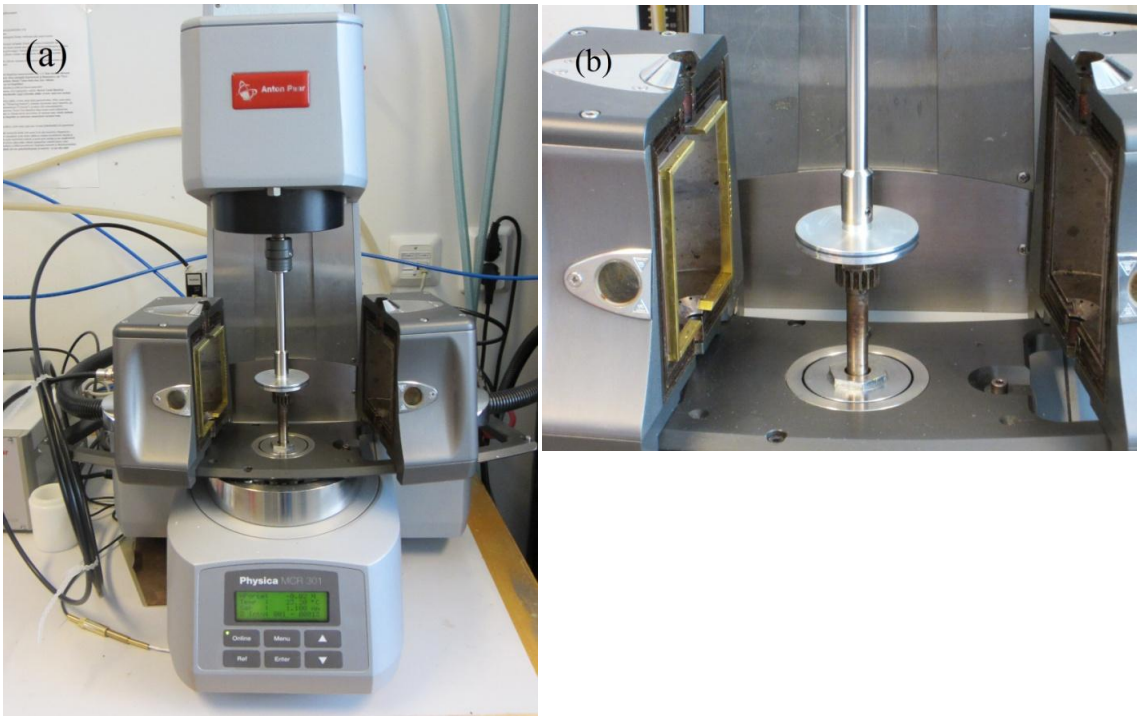

Figure 3.7. (a) Physica MCR 301 rotational rheometer, (b) Plate-plate configuration

Table 3.5. Viscosity measurement parameters

Mode	Function	Temperature	Shear rate	Configuration
Shear	Temperature	23°C - 65°C	10 1/s	Plate-plate (1mm gap)
Shear	Shear rate	Room temp.	0 - 100 1/s	Plate-plate (1mm gap)
Oscillating	Temperature	23°C - 65°C	10 1/s	Plate-plate (1mm gap)

3.3.2 Tensile test

Tensile test was performed to the samples in order to analyze their mechanical properties. Tensile test gives information about the tensile strength and modulus of the samples. The force that is needed to break the sample and the elongation until the breaking point are measured during the test. Modulus can be calculated from the data of the stress-strain curve. [69]

Tensile strength is the maximum tensile stress that is recorded during tension. [70] It is very dependent on the interactions between the matrix and the fillers. [18] Tensile stress can be calculated with the Equation 3:

$$\sigma = \frac{F}{A} \qquad (3)$$

where F is the force in Newtons (N), and A is the cross-sectional area of the sample in square millimetres (mm^2). [71] Modulus describes the material's resistance to deformation. [18] Young's modulus E is calculated from the ratio of the stress difference between σ_1 and σ_2 and the strain difference between ε_1 and ε_2 (Equation 4). The strain difference between ε_1 = 0.0005 and ε_2 = 0.0025 was used in the measurements, according to standard SFS-EN ISO 527-1. [71]

$$E = \frac{\sigma_2 - \sigma_1}{\varepsilon_2 - \varepsilon_1} \qquad (4)$$

An extensometer (Figure 3.8.b) was used to measure the elongation. Extensometer measures the elongation from the narrow part of the sample, because the bone-shaped tensile test sample does not elongate uniformly. [72]

Tensile tests were performed with Instron 5967 tensile test machine according to standards SFS-EN ISO 527-1 and SFS-EN ISO 527-2 using a load cell of 30 kN. The tensile test arrangement is presented in Figure 3.8.a. Thickness, length and width of the narrow portion in the tensile test samples (presented in Figure 3.2.) were 4mm, 150mm and 10mm, respectively. The draw rate of the test was 2 mm/min, gauge length in extensometer 50 mm and the frequency 0.417 1/s. Prior testing, all samples were stored in a humidity room for a few days.

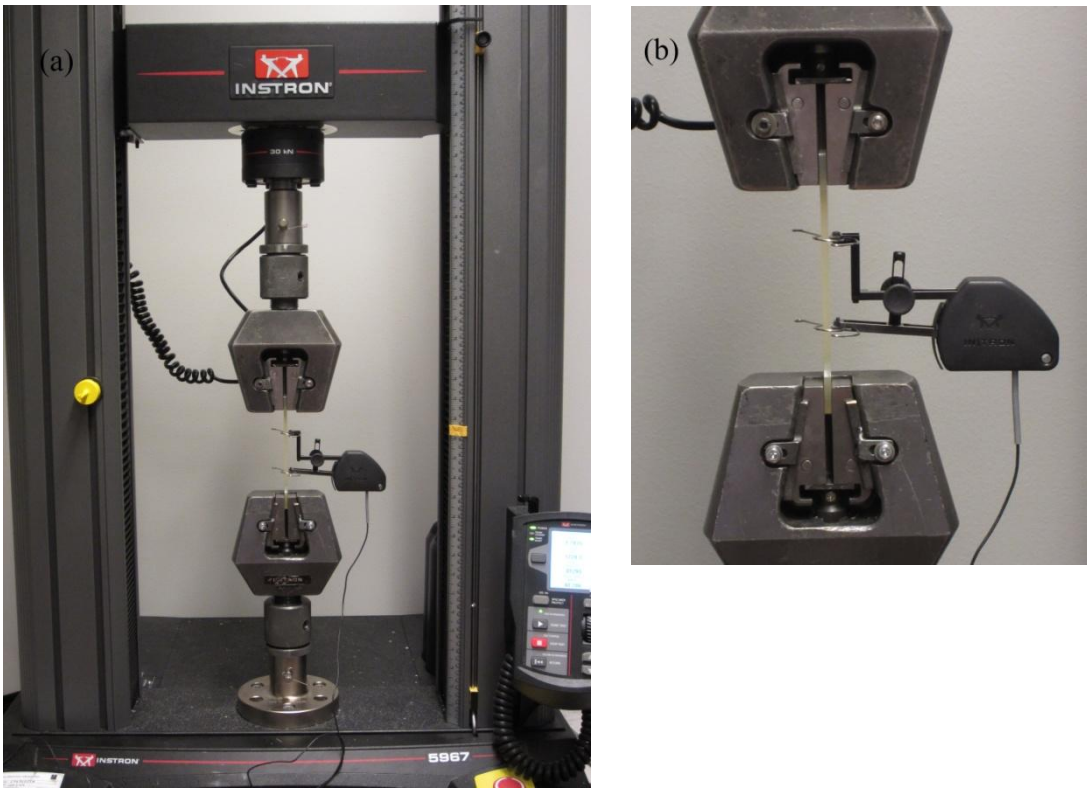

Figure 3.8. Tensile test (a) The arrangement (b) The extensometer

3.3.3 Fracture toughness

Fracture toughness analysis was used to measure the ability of a sample with an existing crack to resist a fracture. Fracture toughness sample is a notched rectangular where a natural crack is cut by a razor on the notch. Fracture toughness analysis can be used to design materials for dynamic applications. It is a very useful test method because it is almost impossible to make a material without any cracks or defects. [33] The theory behind the improved fracture toughness of nanocomposites is the creation of torturous path due to the well dispersed nanoparticles. In that case, the crack propagates along the nanoparticles producing a larger fracture surface area. [73]

Fracture toughness test was determined by standard ASTM D5045-99 with a single-edge-notch bending (SENB) configuration. The critical stress intensity factor K_{Ic}, that can be used to analyze the resistance to fracture, is determined with the equation 5:

$$K_{Ic} = \frac{P_Q}{BW^{1/2}} f(x) \qquad (5)$$

Where P_Q is the critical load for crack propagation, B is the thickness and W is the width of the sample, and f(x) is a non-dimensional shape factor expressed as:

$$f(x) = 6\sqrt{x}\,\frac{\left[1.99 - x(1-x)(2.15 - 3.93x + 2.7x^2)\right]}{(1+2x)(1-x)^{3/2}} \qquad (6)$$

where a is the crack length (machined notch plus razor crack) and x = a/W. [33] [74]

Fracture toughness sample (Figure 3.9.) is a notched rectangular, where a natural crack is cut on the notch by a razor. Fracture toughness sample dimensions were 8 mm x 4 mm x 35 mm and they were cut from the square samples with a disc cutter (using water). The 4 mm deep notch was cut with a circular saw (dry) and the natural crack (length about 0.1 mm) was mad by a sharp knife at the tip of the notch. Six samples from each material were tested and the samples were stored in a humidity room for a few days before testing.

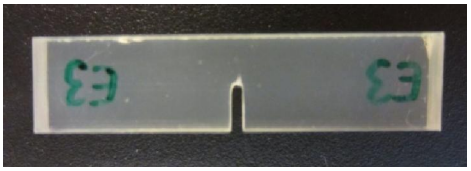

Figure 3.9. The fracture toughness sample

Tests were performed with Instron 5967 tensile test machine using a rate of 3mm/min and a load cell of 30 kN. A special bending fixture was used for the tests (Figure 3.10.b), where the upper tensile jaw moved freely upon the fixture (Figure 3.10.a). The force created by the weight of the upper jaw, 9N, was added on the results since the weight was already on the sample before the test started. The fracture toughness sample was placed on the fixture with the notch pointed down like it is shown in Figure 3.9.

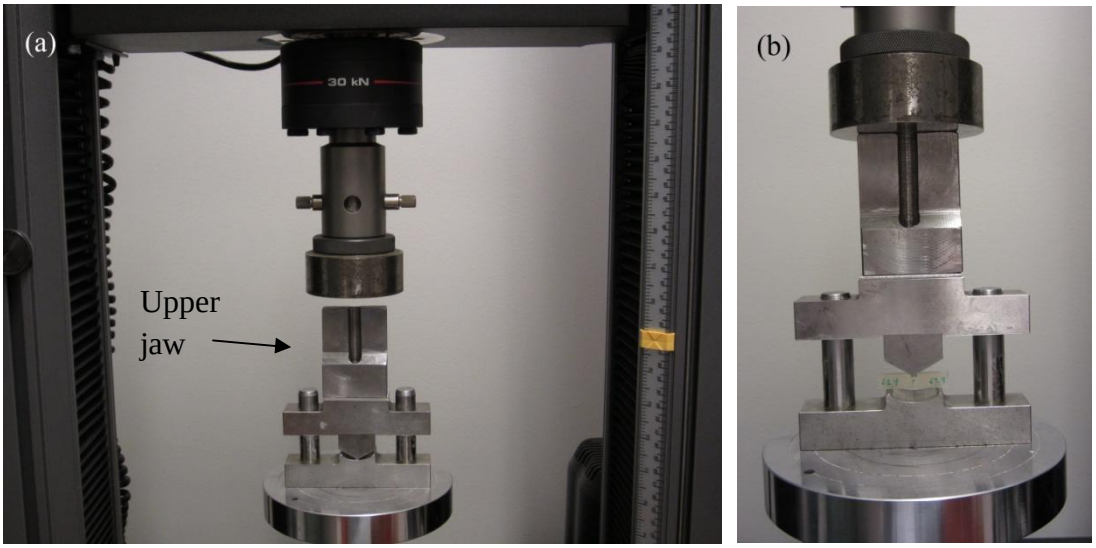

Figure 3.10. Fracture toughness: (a) Test arrangement, (b) Test fixture

3.3.4 Differential scanning calorimetry (DSC)

Differential scanning calorimetry was used to determine the degree of cure and the glass transition temperature of the samples. [72] DSC is based on a temperature difference between the sample (weight generally between 5-10 mg) and the reference material during heating or cooling. [75] [72] An electric signal, given by the temperature difference, is converted to a heat-flow signal which is plotted against temperature. [75] Two heating cycles are usually performed for polymers, because the first one is strongly affected by the thermal history of the sample. [72] If the sample is not fully cured, some residual curing may occur during the first heating, which can be seen as an exothermic peak on the results. During the second heating, the test produces only glass transition peak. [76] The higher is the glass transition temperature, the higher is the degree of cure. [77] An increase in T_g with fillers is considered to result from strong interaction between the filler and the matrix. Reduction in T_g is an indication of reduction in crosslink density. [78] The mid-point temperature of the T_g curve is the most commonly used definition for the glass transition (presented in Figure 3.11.). T1 and T2 are the onset and endset temperatures respectively, Tb represents the very beginning of the change in heat flow and the Te the very end of the detection of the glass transition event. [79] The sample does not necessarily have to be fully cured, thermoset samples can also be analyzed as uncured or partially cured. Heat development can be then monitored during curing. [33]

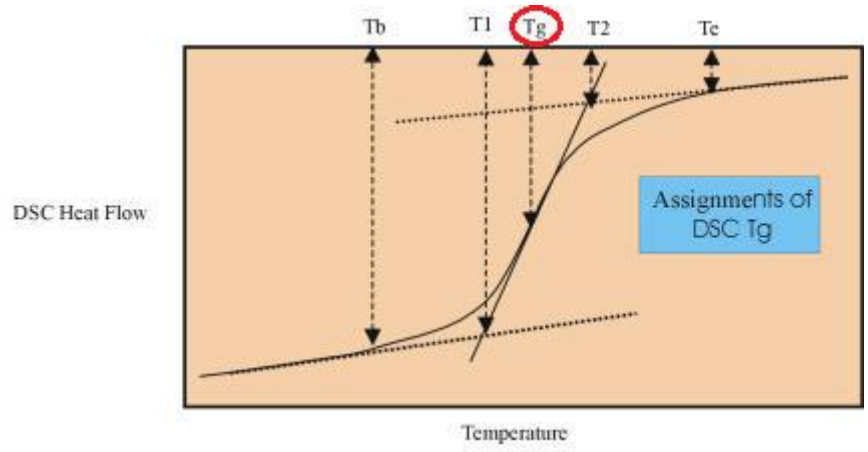

Figure 3.11. Determination of the T_g [79]

The DSC analysis was performed with Netzsch DSC 204F1 instrument, presented in Figure 3.12.a. The test sample and the reference can be seen in the middle of the Figure 3.12.b in the chamber. The samples were heated two times from 20°C to 270°C at a heating rate of 20°C/min under nitrogen atmosphere. Generally only one measurement was done for each sample, but pure epoxy and the sample EP/0.5 wt.% of MWCNT was tested twice.

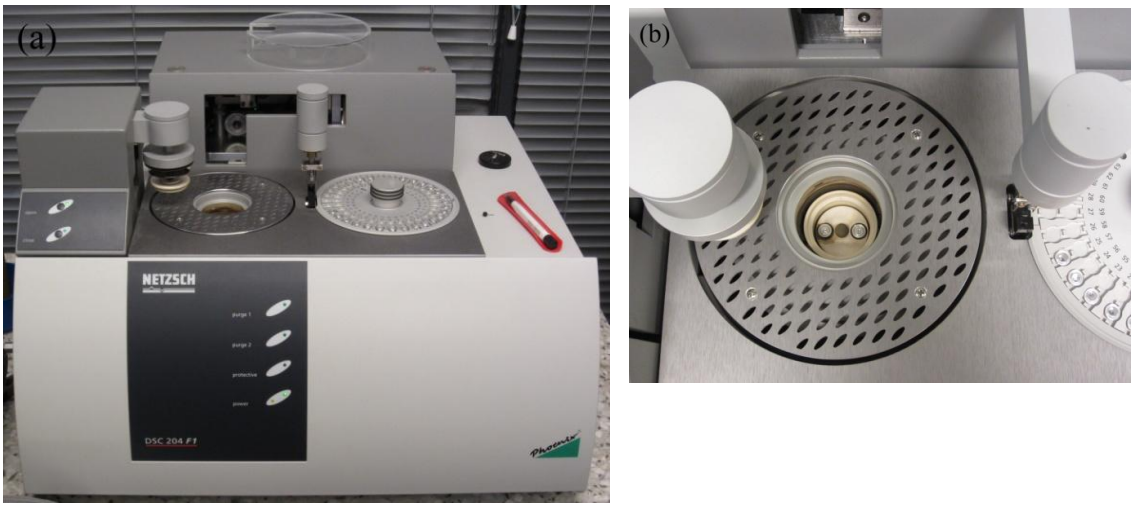

Figure 3.12. (a) DSC instrument, (b) Sample and the reference inside the test chamber

3.3.5 Dynamic mechanical analysis (DMA)

Dynamic mechanical analysis was used to examine the effect of nanofillers on the viscoelastic properties of the resin. [1] Under external loading, the viscoelastic materials have a behaviour that varies between elastic and viscous. Totally viscous system converts all work as heat and cannot be recovered after the force is released. Totally elastic system is able to store all work as potential energy. [24] [3] DMA is able to give information about both of these properties as a function of temperature. [72]

DMA applies a small deformation on the sample and examines the stiffness of the sample. [80] Storage modulus (E') gives information on the elastic properties, and loss modulus (E'') on the viscous properties of the sample. [1] Tan δ measures the energy dissipation of the material and it is the ratio between the loss and storage modulus. [80] The higher the tan δ value is, the better the damping performance of the material. [15] Glass transition temperature can also be determined by the results, but the determination varies with industry. Most commonly the T_g is defined by the onset of the E' drop, the peak of the tan delta or the peak of the E' curve. [80] In this work the T_g was determined by the peak of the tan delta curve.

Dynamic mechanical analysis measurements were performed with Perkin Elmer Pyris Diamond DMA (Figure 3.13.) with three-point bending mode and frequency of 1 Hz. The samples were sawed from the square samples to the size of 3 mm x 4 mm x 40 mm. The temperature range used was 20-340°C with a heating rate of 2°C/min under nitrogen (inert) atmosphere. Only one measurement was done for each sample.

Figure 3.13. DMA instrument

3.3.6 Thermogravimetric analysis (TGA)

Thermogravimetric analysis was used to study the thermal stability of the samples. During TGA test, the mass of the sample is continuously recorded either as a function of time in isothermal mode or as a function of temperature in dynamic mode (the most widely used method [72]). [75] Test atmosphere can be either inert or oxidizing. [72] The mass loss of the sample gives information about the thermal decomposition of the samples and the volatile contents of the material components. [75]

Thermogravimetric analysis was performed with PerkinElmer STA 6000 (Figure 3.14.). Samples were heated from 25°C to 995°C with a heating rate of 10°C/min under nitrogen (inert) atmosphere. Only one measurement was done for each sample. Pure epoxy and the sample EP/0.5 wt.% of MWCNT was tested also under oxygen atmosphere.

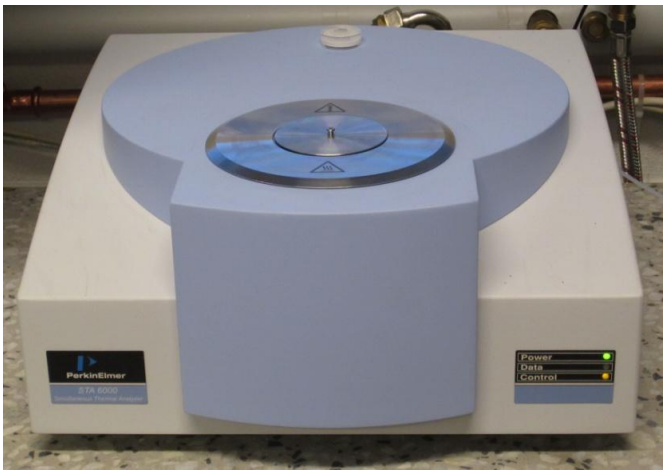

Figure 3.14. TGA instrument

3.3.7 Scanning electron microscopy (SEM)

Scanning electron microscope can be used to inspect the fracture structure of the samples, analyse the dispersion of the nanoparticles and study the arrangement, distribution and geometrical features of nanofillers. [23] Scanning electron microscope produces topographical images with high resolution [33] and it is based on a focused beam of high-energy electrons that is focused on the sample surface. The beam produces signals from the sample that are based on the interactions between the sample surface and the electrons. [81] This requires that the sample has a moderate electrical conductivity [23] to prevent charging. Therefore the sample surface is coated with gold or carbon. [33] The primary electron beam that sweeps over the sample generates secondary electrons, backscattered electrons, Auger electrons and x-rays. Secondary electrons produce the topographical images of the samples. Auger electrons and x-rays can be used to analyse the spectroscopic or chemical composition of the sample. [23]

Philips XL-30 scanning electron microscope (Figure 3.15.) was used for the examination of the fracture surfaces of the tensile test samples using an acceleration voltage of 15 kV. Before the examination, the specimens were coated with gold.

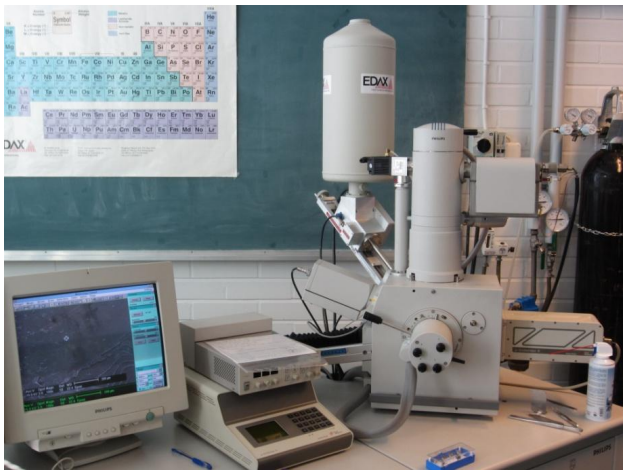

Figure 3.15. Scanning electron microscope Philips XL-30

3.3.8 Field emission scanning electron microsopy (FESEM)

The nanoparticle dispersion was characterized also with field emission scanning electron microscope (FESEM). The advantage compared to conventional SEM is the high resolution with low accelerating voltages that enables to analyze nanostructures and other delicate materials like biological samples. [82]

FESEM Zeiss ULTRAplus (Figure 3.16.) was used to perform the FESEM analysis using an acceleration voltage of 5 kV. The examined surface was cut by liquid nitrogen from the tensile test samples and covered with carbon to make the sample conductive.

Figure 3.16. Zeiss ULTRAplus field emission scanning electron microscopy [83]

3.3.9 Electrical conductivity

Polymeric materials are generally good insulators with the surface resistivity value ranging from 10^{14} to 10^{18} ohm. Conductivity can be increased (resistivity decreased)

with the compounding with carbon based fillers. [84] Resistivity of carbon nanotubes is 5-50 μΩ cm. [52] With polymers, resistivity is often measured from the surface, while metals are usually measured through the volume due to their high conductivity. [84] The measurements are based mostly on the standard ASTM D 257-99: Standard Test Method for DC Resistance or Conductance of Insulating Materials.

In this study, electrical conductivity was measured only with the sample EP/0.5 wt.% of MWCNT (sample size 10 cm x 10 cm, thickness 4 mm). Prior to testing, the samples surface was cleaned with acetone and paper towel. Measurement was done attaching two electrodes to the sample surface with 500 volts between them. Dimensions of the electrode are presented in Figure 3.17.

D1 = 3.00 cm
D2 = 5.70 cm
D3 = 6.35 cm
g = D2 - D1 = 1.35 cm
D0 = D1 + g = 4.35 cm
P = ð * D0 = 13.67 cm

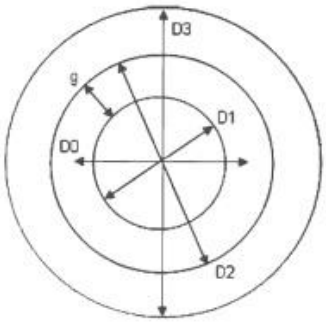

Figure 3.17. Electrode dimensions

Surface resistance is measured using the equation $R_s = U/I$ (where R_s is surface resistance, U is voltage and I is current). Surface resistivity is measured using the surface resistance and the equation $P_s=(P\cdot R_s)/g$. The ratio P/g using the electrodes described above is 10.123 (= 13.67mm/1.35mm), so the surface resistivity can be calculated by multiplying the surface resistance with this constant.

Volume resistance can be calculated with the equation $R_v = U/I$. Volume resistivity (Ω·cm), on the other hand, is calculated with the equation $P_v = (A\cdot R_v)/t$, where t is the sample thickness and A is calculated using the equation 7. [85]

$$A = \frac{\pi \cdot (D1 + g)^2}{4} = 14.86\ \text{cm}^2 \qquad (7)$$

4 RESULTS

4.1 Viscosity

4.1.1 Viscosity observations during processing

Considerable differences in the viscosities of the nanofilled epoxy resin samples were observed during manufacturing. The high viscosity of the samples EP/2 wt.% nano-SiO_2 and EP/2 wt.% nanoclay made the removal of the air bubbles after mixing challenging. Both samples had to be vacuumed and heated several times so that the casting of the samples was done on a following day after the first mixing. With the sample EP/2 wt.% nanoclay, several vacuuming and heating cycles enhanced the air bubble removal resulting samples, which were free of visible air bubbles. For sample EP/2 wt.% SiO_2, similar amount of air bubbles was left on the resin when casting the samples after only a few times of vacuuming and heating than with continuing the vacuuming process until the next day. The viscosity was so high that the mixture formed gel-like structure on the edges of the container after it had been standing in a mixing cup overnight. The sample EP/0.5 wt.% MWCNT, on the other hand, had significantly higher viscosity than the other samples. The mixture did not even out in the moulds after casting and the final samples were left slightly uneven. Furthermore, the removal of air bubbles was not successful during manufacturing. It was noticed that several vacuuming and heating cycles did not have a marked effect on the appearance of the mixture nor the amount of air bubbles in the structure. Therefore, MWCNT-mixture was vacuumed only once for half an hour. Due to the inefficient air bubble removal, the final specimens of the sample with 2 wt.% of nano-SiO_2 and 0.5 wt.% of MWCNT still had some visible air bubbles. Trapped air bubbles in the matrix are not desirable because they act as weak spots in the material, serving as initial points for microcracks. They also reduce the cross-sectional area of the specimens. [86] Hindered degassing process by high viscosity has also been noticed in the literature. Yasmin et al. [87] observed the foamy and viscous properties of nanoclay-epoxy mixture and the difficulty of degassing, which resulted as nanovoids in the final samples. Romhány et al. [86] also observed the processing difficulties due to viscosity increase by the addition of MWCNT (2 wt.%) and stated that air bubbles can be trapped in the matrix due to high viscosity.

Oh. et al. [46] and Thelakkadan et al. [88] also observed the high viscosity of nanoclay filled resin. They also stated that high viscosity can hinder the exfoliation of the clay particles, preventing the separation of the clay layers into individual layers.

High viscosity of the MWCNT-filled epoxy has also been noticed widely in the literature. He et al. [89] observed the viscosity as a function of temperature with 1 wt.% of MWCNT to be about 7 Pa·s between 30-40°C. With the filler content half lower (the sample EP/0.5 wt.% MWCNT) the viscosity was 3.6 Pa·s at 35°. The relation between

the viscosity of the nanofilled resin and the nanoparticle dispersion is unclear. According to Huang et al. [90] it is not yet possible to characterize the state of dispersion by the rheological data. However, He et al. [89] observed that functionalized MWCNTs gave lower viscosity due to better dispersion (observed by scanning electron microscopy). According to Hosur et al. [29] it is easier to achieve better dispersion when the viscosity is low. This can be achieved by using solvents. Sun et al. [54], on the other hand, indicated that at higher CNT loadings the epoxy/CNT viscosity increases dramatically especially when the dispersion is good.

SiO_2-particles with very high specific surface areas agglomerate very easily and form a three-dimensional network in the molten polymer matrix. [10] The lack of surface modification may enhance the formation, because unmodified nano-SiO_2 forms agglomerates more easily than modified nano-SiO_2. [4] Chemical reactions may have also occurred between epoxy groups and silanol groups on the surface of nano-SiO_2. This mainly happens before adding the hardener, but it is believed that the reactions proceed further during addition of hardener and at high temperature curing. [91]. When the particles are clustered together, only the nano-SiO_2 particles on the surface of the cluster can react with the polymer. This leads to encapsulation of the particles inside the matrix. Good dispersion may be difficult to achieve even if the mixing methods are efficient and the particles are surface treated. Tzetzis at al. [92] observed microsize clusters of fumed nano-SiO_2 particles regardless of the mixing with high shear and sonication, and the surface treatment of the particles.

Huang et al. [90] also noted that higher filler contents of nanofillers are more sensitive to reagglomeration during long standing times. Therefore, long vacuuming times are not advisable for the nanofilled mixtures.

With nano-SiO_2 the original plan was to manufacture also samples with 4 wt.% of nano-SiO_2. However, mixing of 4 wt.% of nano-SiO_2 with the epoxy resin increased the viscosity so much that the proper processing was not possible anymore. The mixture was processed in the high shear mixer for 5 minutes until it formed a gel-like structure and did not flow evenly on the container anymore (Figure 4.1.). Therefore, casted samples for mechanical testing were not prepared.

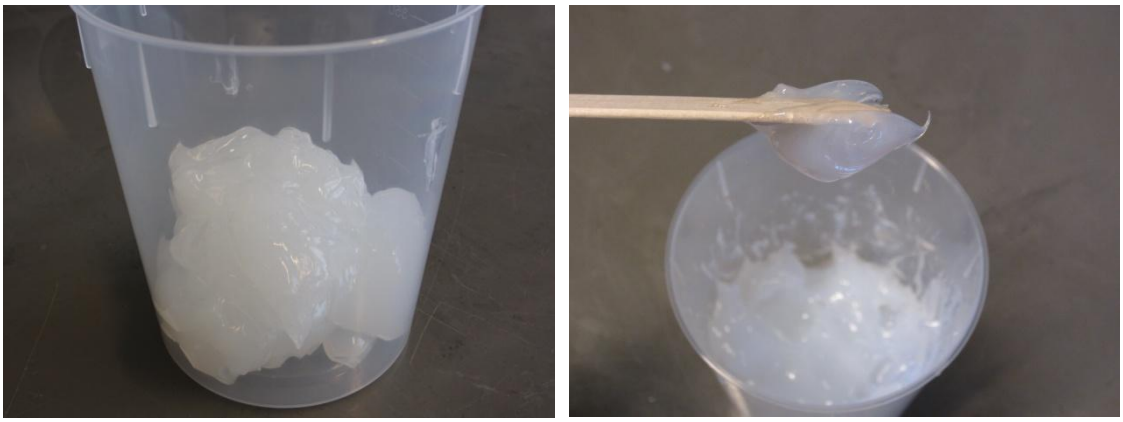

Figure 4.1. High viscosity of the EP / 4 wt.% nano-SiO_2

4.1.2 Viscosity as a function of temperature

Viscosity results for the nanofilled resin samples as a function of temperature between 23°C and 65°C with shear rate of 10 1/s are presented in Figures 4.2 and 4.3 and Table 4.1. The results support well the conclusions obtained from the manufacturing: at room temperature, the viscosity of the MWCNT-filled sample was about ten times higher than for pure epoxy. Both samples with nano-SiO_2 (Figure 4.2.) had abnormal viscosity curves: with 1 wt.% of nano-SiO_2, the viscosity decrease slows down notably after 30°C while in the case of 2 wt.% of nano-SiO_2, the viscosity starts to increase significantly after about 42°C. Viscosity of the samples with nanoclay decreased linearly with the increasing temperature so that the sample with 2 wt.% of nanoclay has a little higher viscosity than the sample with 1 wt.% of nanoclay.

Viscosities of the nano-SiO_2 samples were higher than with the nanoclay samples with the same loadings. This may be due to the different structure of the fillers. Rheology of the nanocomposites is affected by the interactions between the particles and the polymer and the functionality of the fillers. [10] The nano-SiO_2 used was unmodified, while the nanoclay was modified with quaternary ammonium salt. The higher viscosity of the samples with nano-SiO_2 may be due to the lack of surface modification.

The viscosity values for pure epoxy measured by the manufacturer are close to the values presented in Table 4.1: 0.60-0.64 Pa·s at 25°C, and 0.39-0.41 Pa·s at 30°C. [63]

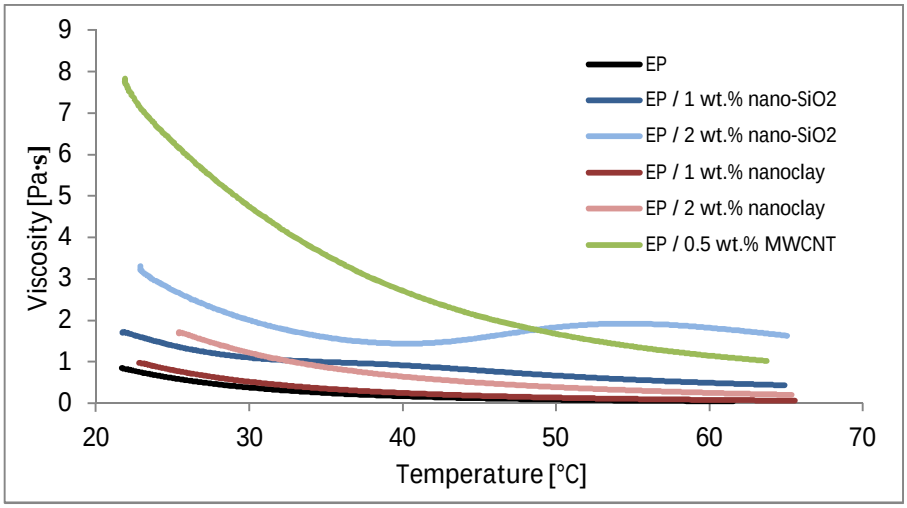

Figure 4.2. Viscosity of the nanofilled resin samples as a function of temperature with 10 1/s shear rate (1 mm gap)

Table 4.1. Viscosity results between 25°C and 60°C with shear rate of 10 1/s

Sample	Viscosity [Pa·s]				
	25°C	**30°C**	**40°C**	**50°C**	**60°C**
EP	0.60	0.38	0.16	0.08	0.05
EP / 1 wt.% nano-SiO_2	1.40	1.10	0.91	0.66	0.49
EP / 2 wt.% nano-SiO_2	2.72	2.00	1.44	1.83	1.82
EP / 1 wt.% nanoclay	0.80	0.52	0.25	0.14	0.08
EP / 2 wt.% nanoclay	1.68	1.21	0.64	0.39	0.25
EP / 0.5 wt.% MWCNT	6.26	4.76	2.72	1.67	1.15

The viscosity of the gel-like EP/4 wt.% of nano-SiO_2 (see Figure 4.1) was measured two times and the results are presented in Figure 4.3 along with other nano-SiO_2 samples to give a reference. In both measurements, the viscosity of the sample EP/4 wt.% of nano-SiO_2 first increases, in the first measurement after 40°C and in the second after 30°C. After that the viscosity decrease is very unstable. This may be due to the large agglomerates that most likely exist in the resin due to the incomplete mixing.

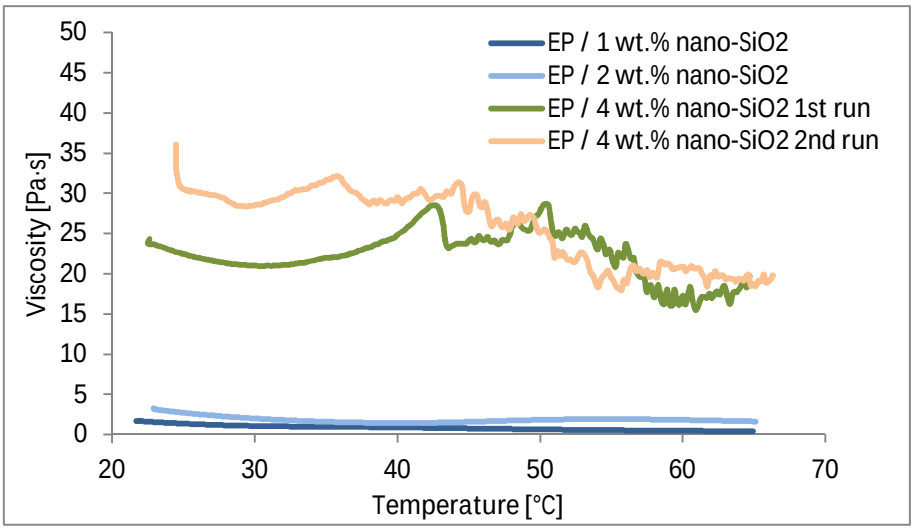

Figure 4.3. Viscosity results of the silica samples as a function of temperature with shear rate of 10 1/s

Due to the abnormality of the viscosity curves with the shear mode, the samples with 2 and 4 wt.% of nano-SiO_2 were also measured with an oscillating mode at angular frequency of 10 rad/s and gap width of 1mm. Measurements were done as a function of temperature between 25°C and 60°C. The results show that the viscosity increase of the sample with 2 wt.% of nano-SiO_2 (Figure 4.4.a) was significant already after 30°C, about 10°C earlier than with the shear mode. The viscosity for the sample with 4 wt.% of nano-SiO_2 (Figure 4.4.b) started to increase straight from the beginning and continued to rise during the whole measurement, slowing down a little after 40°C.

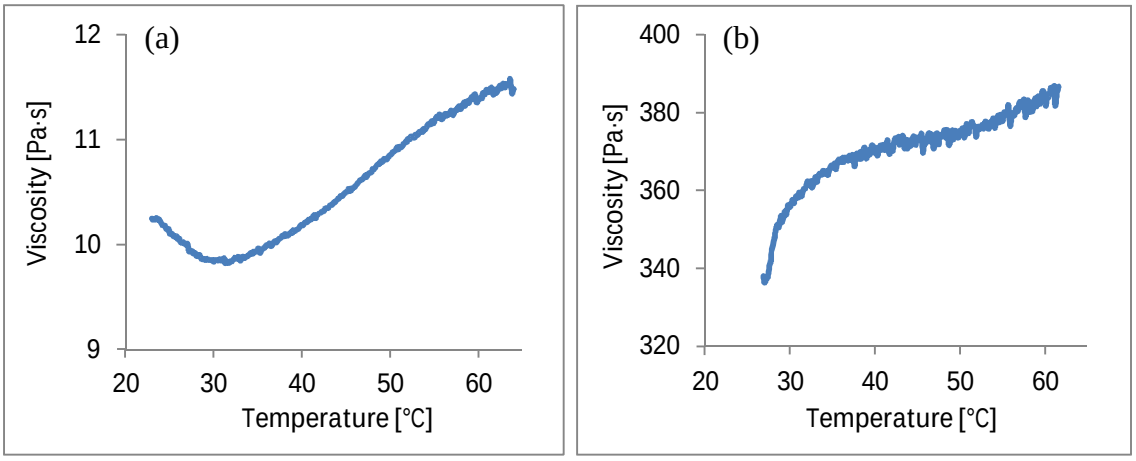

Figure 4.4. Oscillating mode of the (a) EP / 2 wt.% nano-SiO_2 and (b) EP / 4 wt.% nano-SiO_2 as a function of temperature with 10 rad/s

4.1.3 Viscosity as a function of shear rate

Viscosity results for all tested materials as a function of shear rate at room temperature are presented in Figure 4.5 and Table 4.2. The results supported the previous viscosity results since the sample EP/0.5 wt.% of MWCNT had the highest viscosity of all the samples. Furthermore, the viscosity of the sample EP/2 wt.% of nano-SiO_2 was also slightly higher than for the rest of the samples, especially at lower (< 40 1/s) shear rates. The viscosity values of all the other samples were close to each other already at low shear rates.

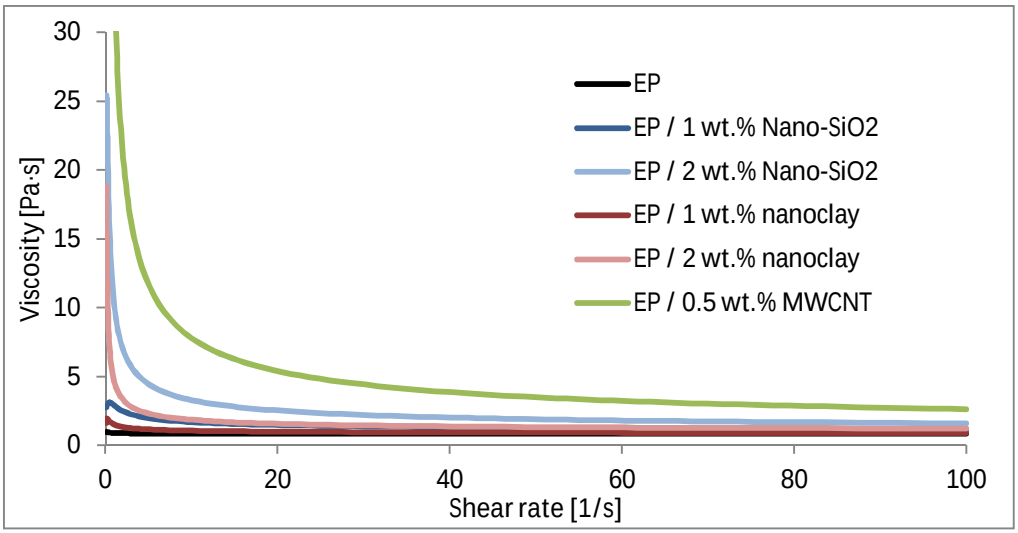

Figure 4.5. Viscosity results as a function of shear rate

Table 4.2. Viscosity results for the samples between shear rates 1 and 100 1/s

Sample	Viscosity [Pa·s]		
	1 [1/s]	**10 [1/s]**	**100 [1/s]**
EP	0.9	0.9	0.8
EP / 1 wt.% nano-SiO_2	2.9	1.7	1.2
EP / 2 wt.% nano-SiO_2	10.3	3.3	1.6
EP / 1 wt.% nanoclay	1.5	1.1	0.9
EP / 2 wt.% nanoclay	4.7	1.9	1.2
EP / 0.5 wt.% MWCNT	34.7	7.8	2.6

The effect of gap distance on the viscosity results were investigated for the sample with 4 wt.% of nano-SiO_2 (Figure 4.6 and Table 4.3). Measurements were done with the shear mode as a function of shear rate between 1 and 100 1/s at room temperature and the gap distances were varied between 0.3 mm and 1 mm. The results show that only the beginning of the measurement shows some differences between viscosities measured with different gap distances. After the shear rate of 0.6 1/s, the curves are overlapping each other. Therefore, it can be concluded that the abnormal viscosity curves of nano-SiO_2 samples shown before are not caused by the chosen gap width. The viscosity differences most likely result from the properties of the different nanofillers and their high tendency to agglomerate.

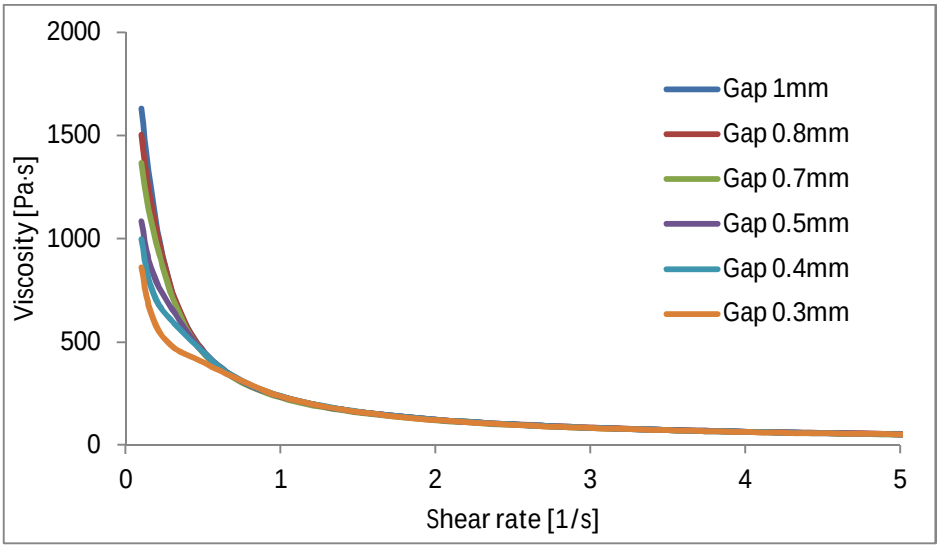

Figure 4.6. Sample EP / 4 wt.% of nano-SiO_2 with different gap distances as a function of shear rate at room temperature

Table 4.3. Sample EP / 4 wt.% of nano-SiO_2 with different gap distances as a function of shear rate at room temperature

	Viscosity [Pa·s]			
Gap	**0.1 [1/s]**	**1 [1/s]**	**10 [1/s]**	**100 [1/s]**
1.0 mm	1629.40	237.3	29.423	6.4452
0.8 mm	1502.60	235.98	30.481	6.5006
0.7 mm	1365.40	231.22	28.984	6.4108
0.5 mm	1085.10	236.36	29.603	6.5419
0.4 mm	996.99	238.66	29.587	6.4662
0.3 mm	861.38	237.56	29.390	6.4147

4.2 Tensile test

Results of the tensile tests are presented in Table 4.5. and Figures 4.8. - 4.11. All the tensile test curves for the tested samples can be found in Appendix 1. The measured thicknesses of the samples are presented in Table 4.4. while the average width of the samples was 10.1 mm. Especially samples with 2 wt.% of nano-SiO_2 and 0.5 wt.% of MWCNT had some visible air bubbles. Also, high viscosity left the MWCNT-samples slightly uneven, which may have caused higher standard deviation in the Young's modulus values. In fact, air bubbles were observed in some tensile test bars, as in Figure 4.7. with the sample EP/2 wt.% nano-SiO_2 where the fracture is initiated from the air bubble.

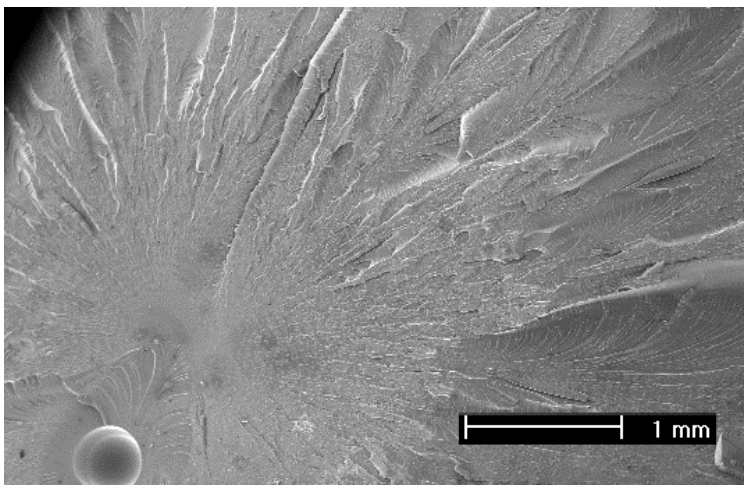

Figure 4.7. Fracture surface of sample EP/2 wt.% nano-SiO_2

The tensile test results show that the most significant improvements were observed in tensile strain at break with the sample EP/1 wt.% of nano-SiO_2 (improvement compared to neat epoxy was 27%) and in Young's modulus with the sample EP/0.5 wt.% of MWCNT (improvement compared to neat epoxy was 41%). Surprisingly,

nanoclay did not improve the tensile properties of epoxy although this has been widely verified in the literature. Ngo et al. [93] [94], for example, observed the tensile strength and modulus to increase by the clay loading. Also, Mohan et al. [95] observed the modulus and tensile strength of epoxy to increase up to 66.3 MPa with 3 wt.% of nanoclay. However, opposite views have also been obtained. According to Nordin et al. [96] the tensile strength decreased with increasing nanoclay content. The brittle behaviour compared to neat epoxy was considered to be due to the agglomerated nanoclay particles, which bring premature fracture on the sample when they break. The Young's modulus, however, increased with 1 wt.% of nanoclay, but decreased with 2 and 3 wt.%. [96] Oh and al. [46] also observed the tensile strength to decrease with increasing nanoclay loading, but the elastic modulus to increased. High viscosity of the nanoclay filled mixture and the decrease in tensile strength has been observed also by Yasmin et al. [87], having also problems with hindered air bubble removal due to the viscosity increase. However, elastic modulus was also observed to increase with increasing nanoclay content. [87]

The resin manufacturer gave the following results for the tensile test properties for the pure epoxy: tensile strength 73 MPa, tensile modulus 3.5 GPa and strain to failure 3.5 %. These values are slightly lower than the results in this work. The manufacturer cured the samples for 16 hours at 50°C, which was the other option for the curing conditions. The sample dimensions the manufacturer used were not mentioned. [63]

Table 4.4. Tensile test samples

Sample	**AVG Thickness [mm]**
EP	3.6
EP / 1 wt.% nano-SiO_2	4.1
EP / 2 wt.% nano-SiO_2	3.6
EP / 1 wt.% nanoclay	4.1
EP / 2 wt.% nanoclay	4.1
EP / 0.5 wt.% MWCNT	4.3

Table 4.5. Tensile test results

Sample	**Tensile strength [MPa]**	**Tensile strain at break [%]**	**Young's modulus [GPa]**
EP	75.9±1.3	4.9±0.3	3.4±0.1
EP / 1 wt.% nano-SiO_2	76.1±0.4	6.2±1.7	3.4±0.4
EP / 2 wt.% nano-SiO_2	74.0±0.4	4.2±0.4	3.1±0.2
EP / 1 wt.% nanoclay	63.2±1.8	2.7±0.2	3.1±0.3
EP / 2 wt.% nanoclay	48.4±3.5	1.8±0.2	2.9±0.2
EP / 0.5 wt.% MWCNT	58.3±6.2	2.6±0.8	4.8±1.8

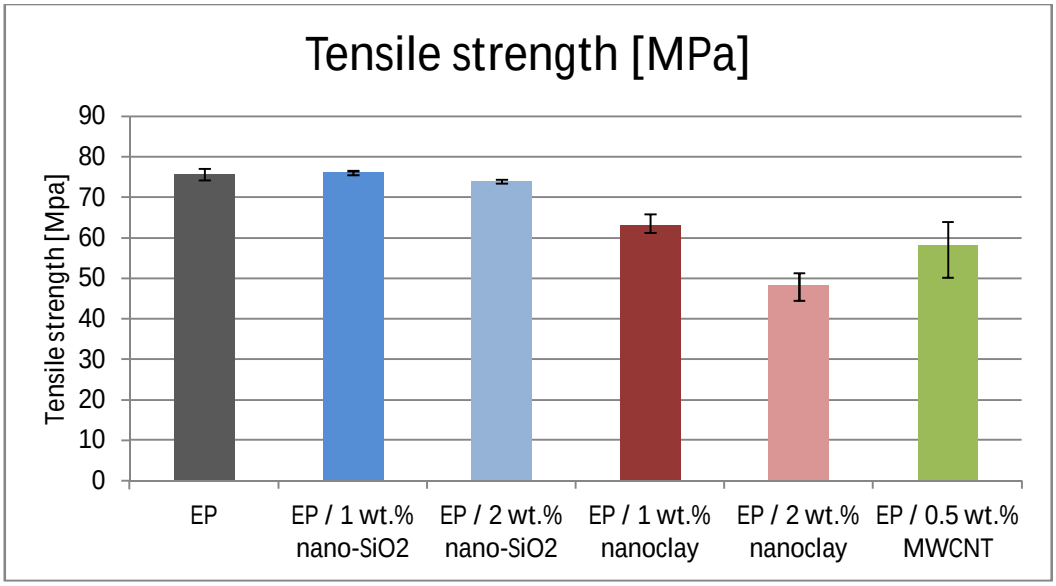

Figure 4.8. Tensile strength values

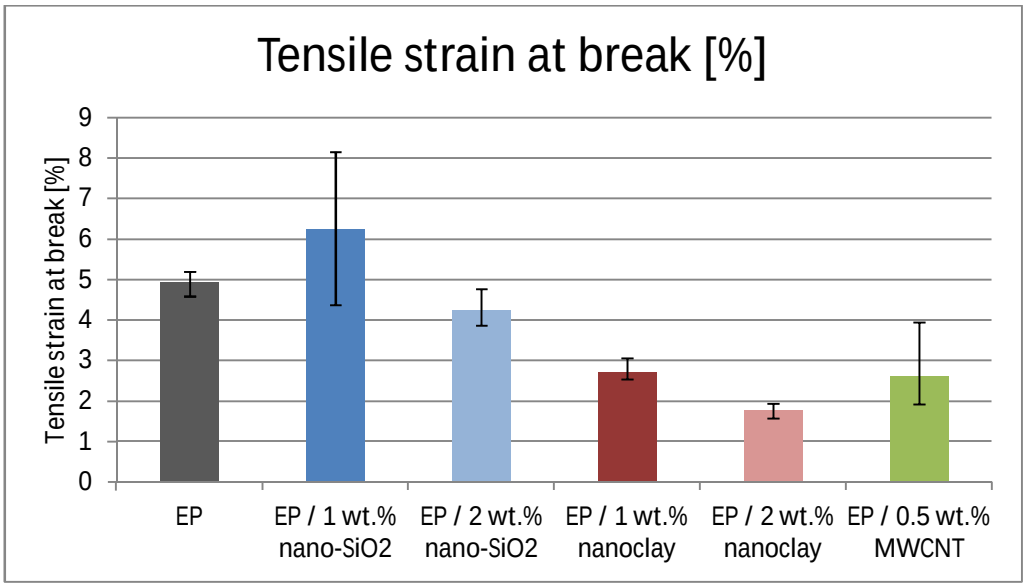

Figure 4.9. Results for the tensile strain at break

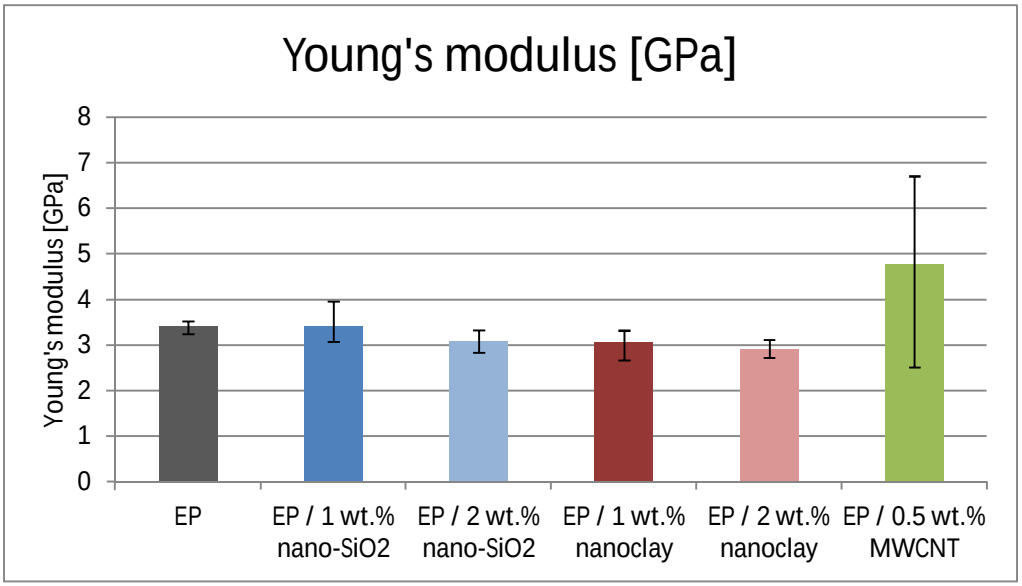

Figure 4.10. Young's modulus results

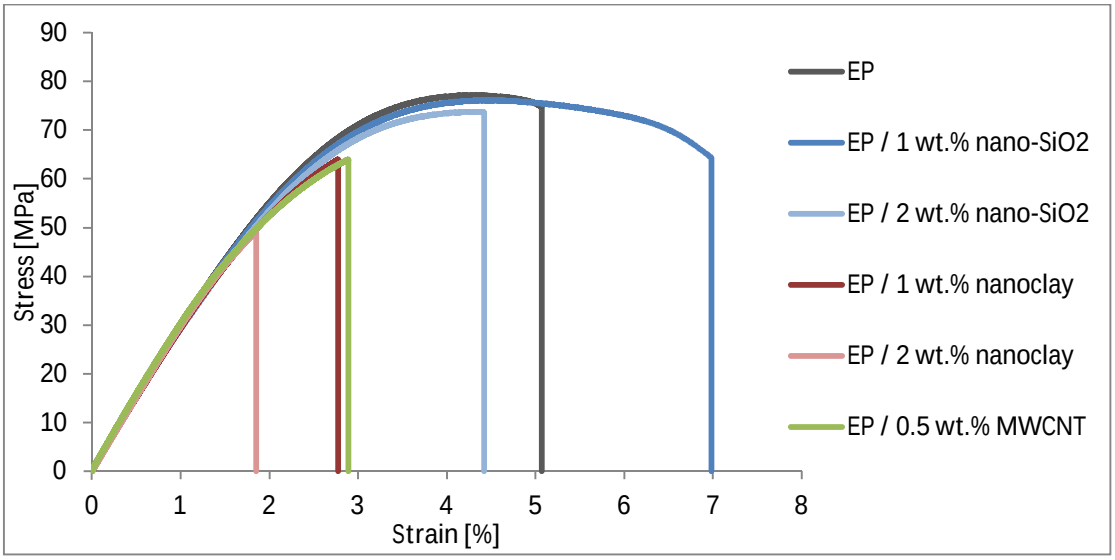

Figure 4.11. Examples of the tensile test curves (middle curve has been chosen for each material)

4.3 Fracture toughness

The dimensions of the fracture toughness samples are presented in Table 4.6 and the test results in Table 4.7. and Figures 4.12 and 4.13. All the fracture toughness curves for the tested samples can be found in Appendix 2. It can be seen that 1 and 2 wt.% of nano-SiO_2 improved the fracture toughness of epoxy 14% and 41%, respectively. Furthermore, small amount of MWCNT had marked effect on the fracture toughness of epoxy (improvement of 32%). Similar results have been obtained in the literature. Zamanian et al. [97], for example, observed the fracture toughness to increase roughly 17% with 1 wt.% of nano-SiO_2 compared to neat epoxy. Jyotishkumar et al. [41] observed the fracture toughness to increase by 38% with 0.22 wt.% of MWCNTs compared to neat epoxy. Nanoclay, on the other hand, showed poorer results with the 2 wt.% content compared to pure epoxy, which is in line with the tensile test results. The decrease of fracture toughness by nanoclay loading has been observed also by others. Lu et al. [98] observed the fracture toughness of nanoclay/epoxy nanocomposites to decrease with the increasing nanoclay content. The brittleness of the samples appeared to increase by the addition of nanoclay particles.

Table 4.6. Dimensions of the fracture toughness samples (a = crack length, W = width, B = thickness, and x = ratio a/W)

Sample	a [mm]	W [mm]	B [mm]	x
EP	3.7	7.6	4.0	0.49
EP / 1 wt.% nano-SiO_2	3.8	8.2	3.4	0.46
EP / 2 wt.% nano-SiO_2	3.8	7.9	3.1	0.48
EP / 1 wt.% nanoclay	3.7	7.9	3.8	0.47
EP / 2 wt.% nanoclay	3.7	7.6	4.1	0.49
EP / 0.5 wt.% MWCNT	3.8	8.7	4.0	0.44

Table 4.7. Fracture toughness results. Force caused by the test fixture (9 N) is added on the results.

Sample	P_{max} [N]	K_{ic} [MPa·m$^{1/2}$]
EP	65.5 ± 13.0	2.2 ± 0.5
EP / 1 wt.% nano-SiO_2	73.0 ± 13.9	2.5 ± 0.5
EP / 2 wt.% nano-SiO_2	75.7 ± 13.6	3.1 ± 0.4
EP / 1 wt.% nanoclay	73.3 ± 9.6	2.3 ± 0.2
EP / 2 wt.% nanoclay	59.0 ± 11.5	1.9 ± 0.2
EP / 0.5 wt.% MWCNT	112.7 ± 28.3	2.9 ± 0.7

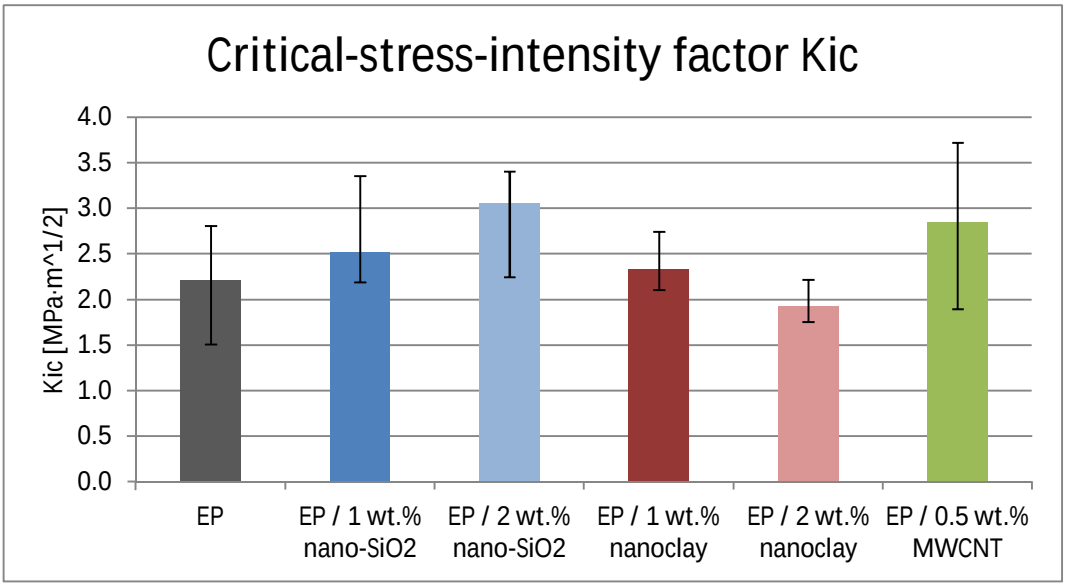

Figure 4.12. Fracture toughness results

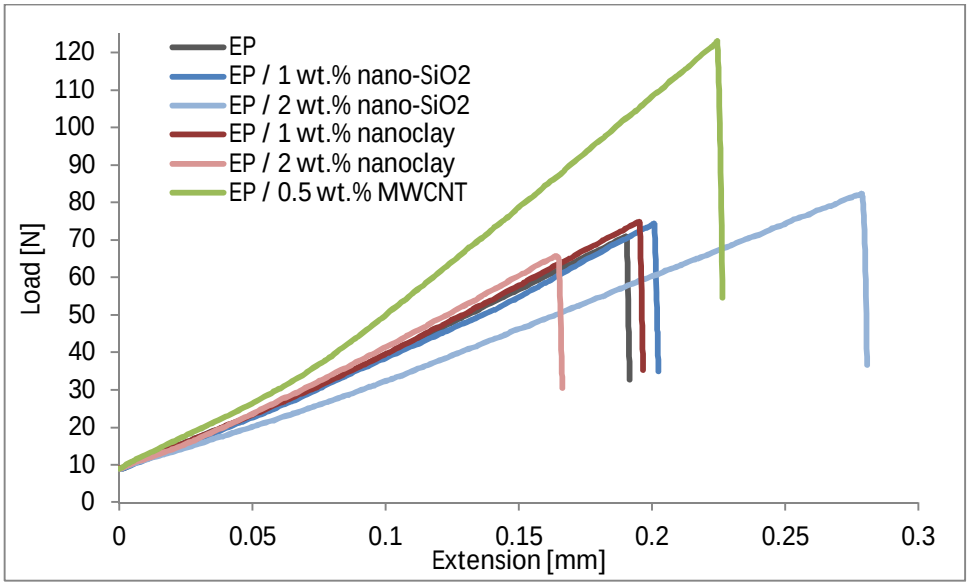

Figure 4.13. Examples of the fracture toughness curves. Middle curve has been chosen for each material (n=6). Force caused by the test fixture (9 N) is added on the results.

4.4 Differential scanning calorimetry (DSC)

Differential scanning calorimeter results have been presented in Tables 4.8 and 4.9 and Figures 4.14 - 4.17. DSC curves in Figure 4.14. show that after the T_g the samples have a slight exothermic reaction. This may indicate that some curing has occurred during the first heating. Second heating (Figure 4.15) indicate that the samples are fully cured (line is straight after T_g) [99] and because of that the T_g values are slightly shifted to higher temperatures compared to the first heating. The T_g values of the second heating with the nanofilled samples are slightly lower compared to the pure epoxy. This may be caused by the fact that nanofillers may disturb the crosslinking reaction. [100] Especially high viscosity, which was observed with the 2 wt.% of nano-SiO_2 and nanoclay and the MWCNT-sample, may reduce the available free volume to move around in the resin and hinder the orientation of the crosslinking network, resulting in decrease of T_g. [29] Similar results for the T_g have been obtained also in the literature. Thelakkadan et al. [88], for example, observed the T_g to decrease with increasing nanoclay content. The nanoclay seems to increase the curing rate which may be caused by a catalytic activity of the clay during the crosslinking reaction. The concentration of the epoxy also decreases as the filler content increases. [88] Rashmi et al. [101] observed the T_g to increase at 2 wt.% of nanoclay, but decrease at higher contents. Reason for the increase in T_g was suggested to be due to formation of a few crosslinks between the nanoclay and the epoxy matrix. The decrease of T_g might result from the failure of nanoclay particles to establish more crosslinks. [101] Zheng et al. [102] observed the T_g values of nano-SiO_2 filled nanocomposites to be just a little lower than for the pure epoxy while Abdalla et al. [103] reported similar T_g values for MWCNT-filled nanocomposite and neat epoxy. This indicated that the samples were equally cured.

Table 4.8. DSC results (heating rate 20°C/min, N_2)

	First heating			**Second heating**		
Sample	**Onset T_g [°C]**	**Mid T_g [°C]**	**Delta C_p [J/gK]**	**Onset T_g [°C]**	**Mid T_g [°C]**	**Delta C_p [J/gK]**
EP	75	79	0.34	85	94	0.37
EP / 1 wt.% nano-SiO_2	78	81	0.40	84	92	0.35
EP / 2 wt.% nano-SiO_2	76	79	0.42	83	91	0.37
EP / 1 wt.% nanoclay	76	78	0.30	81	90	0.35
EP / 2 wt.% nanoclay	73	80	0.55	84	93	0.36
EP / 0.5 wt.% MWCNT	74	78	0.50	82	90	0.35

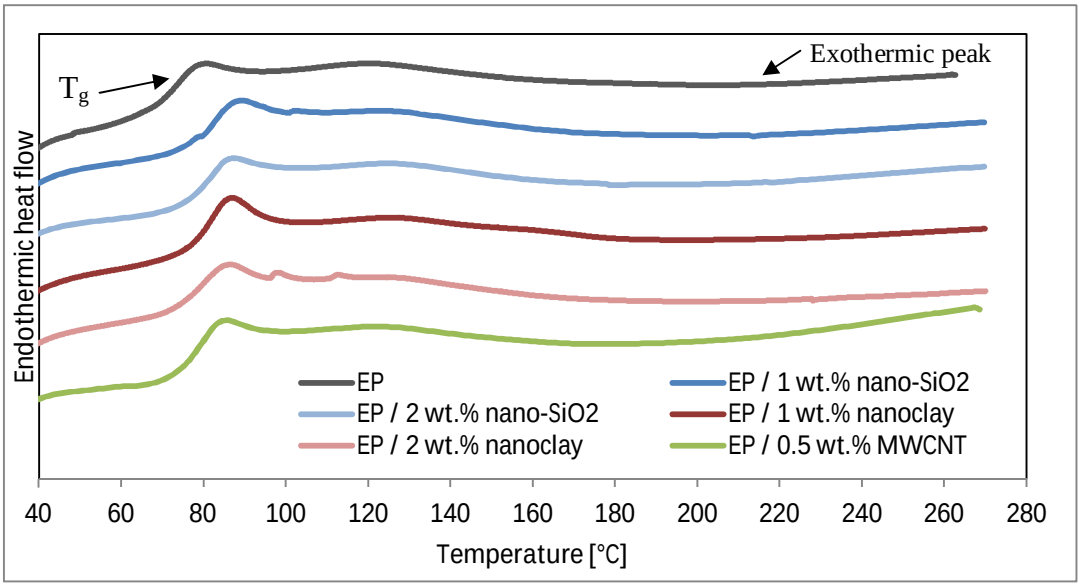

Figure 4.14. First heating curves (heating rate 20°C/min, N_2)

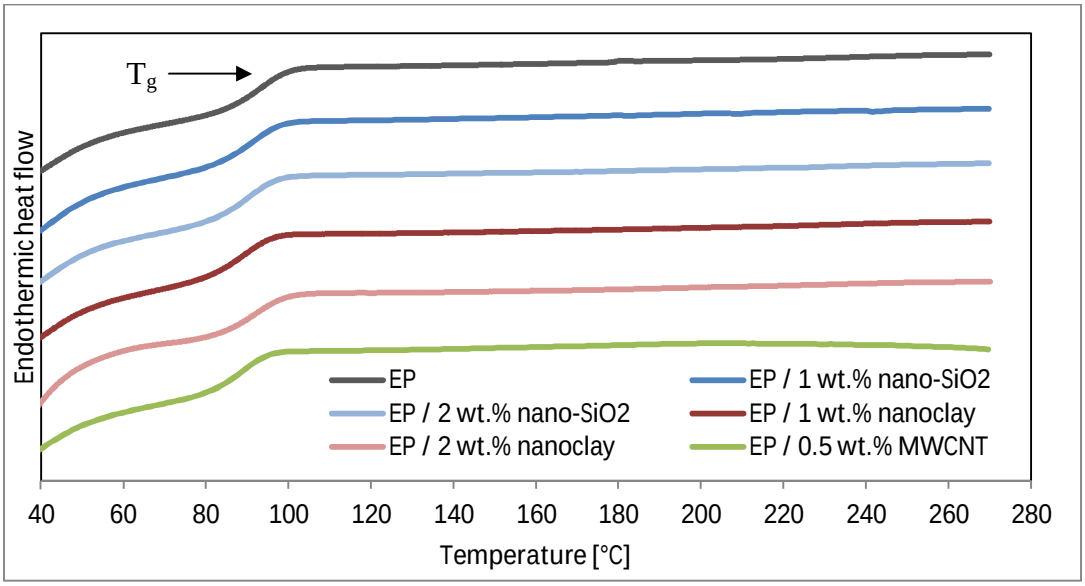

Figure 4.15. Second heating curves (heating rate 20°C/min, N_2) with heating rate of 20°C/min at nitrogen atmosphere

DSC-measurements discussed above were done only once for every sample. Furthermore, secondary measurements were done for pure epoxy and the sample EP/0.5 wt.% of MWCNT (Table 4.9 and Figures 4.16 and 4.17). The samples were from the same batch as in the previous measurements, but there was about two month difference between the measurements. However, similar results were obtained in both measurements.

Table 4.9. Results from the first heating

Sample	First heating			Second heating		
	Onset T_g [°C]	Mid T_g [°C]	Delta C_p [J/gK]	Onset T_g [°C]	Mid T_g [°C]	Delta C_p [J/gK]
EP / Sample 1	74.9	78.7	0.34	85.3	94.0	0.37
EP / Sample 2	73.6	81.2	0.54	82.4	91.2	0.37
EP / 0.5 wt.% MWCNT / Sample 1	74.3	78.1	0.50	81.8	89.5	0.35
EP / 0.5 wt.% MWCNT / Sample 2	72.6	77.3	0.59	79.0	86.7	0.39

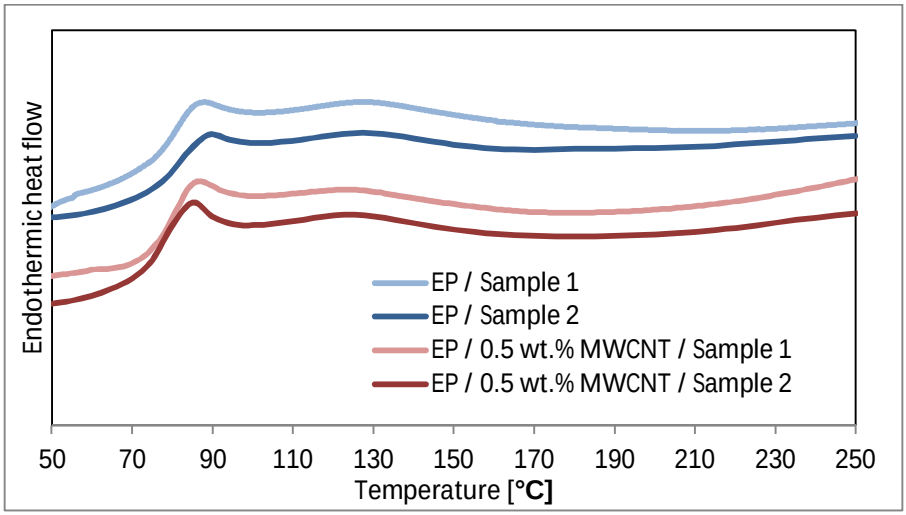

Figure 4.16. First heating curves (heating rate 20°C/min, N_2)

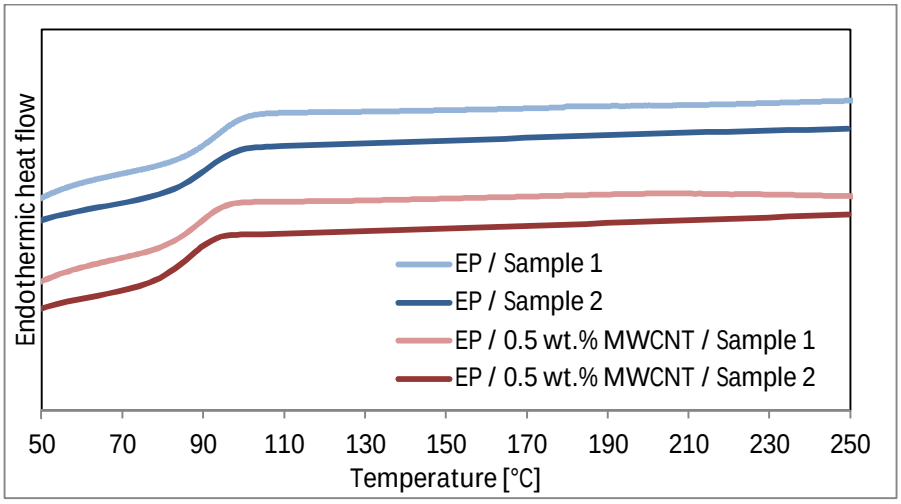

Figure 4.17. Second heating curves (heating rate 20°C/min, N_2)

4.5 Dynamic mechanical analysis (DMA)

Results from the dynamic mechanical analysis are presented in Table 4.10. and Figures 4.18 - 4.20. Storage modulus values were higher than the loss modulus, which is indicative of an elastic behaviour of the samples. [104] Samples with nano-SiO_2 gave higher elastic modulus results than pure epoxy, while nanoclay and MWCNT-filled samples gave lower results compared to pure epoxy. The tan δ values for nanofilled samples are lower (except EP/2 wt.% of nano-SiO_2 that was the same) than for pure epoxy. Nanofillers often lead to decrease of tan δ because of weak interaction between the filler and the matrix. [15]

Table 4.10. DMA results (heating rate of 2°C/min, N_2)

	Peak E'		Peak E''		Peak Tan δ	
Sample	**°C**	**MPa**	**°C**	**MPa**	**°C**	
EP	74.7	1500	77.6	320	88	1.17
EP / 1 wt.% nano-SiO_2	72.9	2200	75.3	260	88	1.09
EP / 2 wt.% nano-SiO_2	74.4	2900	77.7	410	87	1.17
EP / 1 wt.% nanoclay	74.7	3000	77.9	450	87	1.16
EP / 2 wt.% nanoclay	75.1	1200	76.7	260	89	1.07
EP / 0.5 wt.% MWCNT	72.7	1800	78.1	330	88	1.15

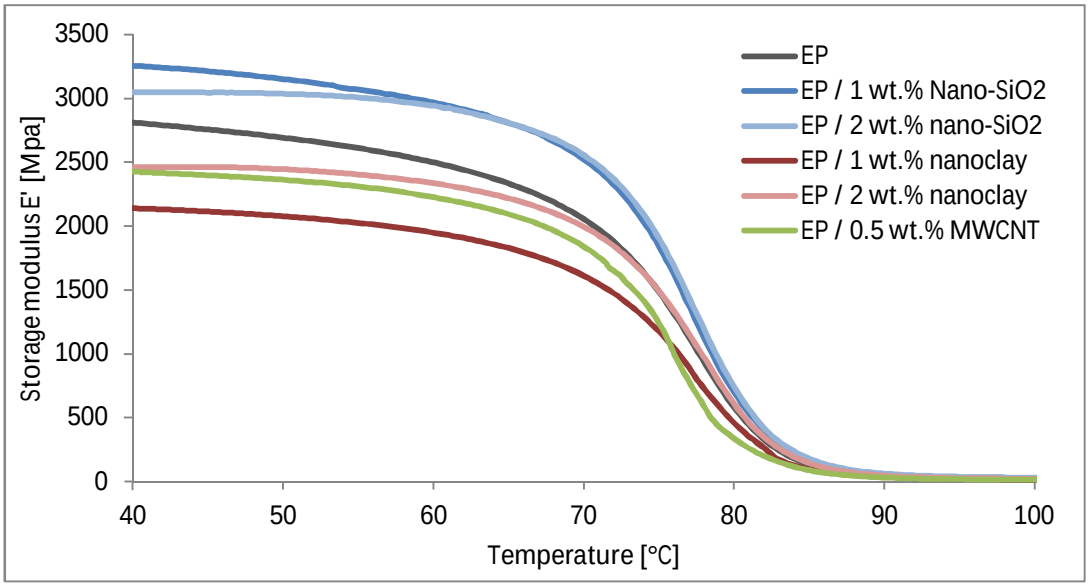

Figure 4.18. Storage modulus of the samples (heating rate of 2°C/min, N_2)

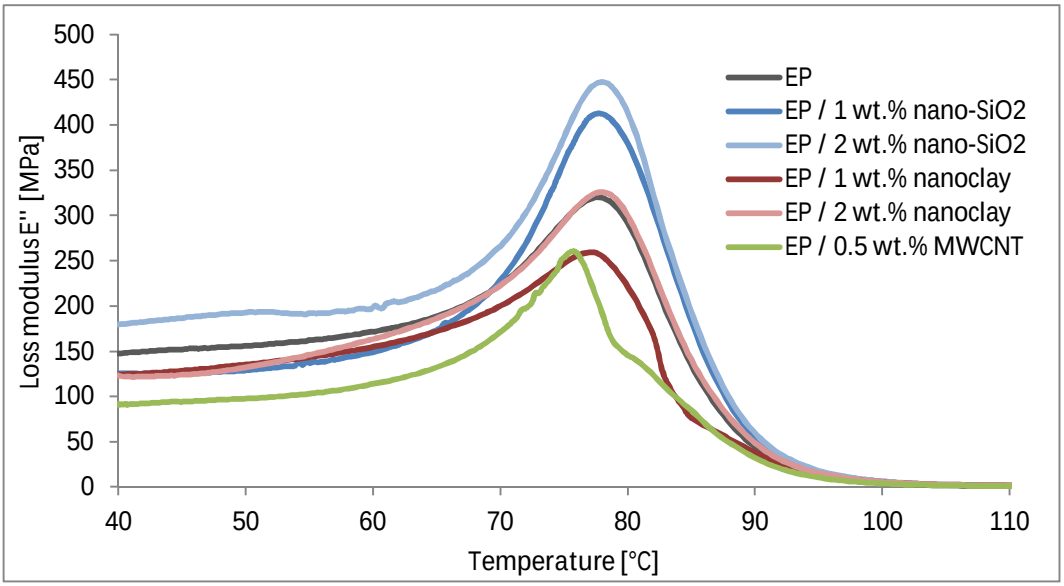

Figure 4.19. Loss modulus of the samples (heating rate of 2°C/min, N_2)

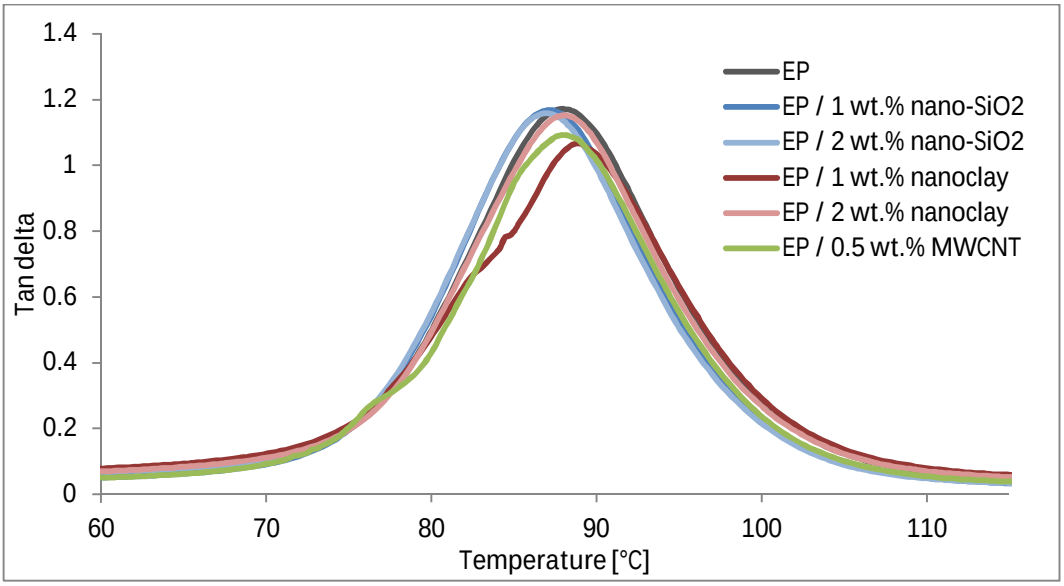

Figure 4.20. Tan delta of the samples (heating rate of 2°C/min, N_2)

4.6 Thermogravimetry (TGA)

Results of the thermogravimetric analysis are presented in Table 4.11. and Figures 4.21 - 4.24. There are no significant differences between the thermal degradation behaviour of the prepared samples. The filler addition does not change the initial degradation temperature, which is roughly 300°C for all the samples. Also, the degradation occurs in a similar manner for all the samples. The nanofilled samples (except EP/2 wt.% of nanoclay) had 1 - 6°C and 1 - 2°C lower degradation temperature than pure epoxy at 5 % and 10 % weight loss (Table 4.11.), respectively. The sample EP/2 wt.% of nanoclay

had 3°C higher degradation temperature than epoxy at 10% weight loss. Differences between the nanofilled samples are clearest between temperatures of 400°C and 700°C.

Minor changes in the degradation temperature have occurred also for others. According to Yu et al. [105] the addition of 4 wt.% of unmodified nano-SiO_2 on epoxy resin had a slight decrease on the thermal properties. The onset decomposing temperature decreased from 368.4°C (for pure epoxy) to 352.3°C (SiO_2-filled) and at 50% weight loss the temperature decreased from 439.2°C to 433.4°C. Nano-SiO_2 has a very high thermal stability due to the high Si – O bond energy, but the high tendency of the SiO_2 particles to agglomerate makes the manufacturing of a stable nanocomposite with improved thermal properties challenging. [105] For the nanoclay, Rashimi et al. [101] observed that it had no significant influence on the degradation temperature of epoxy filled with 2-7 wt.% of nanoclay. Miyagawa et al. [106], on the other hand, observed the thermal stability to slightly improve with nanoclay loading up to 5 wt.%. Hosur et al. [29] observed that 0.4 wt.% of MWCNT increased the decomposition temperature of epoxy by 12°C (in nitrogen atmosphere). The lack of significant improvement was suggested to be due to the fact that at high temperatures the molecular chains move freely and the interactions between epoxy and MWCNT become weak. [29]

Table 4.11. Temperature at the weight loss of 5 wt.% and 10 wt.%

Sample	**$T_{5\%}$ [°C]**	**$T_{10\%}$ [°C]**
EP	332.4	340.6
EP / 1 wt.% nano-SiO_2	326.6	339.2
EP / 2 wt.% nano-SiO_2	328.8	339.0
EP / 1 wt.% nanoclay	326.0	338.8
EP / 2 wt.% nanoclay	334.7	343.1
EP / 0.5 wt.% MWCNT	331.1	339.1

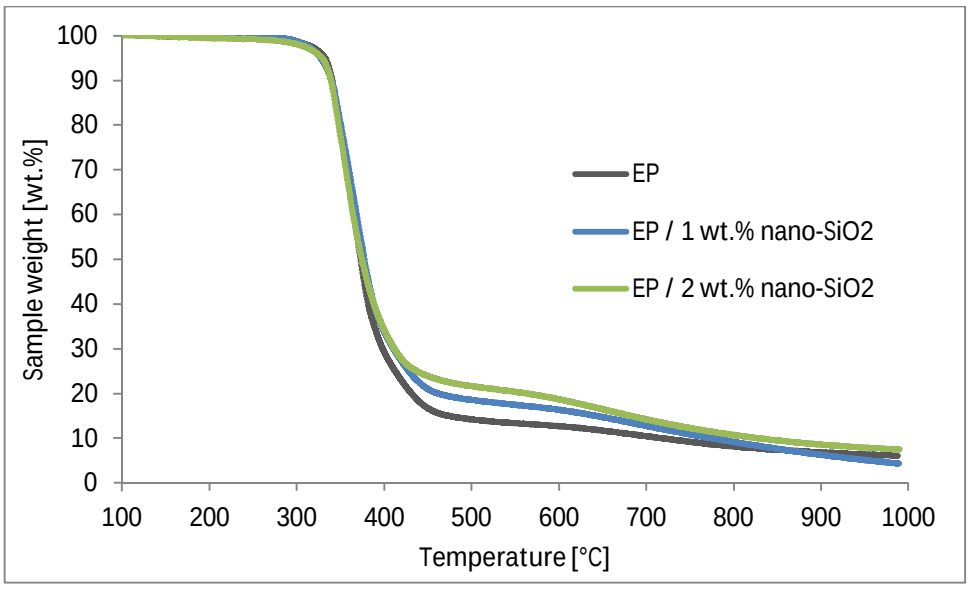

Figure 4.21. TGA curves of nano-SiO_2 samples (heating rate of 10°C/min, N_2)

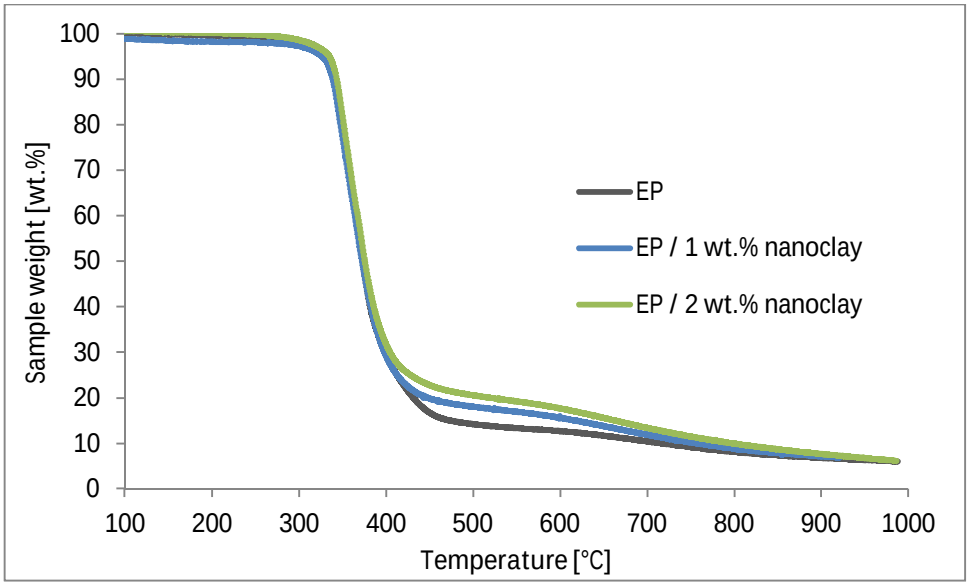

Figure 4.22. TGA curves of nanoclay samples (heating rate of 10°C/min, N_2)

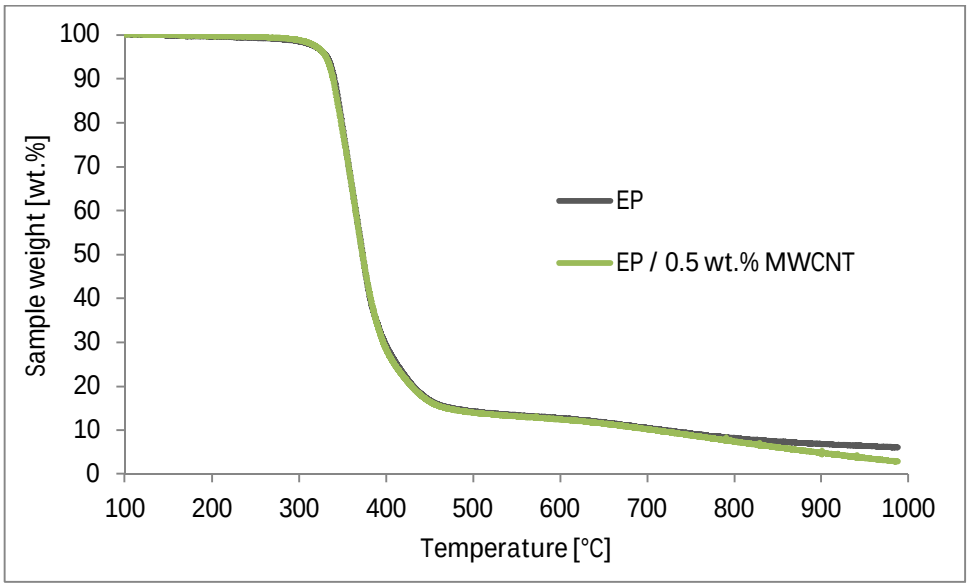

Figure 4.23. TGA-curve of MWCNT sample (heating rate of 10°C/min, N_2)

Because the thermogravimetric analysis gave abnormal results for the MWCNT-sample (the final weight was lower for the MWCNT-sample than for pure epoxy), the analysis was conducted also under oxygen atmosphere. The results are presented in Figure 4.24. The degradation temperature for 5 wt.% weight loss decreased from 320.8°C (for pure epoxy) to 296.1°C (for EP/0.5 wt.% MWCNT), and for 10 wt.% weight loss from 337.7°C to 330.7°C. Therefore, improvement in initial degradation temperatures was not detected in oxygen atmosphere either.

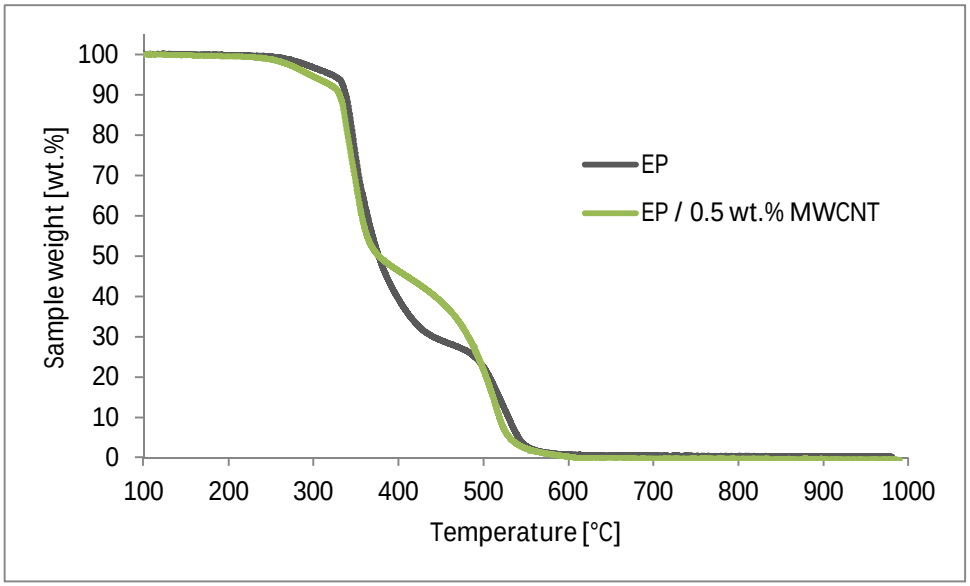

Figure 4.24. TGA-curve of MWCNT sample (heating rate of 10°C/min, O_2)

4.7 Scanning electron microscopy (SEM)

The surface structures of the fractured tensile test bars were studied using Philips XL scanning electron microscope (Figures 4.25 and 4.26 and Appendix 3). Presence of nanoparticles can be seen as the roughness on the fracture surface of the nanofilled samples (4.25.b-f) compared to smooth surface of the pure epoxy (4.25.a). [107] The smooth surface is indicative of brittle failure. The rough surface of the nanofilled samples is assumed to be due to the resistance of crack propagation and an increased tortuous path of crack propagation, which increases the strength to failure. [95] Stacks of clay particles can be seen in Figures 4.26.d and 4.26.e, and MWCNT agglomerates are pointed with an arrow in Figure 4.26.f.

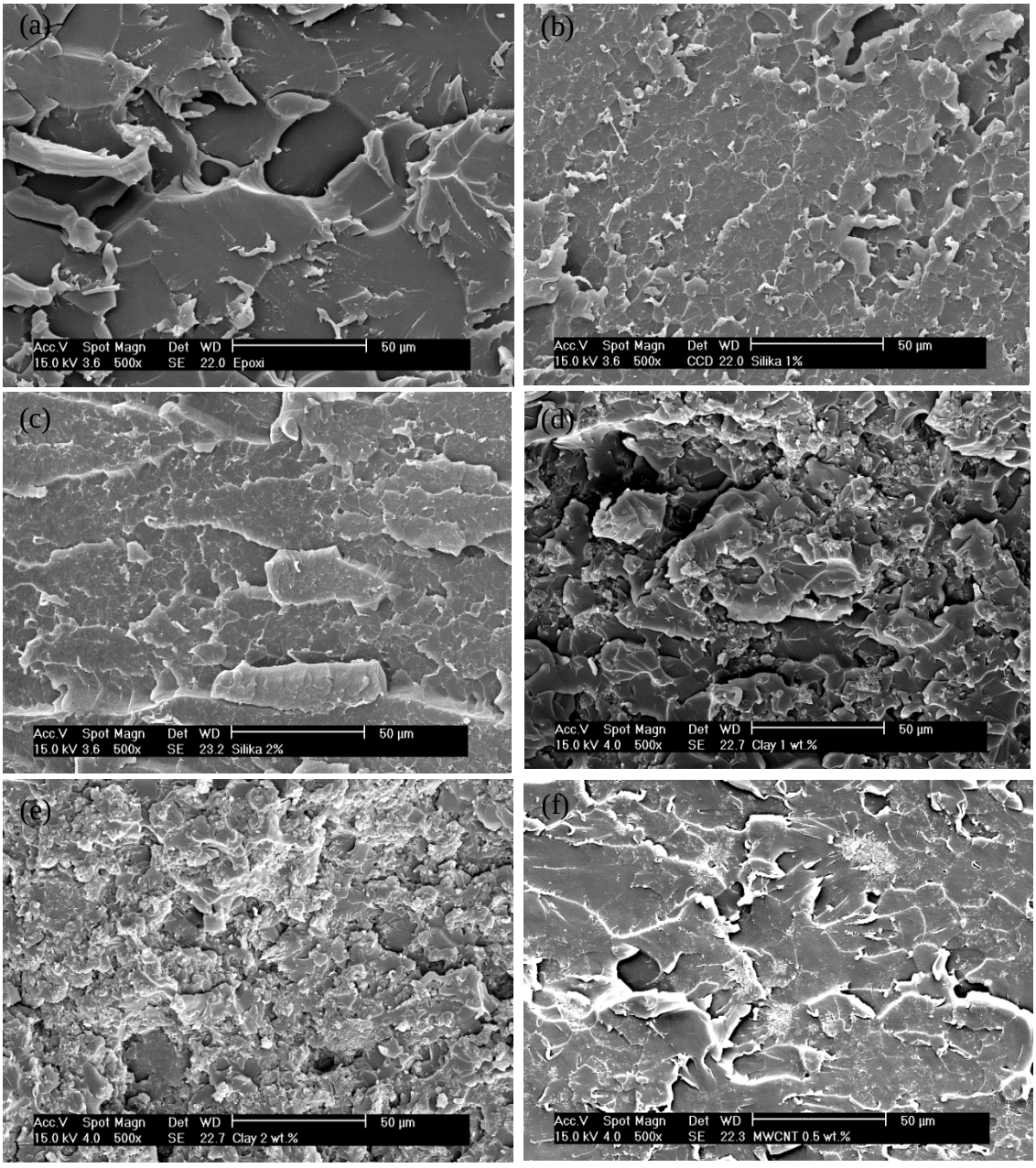

Figure 4.25. SEM images of (a) pure epoxy (b) EP / 1 wt.% SiO_2 (c) EP / 2 wt.% SiO_2 (d) EP / 1 wt.% nanoclay (e) EP / 2 wt.% nanoclay and (f) EP / 0.5 wt.% MWCNT (magnification of 500)

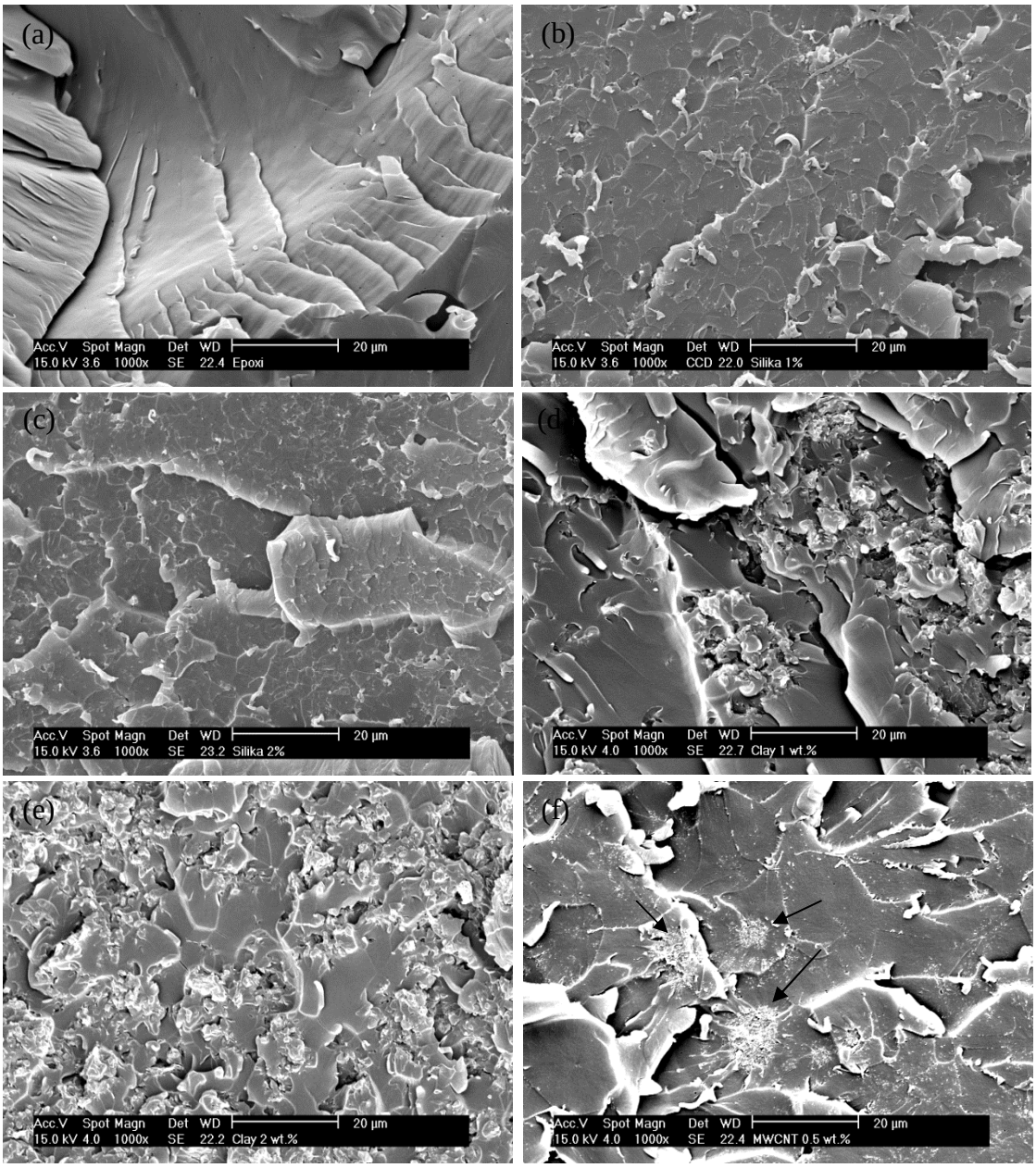

Figure 4.26. SEM images of (a) pure epoxy (b) EP / 1 wt.% SiO_2 (c) EP / 2 wt.% SiO_2 (d) EP / 1 wt.% nanoclay (e) EP / 2 wt.% nanoclay and (f) EP / 0.5 wt.% MWCNT (magnification of 1000)

4.8 Field emission scanning electron microscopy (FESEM)

Dispersion of the nanoparticles and their adhesion to matrix were observed successively using field emission scanning electron microscope (Zeiss UltraPlus). Pure epoxy shows smooth surfaces compared to the nanoparticle filled samples as was seen in previous chapter and in Figure 4.27.a. FESEM images of the nanofilled samples (Figures 4.27 and 4.28 and Appendix 4 and 5) indicate that small air bubbles and agglomerated nanoparticles are present in the structures. FESEM images of the samples with nano-SiO_2 (Figure 4.27.b and c) indicate that the nanosized particles form agglomerates with a size of several micrometers. However, individual particles could also be seen. There were also some small air bubbles left in the structure. The measured diameter of silica particles was generally between 30-60 nm, which is slightly higher than the averaged diameter value reported in the datasheet (12 nm). That may be due to the epoxy around the particles. Adhesion between epoxy and nano-SiO_2 particles seems to be good, because the particles are left attached on the matrix surface after fracture, and they are well covered with the resin (no large voids around the particles). Large nanoclay clusters (with a size of 1-5µm) were also seen in both nanoclay samples (Figures 4.27.d and e). The agglomerates seem to indicate a lack of clay exfoliation. The MWCNT-sample also contained agglomerates (a size of 40µm in the figure f in Appendix 4). Nanotube structure can be clearly seen in Figure 4.28.f. Very small air bubbles can be seen with pure epoxy and the nano-SiO_2 samples in Appendix 5 in Figures a-c.

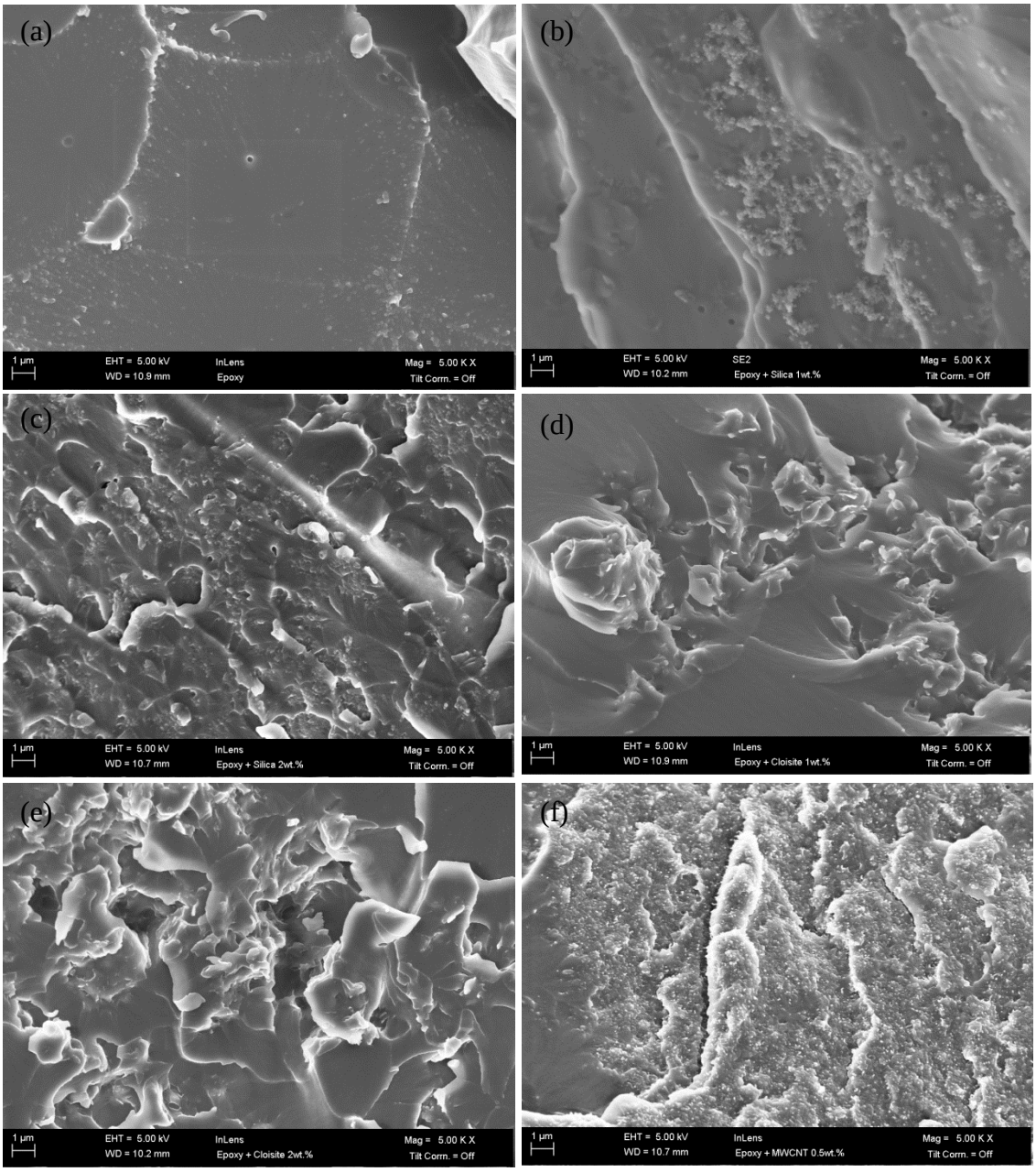

Figure 4.27. FESEM images of (a) pure epoxy (b) EP / 1 wt.% SiO_2 (c) EP / 2 wt.% SiO_2 (d) EP / 1 wt.% nanoclay (e) EP / 2 wt.% nanoclay and (f) EP / 0.5 wt.% MWCNT (magnification of 5000)

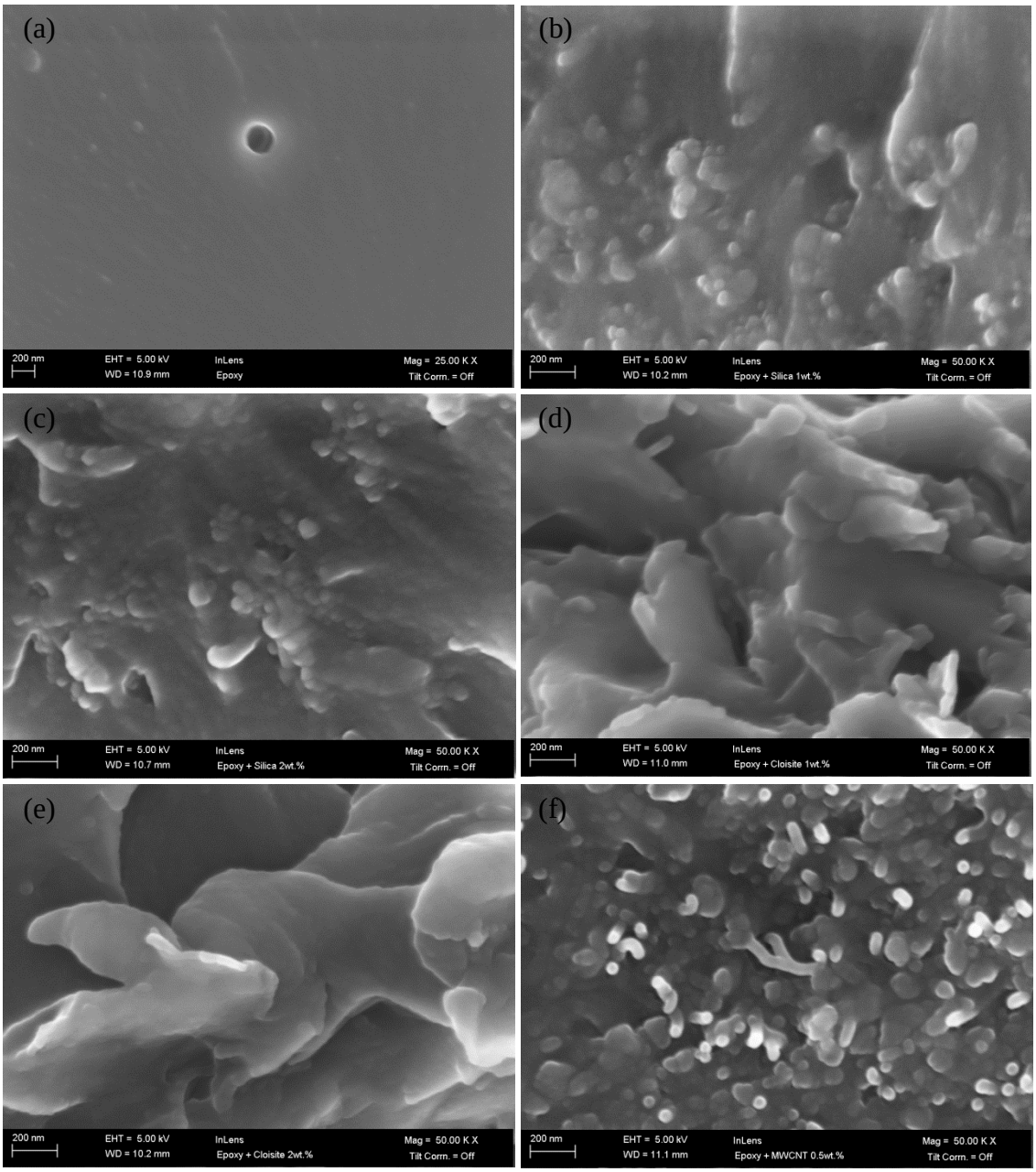

Figure 4.28. FESEM images of (a) pure epoxy (b) EP / 1 wt.% SiO_2 (c) EP / 2 wt.% SiO_2 (d) EP / 1 wt.% nanoclay (e) EP / 2 wt.% nanoclay and (f) EP / 0.5 wt.% MWCNT (magnification of 50 000)

4.9 Electrical conductivity

Electrical conductivity measurements (Table 4.12.) indicate that the surface resistivity is markedly decreased with the addition of 0.5 wt.% of MWCNT compared to pure epoxy.

Table 4.12. Electrical conductivity measurements

Sample	**Surface resistivity [Ω]**	**Volume resistivity [Ωcm]**
EP	$1.41 \cdot 10^{14}$	-
EP / 0.5 wt.% MWCNT	$3.35 \cdot 10^{6}$	$1.56 \cdot 10^{13}$

Metals have a resistivity value around 10^{-8} Ω and insulators around 10^{16} Ω. [108] The measured surface resistivity of the MWCNT-sample can be compared with the literature value: Wladyka-Przybylak et al. [109] have measured a surface resistivity value of $1.78 \cdot 10^{7}$ Ω with a MWCNT concentration of 0.5 wt.% in epoxy matrix.

5 CONCLUSIONS

Nanocomposites offer new prospects for the polymer industry since key properties, such as mechanical and thermal properties can be improved with only a small filler amount. However, the processing methods are still under investigation due to the challenges in the processing of nanoscale fillers. Nanoparticles have a high tendency to agglomerate and the improved properties cannot be achieved if the dispersion is poor.

In this study, nanocomposites based on epoxy resin were manufactured and characterized using three different nanofillers: nano-SiO_2, nanoclay and multi-walled carbon nanotubes. The concentrations of nano-SiO_2 and nanoclay in the matrix were 1 and 2 wt.% while the MWCNT-sample had a filler content of 0.5 wt.%. Nanofillers were mixed with high shear mixer under vacuum. Viscosity of the nanofilled resin was measured and the final samples were tested with tensile test, fracture toughness analysis and thermal analysis methods. The dispersion and adhesion of the nanofillers were also investigated with scanning electron microscopes.

During nanocomposite preparation, some difficulties were observed. Firstly, a large amount of air bubbles were formed on the resin during the nanofiller mixing and thus all mixtures had to be vacuumed prior to the hardener addition. Especially, mixing of samples with 2 wt.% of nano-SiO_2, 2 wt.% of nanoclay and 0.5 wt.% of MWCNT created high amount of air bubbles and the high viscosity of the mixtures made their removal extremely slow. Therefore, during the removal process, the filler particles may have started to reagglomerate. Also, final samples with 2 wt.% of nano-SiO_2 and 0.5 wt.% of MWCNT contained visible air bubbles, which may have affected the tensile test and fracture toughness results. The preparation of higher filler contents was restricted by the viscosity increase. Epoxy with only 0.5 wt.% of MWCNT had already a very high viscosity, which left the samples slightly uneven. Epoxy with 4 wt.% of nano-SiO_2 could not be prepared because the high viscosity prevented proper mixing.

The only distinct improvement in tensile properties was in tensile strain at break with 1 wt.% of nano-SiO_2 (improvement compared to neat epoxy was 27%) and in Young's modulus with 0.5 wt.% of MWCNT (improvement compared to neat epoxy was 41%). Fracture toughness was slightly improved with 1 and 2 wt.% of nano-SiO_2 and with 0.5 wt.% of MWCNT. Nanoclay samples gave poor results with both tests, which may be due to the lack of nanoclay compatibility into the epoxy resin which resulted in stacking of clay platelets. Furthermore, adhesion between clay particles and epoxy was poor. SEM and FESEM images of the samples indicate that the nanofilled samples contained agglomerates with a size of several micrometers. The images also revealed some very small air bubbles in the matrix. These factors may have affected on the tensile test and fracture toughness results.

According to the results, it can be concluded that high shear mixing is not enough to create proper dispersion for the nanoparticles. Therefore, other methods, such as ultrasonication or solvents, should be used in addition to the high shear mixing. Formation of air bubbles during the processing needs to be minimized using, for

example, more effective vacuum. Right nanofiller content and proper surface treatment according to the matrix polymer should also improve the interaction between the matrix and the nanoparticles and the properties of the formed composite. All in all, further research is needed to improve the processing methods to make the nanocomposite preparation more effective and to achieve the desired properties.

REFERENCES

1. Kotsilkova, R. Thermoset nanocomposites for engineering applications. Smithers Rapra Technology Limited, 2007. 326 p.
2. Gogotsi, Y. Nanomaterials Handbook. CRC Press, 2006. 780 p.
3. Sperling, L. H. Introduction to Physical Polymer Science. John Wiley & Sons, 2005. 845 p.
4. Zander, N. E. Epoxy Nano-Reinforced Composite Systems. Army Research Laboratory, Dynamic Science, Inc., 2008. 20 p.
5. Ji, G., Li, G. Effects of nanoclay morphology on the mechanical, thermal, and fire-retardant properties of vinyl ester based nanocomposite. Materials Science and Engineering A 498(2008)1-2, pp. 327-334
6. El-Sonbati, A. Z. Thermoplastic - Composite Materials. InTech, 2012. 146 p.
7. Shi, X., Wang, J., Jiang, B., Yang, Y. Influence of nanofiller dimensionality on the crystallization behavior of HDPE/carbon nanocomposites. Journal of Applied Polymer Science 128(2013)6, pp. 3609-3618
8. Pramanik, M., Acharya, H., Srivastava, S. K. Exertion of inhibiting effect by aluminosilicate layers on swelling of solution blended EVA/clay nanocomposite. Macromolecular Materials and Engineering 289(2004)6, pp. 562-567
9. Wu, T., Ke, Y. The adsorption and thermal behaviors of PET-SiO_2 nanocomposite films. Polymer Degradation and Stability 91(2006)9, pp. 2205-2212
10. Gupta, R. K., Kennel, E., Kim, K-J. Polymer Nanocomposites Handbook. CRC Press, 2009. 566 p.
11. Periadurai, T., Vijayakumar, C.T., Balasubramanian, M. Thermal decomposition and flame retardant behaviour of SiO_2-phenolic nanocomposite. Journal of Analytical and Applied Pyrolysis 89(2010)2, pp. 244-249
12. Wang, X., Jin, J., Song, M. Cyanate ester resin/graphene nanocomposite: Curing dynamics and network formation. European Polymer Journal 48(2012)6, pp. 1034-1041
13. Akhlaghi, S., Kalaee, M., Jowdar, E., Nouri, A., Mazinani, S., Afshari, M., Famili, M. N., Amini, N., Behrouz, T. Simultaneous study of cure kinetics and rheology of montmorillonite/vinyl ester resin nanocomposites. Polymer for Advanced Technologies 23(2012)3, pp. 534-544
14. Thomas, S., Stephen, R. Rubber Nanocomposites. Wiley, 2007. 705 p.
15. Zhao, X-Y., Xiang, P., Tian, M., Fong, H., Jin, R., Zhang, L-Q. Nitrile butadiene rubber/hindered phenol nanocomposites with improved strength and high damping performance. Polymer 48(2007)20, pp. 6056-6063
16. Tarrío-Saavedra, J., López-Beceiro, J., Naya, S., Gracia, C., Artiaga, R. Controversial effects on fumed silica on the curing and thermomechanical properties of epoxy composites. eXPRESS Polymer Letters 4(2010)6, pp. 382-395

17. Friedrich, K., Fakirov, S., Zhang, Z. Polymer composites, From nano- to macro-scale. Springer, 2005. 367 p.
18. Bhattacharya, S. N., Kamal, M. R., Gupta, R. K. Polymeric Nanocomposites – Theory and Practice. Hanser Publishers, 2008. 383 p.
19. Gao, F. Clay/polymer composites: the story. Materials Today 7(2004)11, pp. 50-55
20. Hussain, F., Hojjati, M., Okamoto, M., Gogra, R. E. Review article: Polymer-matrix nanocomposites, processing, manufacturing, and application: An overview. Journal of Composite Materials 40(2006)17, pp. 1511-1575
21. Wypych, G. Handbook of Fillers. 3rd edition. ChemTec Publishing, 2010. 840 p.
22. Rothon, R.N. Particulate-filled polymer composites. Smithers Rapra Technology, 2003. 571 p.
23. Ma, P-C., Kim, J-K. Carbon nanotubes for polymer reinforcement. Taylor and Francis Group, 2011. 224 p.
24. Shenoy, A. V. Rheology of filled polymer systems. Kluwer academic publishers, 1999. 475 p.
25. Rauwendaal, C. Polymer Mixing: A Self-Study Guide. HanserGardner Publications, 1998. 255 p.
26. Martone, A., Formicola, C., Piscitelli, F., Lavorgna, M., Zarrelli, M., Antonucci, V., Giordano, M. Thermo-mechanical characterization of epoxy nanocomposites with different carbon nanotube distributions obtained by solvent aided and direct mixing. eXPRESS Polymer Letters 6(2012)7, pp. 520-531
27. Benedito, A., Buezas, I., Giménez, E., Galindo, B., Ortega, A. Dispersion and characterization of thermoplastic polyurethane/multiwalled carbon nanotubes by melt mixing. Journal of Applied Polymer Science 122(2011)6, pp. 3745-3751
28. Cho, B-M., Kim, G-H. Effect of processing parameters on the surface resistivity of acrylonitrile-butadiene rubber/multiwalled carbon nanotube nanocomposites. Journal of Applied Polymer Science 116(2010)1, pp. 555-561
29. Hosur, M., Barua, R., Zainuddin, S., Kumar, A., Trovillion, J., Jeelani, S. Effect of processing techniques on the performance of epoxy/MWCNT nanocomposites. Journal of Applied Polymer Science 127(2013)6 pp. 4211-4224
30. Innovative dispersion systems for laboratory and pilot plant, Manufacturer's guide, VMA-Getzmann GMBH, Verfahrenstechnik, Dispermat, Torusmill
31. Introduction to dispersion technology with the DISPERMAT Dissolver. Accessed on 28.2.2013. Available at: http://www.vma-getzmann.com/english/dispersion_know-how/dispersion_with_dissolvers/dispersion_with_dissolvers_0_935_987_1809.html
32. Callister, W. D., Jr. Materials Science and Engineering: An Introduction. 7th Edition. John Wiley & Sons, 2007. 721 p.

33. Ratna, D. Handbook of Thermoset Resins. Smithers Rapra Technology, 2009. 410 p.
34. Systems, Sp. Guide to Composites. Accessed on 2.2.2013. Available at: http://www.aerosol.co.il/files/article/1315851198c98Ug.pdf
35. Tucker, N., Lindsey, K. An Introduction to Automotive Composites. Smithers Rapra Publishing, 2002. 196 p.
36. Boogh, L., Mezzenga, R.. 2.19 – Processing principles for thermoset composites. Polymer Matrix Composites 2(2002), pp. 671-699
37. Mulligan, D. Cure monitoring for composites and adhesives. Smithers Rapra Publishing, 2003. 124 p.
38. Thermoplastic vs Thermoset Resins. About.com, Composites / Plastics. Accessed on 15.1.2013. Available at: http://composite.about.com/od/aboutcompositesplastics/a/Thermoplastic-Vs-Thermoset-Resins.htm
39. Kornmann, X. Synthesis and Characterization of thermoset-clay nanocomposites, Introduction of the Licentiate thesis. 1999. Luleå University of Technology, Division of polymer engineering. 29 p.
40. Mai, Y-W., Yu, Z-Z. Polymer Nanocomposites. Woodhead Publishing, 2006. 594 p.
41. Jyotishkumar, P., Logakis, E., George, S. M., Pionteck, J., Häussler, L., HaBler, R., Pissis, P., Thomas, S. Preparation and properties of multiwalled carbon nanotube/epoxy-amine composites. Journal of Applied Polymer Science 127(2013)4, pp. 3063-3073
42. Hsieh, T. H., Kinloch, A. J., Taylor, A. C., Sprenger, S. The effect of silica nanoparticles and carbon nanotubes on the toughness of a thermosetting epoxy polymer. Journal of Applied Polymer Science 119(2011)4, pp. 2135-2142
43. Zou, H., Wu, S., Shen, J. Polymer/silica nanocomposites: Preparation, characterization, properties, and applications. Chemical Reviews 108(2008)9, pp. 3893-3957
44. Alexandre, M., Dubois, P. Polymer-layered silicate nanocomposites: preparation, properties and uses of a new class of materials. Materials Science and Engineering 28(2000)1-2, pp. 1-63
45. Mallick, P. K. Fiber-Reinforced Composites; materials, manufacturing, and design. Third Edition. CRC Press, 2008. 619 p.
46. Oh, T-K., Hassan, M., Beatty, C., El-Shall, H. The effect of shear forces on the microstructure and mechanical properties of epoxy-clay nanocomposites. Journal of Applied Polymer Science 100(2006)5, pp. 3465-3473
47. Carbon nanotubes, AccessScience. Accessed on 30.1.2013. Available at: http://www.accessscience.com/content/Carbon-nanotubes/800630
48. Thostenson, E. T., Ren, Z., Chou, T-W. Advances in the science and technology of carbon nanotubes and their composites: a review. Composites Science and Technology 61(2001)13, pp. 1899-1921

49. Duksh, Y. S., Kaushik, B. K., Sarkar, S., Singh, R.. Performance comparison of carbon nanotube, nickel silicide nanowire and copper VLSI interconnects. Journal of Engineering, Design and Technology 8(2010)3, pp. 334-353
50. Daniel, S., Rao, T. P., Rao, K. S., Rani, S. U., Naidu, G.R.K., Lee, H-Y., Kawai, T. A review of DNA functionalized/grafted carbon nanotubes and their characterization. Sensors and Actuators B 122(2007)2, pp. 672-682
51. Coleman, J. N., Khan, U, Gun'ko, Y. K. Mechanical reinforcement of polymers using carbon nanotubes. Advanced materials 18(2006)6, pp. 689-706
52. Xie, X-L., Mai, Y-W., Zhou, X-P. Dispersion and alignment of carbon nanotubes in polymer matrix: A review. Materials Science and Engineering R 49(2005)4, pp. 89-112
53. Deng, C.F., Wang, D.Z., Zhang, X.X., Li, A.B. Processing and properties of carbon nanotubes reinforced aluminum composites. Materials Science and Engineering A 444(2007)1-2, pp. 138-145
54. Sun, L., Warren, G. L., Sue, H-J. Partially cured epoxy/SWCNT thin films for the reinforcement of vacuum-assisted resin-transfer-molded composites. Carbon 48(2010)8, pp. 2361-2380
55. Advani, S. G. Processing and Properties of Nanocomposites. World Scientific, 2006. 463 p.
56. Markarian, J. Delivering dispersion in nanocomposites. Compounding World, November 2010 . Available at: http://njmarkarian.home.comcast.net/~njmarkarian/CW_Nov10.pdf.
57. Gupta, M. L., Sydlik, S. A., Schnorr, J. M., Woo, D. J., Osswald, S., Swager, T. M., Raghavan, D. The effect of mixing methods on the dispersion of carbon nanotubes during the solvent-free processing of multiwalled carbon nanotube/epoxy composites. Journal of Polymer Science, Part B: Polymer Physics 51(2013)6, pp. 410-420
58. Li, X., Yuan, G., Westwood, A., Zhang, H., Dong, Z., Brown, A., Brydson, R., Rand, B. The preparation and CVD densification of multi-walled carbon nanotube felt synthesized by a catalytic CVD method. Chemical Vapor Deposition 14(2008)1-2, pp. 40-45
59. Silicon element facts. Accessed on 24.3.2013. Available at: http://www.green-planet-solar-energy.com/silicon-element-facts.html
60. Napierska, D., Thomassen, L. CJ., Lison, D., Martens, J. A., Hoet, P. H. The nanosilica hazard: another variable entity. Particle and Fibre Toxicology 7(2010)1
61. Balamurugan, M., Saravanan, S. Producing nanosilica from Sorghum vulgare seed heads. Powder Technology 224(2012), pp. 345-350
62. Park, J-J., Yoon, K-G., Lee, J-Y. Thermal and mechanical properties of epoxy/micro- and nano- mixed silica composites for insulation materials of heavy electric equipment. Transactions on Electrical and Electronic Materials 12(2011)3, pp. 98-101

63. Epoxy Infusion System. PRIME 20LV, Gurit.
64. Sigma-Aldrich. Carbon nanotube, multi-walled. Accessed on 10.10.2012. Available at: http://www.sigmaaldrich.com/catalog/product/aldrich/724769?lang=fi&region=FI
65. Sigma-Aldrich. Silica nanopowder. Accessed on 10.10.2012. Available at: http://www.sigmaaldrich.com/catalog/product/aldrich/718483?lang=fi&region=FI, and Sigma-Aldrich Technical service 1.2.2013
66. Rockwood Clay Additives. Cloisite 11. Accessed on 10.10.2012. Available at: www.nanoclay.com
67. Chemical book. Accessed on 22.2.2013. Available at: http://www.chemicalbook.com/ProductChemicalPropertiesCB5767904_EN.htm#MSDSA
68. Cloisite 11 Safety data sheet, Rockwood Clay Based Additives
69. Intertek. Tensile testing of polymers and composites materials. Accessed on 31.1.2013. Available at: http://www.intertek.com/polymers/tensile-testing/
70. Grellmann, W., Seidler, S. Polymer Testing. Hanser Gardner Publications, 2007. 674 p.
71. SFS-EN ISO 527-1. Muovit. Veto-ominaisuuksien määrittäminen. Osa 1: Yleiset periaatteet. Suomen standardisoimisliitto
72. Scheirs, J. Compositional and Failure Analysis of Polymers: A Practical Approach. John Wiley & Sons, 2000. 806 p.
73. Kornmann, X. Synthesis and Characterisation of Thermoset-Layered Silicate Nanocomposites. Doctoral thesis. 2001. Luleå University of Technology, Department of materials and manufacturing engineering, division of polymer engineering, 161 p.
74. Standard D 5045-99. Standard test methods for plane-strain fracture toughness and strain energy release rate on plastic materials. ASTM
75. Mathot, V. B.F. Calorimetry and Thermal Analysis of Polymers. Hanser Gardner Publications, 1994. 369 p.
76. Differential Scanning Calorimetry. Department of Chemistry, Colorado State University. Accessed on 29.5.2012. Available at: http://www1.chm.colostate.edu/Files/CIFDSC/dsc2000.pdf
77. Nakamura, T. DSC Measurements of Epoxy Adhesives. Hitachi High-Tech. Accessed on 1.4.2013. Available at: http://www.hitachi-hitec-science.com/en/documents/technology/thermal_analysis/application_TA_055e.pdf
78. Ratna, D., Chakraborty, B. C., Dutta, H., Banthia. A. K. Nanoreinforcement of flexible epoxy using layered silicate. Polymer Engineering & Science 46(2006)12, pp. 1667-1673
79. Sichina, W.J. Measurement of Tg by DSC. Thermal Analysis Application Note. PerkinElmer Instruments

80. Introduction to Dynamic Mechanical Analysis (DMA). A Beginner's Guide. Perkin Elmer, 2008
81. Geochemical Instrumentation and Analysis. Scanning Electron Microscopy (SEM). Accessed on 18.3.2013. Available at: serc.carleton.edu/research _education/geochemsheets/techniques/SEM.html
82. Field emission scanning electron microscope (FESEM). FindNano. Accessed on 29.1.2013. Available at: http://www.findnano.fi/fi/NanoCrmEquipment:UserView/id/1485/Field_Emission_Scanning_Electron_Microscope__FESEM__/
83. Tampereen Teknillinen Yliopisto. Tutkimuslaitteet: Mikroskopia ja kuvantaminen. Accessed on 8.4.2013. Available at: http://www.tut.fi/fi/tietoa-yliopistosta/laitokset/materiaalioppi/tutkimus/tutkimuslaitteet/mikroskopia-ja-kuvantaminen/sem/index.htm
84. MatWeb. Surface resistivity testing on plastics. Accessed on 10.2.2013. Available at: www.matweb.com/reference/surface-resistivity.aspx
85. Resistivity test instruction based on standard ASTM D 257-99
86. Romhány G., Szebényi, G. Preparation of MWCNT reinforced epoxy nanocomposite and examination of its mechanical properties. Plastics, Rubber and Composites 37(2008)5/6, pp. 214-218
87. Yasmin, A., Abot, J. L., Daniel, I. M. Processing of clay/epoxy nanocomposites by shear mixing. Scripta Materialia 49(2003), pp. 81-86
88. Thelakkadan, A. S., Coletti, G., Guastavino, F., Fina, A. Thermomechanical and electrical characterization of epoxy-organoclay nanocomposites. Polymer Engineering & Science 52(2012)5, pp. 1037-1046
89. He, Z., Zhang, X., Chen, M., Li, M., Gu, Y., Zhang, Z., Li, Q. Effect of the filler structure of carbon nanomaterials on the electrical, thermal, and rheological properties of epoxy composites. Journal of Applied Polymer Science 2013
90. Huang, Y. Y., Ahir, S.V., Terentjev, E. M. Dispersion rheology of carbon nanotubes in a polymer matrix. Physical Review B 73(2006)12
91. Ragosta, G., Abbate, M., Musto, P., Scarinzi, G., Mascia, L. Epoxy-silica particulate nanocomposites: Chemical interactions, reinforcement and fracture toughness. Polymer 46(2005)23, pp. 10506-10516
92. Tzetzis, D., Mansour, G., Tsiafis, I., Pavlidou, E. Nanoindentation measurements of fumed silica epoxy reinforced nanocomposites. Journal of Reinforced Plastics and Composites 32(2013)3, pp. 160-173
93. Ngo, T-D., Ton-That, M-T., Hoa, S. V., Cole, K. C. Preparation and properties of epoxy nanocomposites. Part 2: The effect of dispersion and intercalation/exfoliation of organoclay on mechanical properties. Polymer Engineering & Science 52(2012)3, pp. 607-614
94. Ngo, T-D., Ton-That, M-T., Hoa, S. V., Cole, K. C. Reinforcing effect of organoclay in rubbery and glassy epoxy resins, part 1: Dispersion and properties. Journal of Applied Polymer Science 107(2008)2, pp. 1154-1162

95. Mohan, TP., Kumar, M. R., Velmurugan, R. Rheology and curing characteristics of epoxy-clay nanocomposites. Polymer International 54(2005)12, pp. 1653-1659
96. Nordin, A., Baosheng, R., Noda, J., Goda, K. Effect of nanoclay loading on mechanical properties of nanocomposites. Department of Mechanical Engineering, Yamaguchi University
97. Zamanian, M., Mortezaei, M., Salehnia, B., Jam, J. E. Fracture toughness of epoxy polymer modified with nanosilica particles: Particle size effect. Engineering Fracture Mechanics 97(2013), pp. 193-206
98. Lu, H., Roy, S., Sampathkumar, P., Ma, J. Characterization of the fracture behavior of epoxy nanocomposites. 2002
99. Sichina, W.J. Characterization of epoxy resins using DSC. PerkinElmer Instruments, 2002
100. Wang, L., Wang, K., Chen, L., Zhang, Y., Chaobin He, C. Preparation, morphology and thermal/mechanical properties of epoxy/nanoclay composite. Composites: Part A: 37(2006)11, pp. 1890-1896
101. Rashmi, Renukappa, N. M., Chikkakuntappa, R., Kunigal, N. S. Montmorillonite nanoclay filler effects on electrical conductivity, thermal and mechanical properties of epoxy-based nanocomposites. Polymer Engineering and Science 51(2011)9, pp. 1827-1836
102. Zheng, Y., Chonung, K., Wang, G., Wei, P., Jiang, P. Epoxy/nano-silica composites: Curing kinetics, glass transition temperatures, dielectric, and thermal-mechanical performances. Journal of Applied Polymer Science 111(2009)2, pp. 917-927
103. Abdalla, M., Dean, D., Robinson, P., Nyairo, E. Cure behavior of epoxy/MWCNT nanocomposites: The effect of nanotube surface modification. Polymer 49(2008)15, pp. 3310-3317
104. Park, S-D., Han, D-H., Teng, D., Kwon, Y. Rheological properties and dispersion of multi-walled carbon nanotube (MWCNT) in polystyrene matrix. Current Applied Physics 8(2008)3-4, pp. 482-485
105. Yu, Z-Q., You, S-L., Baier, H. Effect of organosilane coupling agents on microstructure and properties of nanosilica/epoxy composites. Polymer Composites 33(2012)9, pp. 1516-1524
106. Miyagawa, H., Rich, M. J., Drzal, L. T. Amine-cured epoxy/clay nanocomposites. I. Processing and chemical characterization. Journal of Polymer Science: Part B: Polymer Physics 42(2004)23, pp. 4384-4390
107. Conradi, M., Zorko, M., Kocijan, A., Verpoest, I. Mechanical properties of epoxy composites reinforced with a low volume fraction of nanosilica fillers. Materials Chemistry and Physics 137(2013)3, pp. 910-915
108. Wikipedia. Electrical resistivity and conductivity. Accessed on 10.02.2013. Available at: en.wikipedia.org/wiki/Electrical_resistivity_and_conductivity

109. Wladyka-Przybylak, M., Wesolek, D., Gieparda, W., Boczkowska, A., Ciecierska, E. Functionalization effect on physico-mechanical properties of multi-walled carbon nanotubes/epoxy composites. Polymers for Advanced Technologies 22(2011)1, pp. 48-59

APPENDIX 1: TENSILE TEST RESULTS

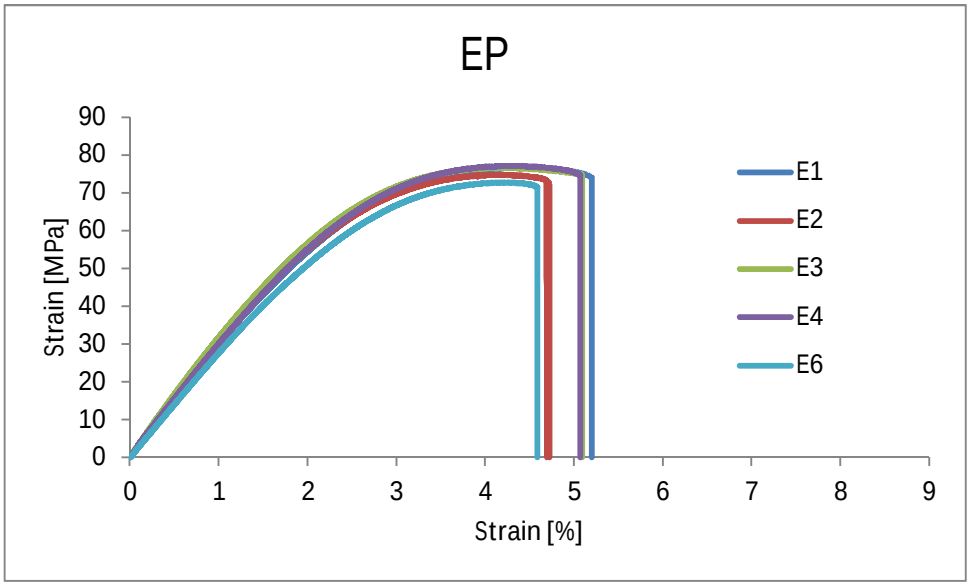

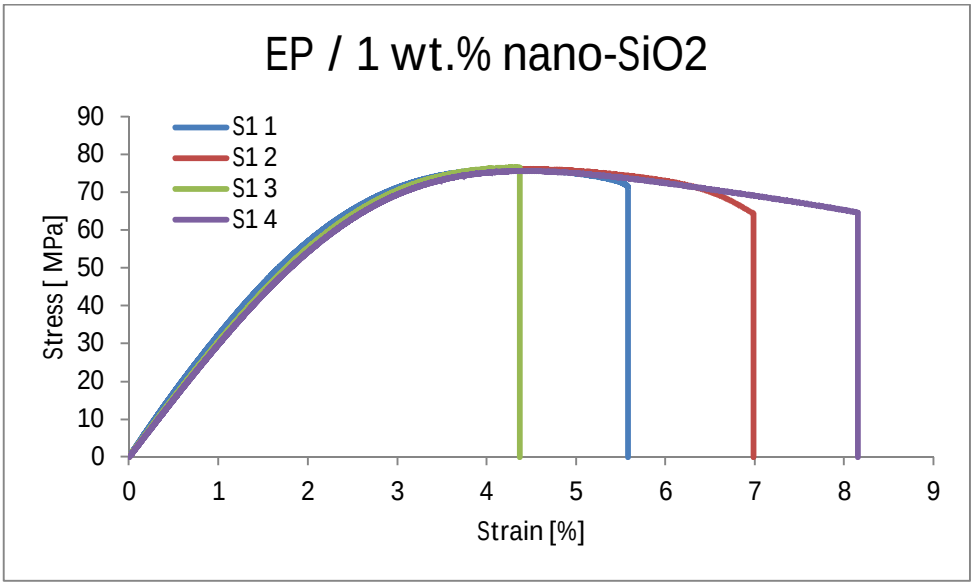

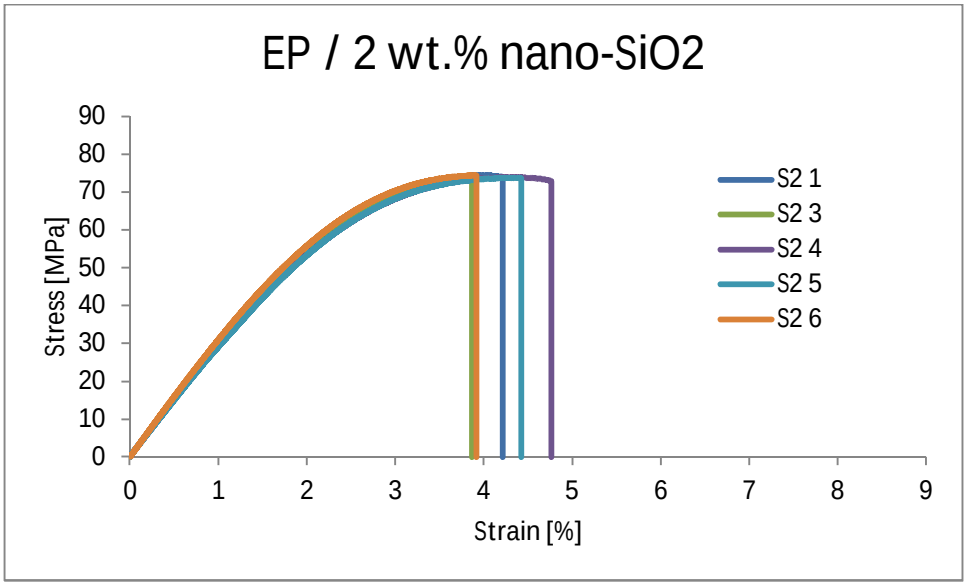

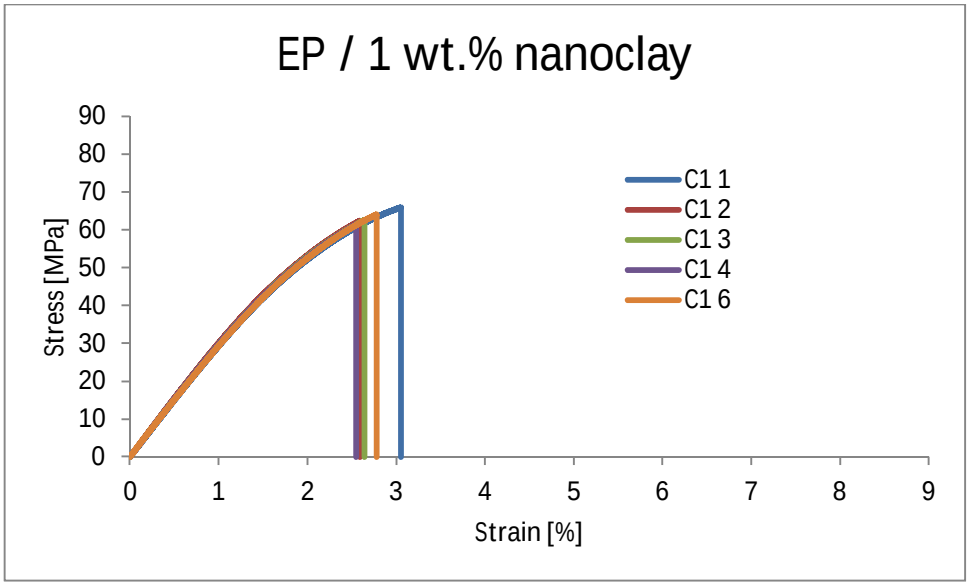
EP / 1 wt.% nanoclay
Stress [MPa]
Strain [%]
C1 1
C1 2
C1 3
C1 4
C1 6

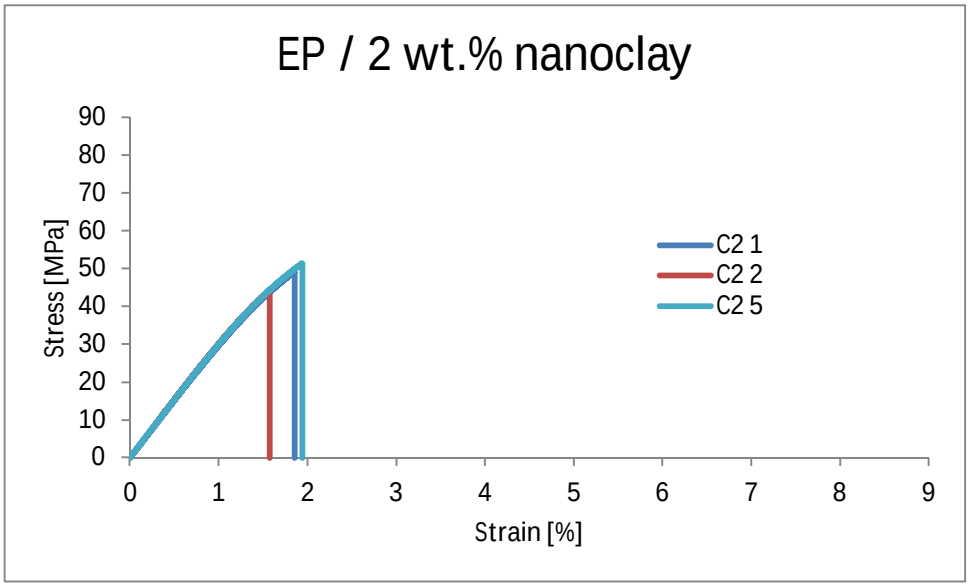
EP / 2 wt.% nanoclay
Stress [MPa]
Strain [%]
C2 1
C2 2
C2 5

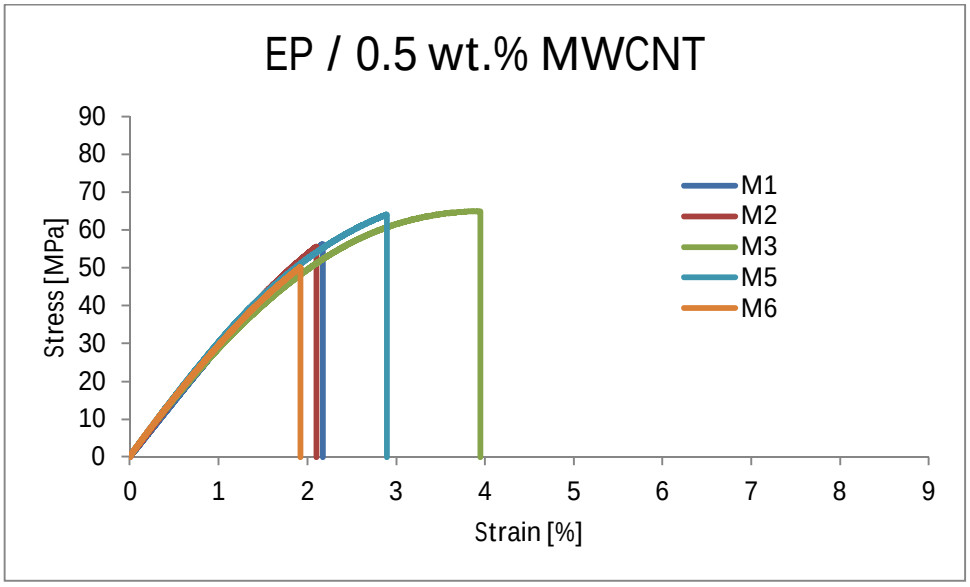
EP / 0.5 wt.% MWCNT
Stress [MPa]
Strain [%]
M1
M2
M3
M5
M6

APPENDIX 2: FRACTURE TOUGHNESS RESULTS

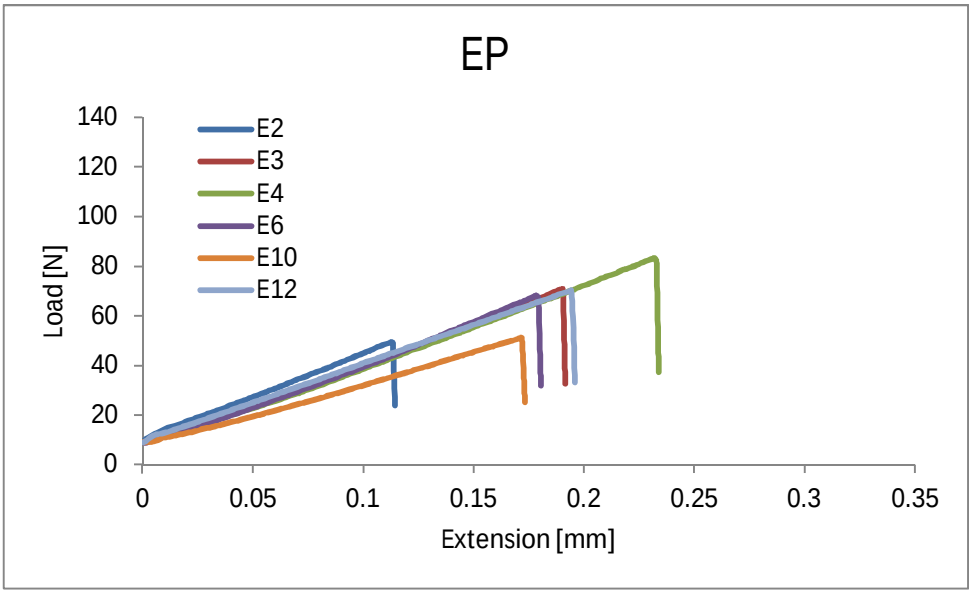

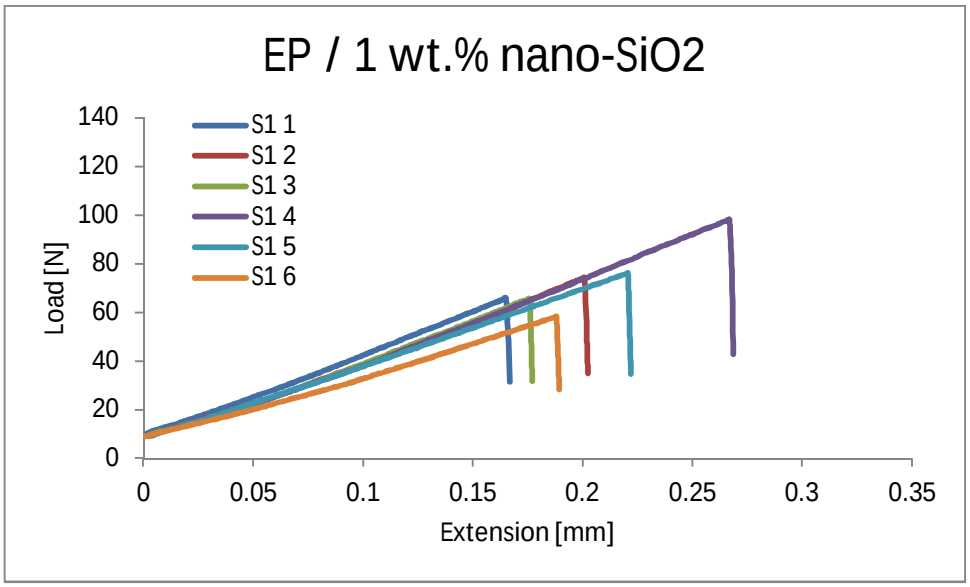

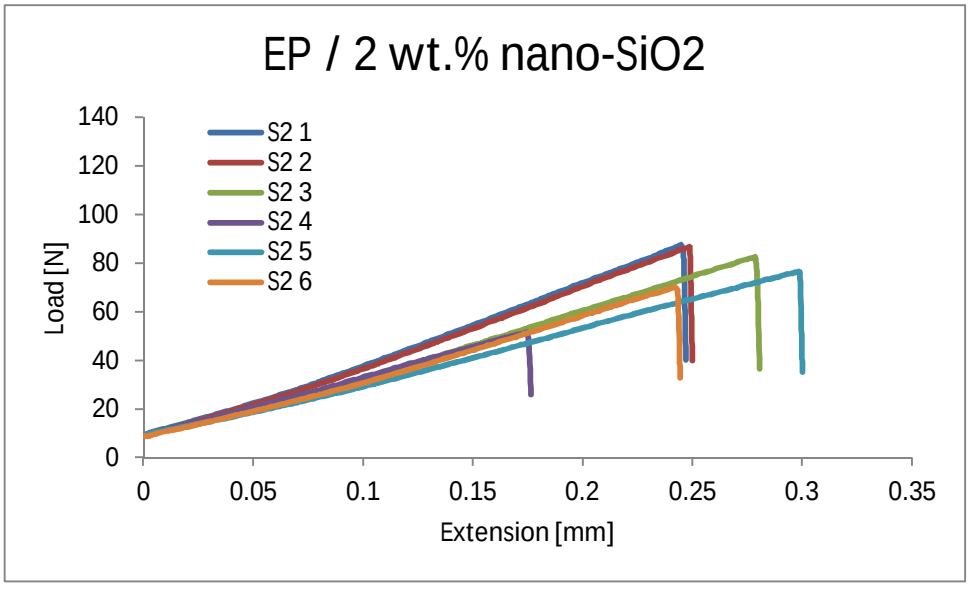

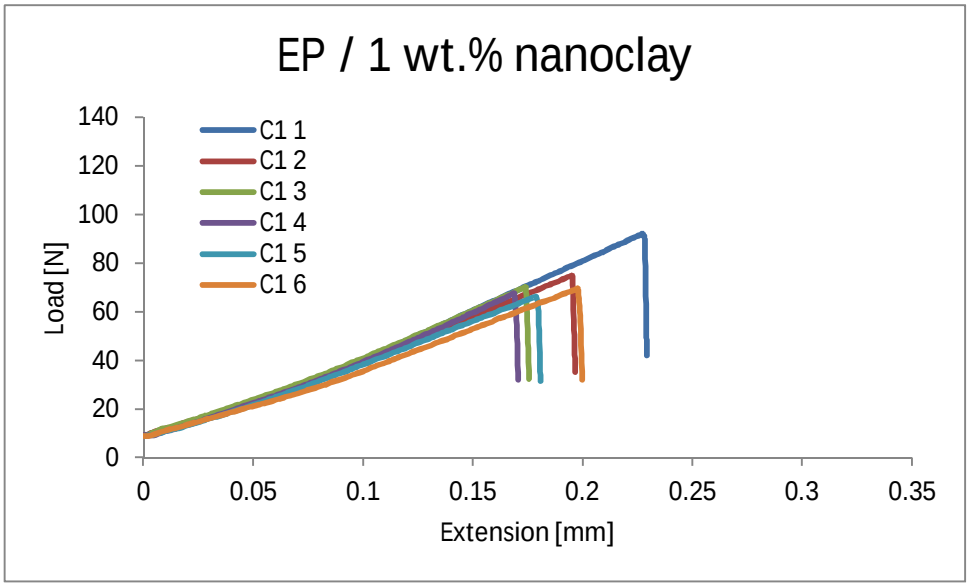
EP / 1 wt.% nanoclay
Load [N]
Extension [mm]
C1 1
C1 2
C1 3
C1 4
C1 5
C1 6
0
20
40
60
80
100
120
140
0
0.05
0.1
0.15
0.2
0.25
0.3
0.35

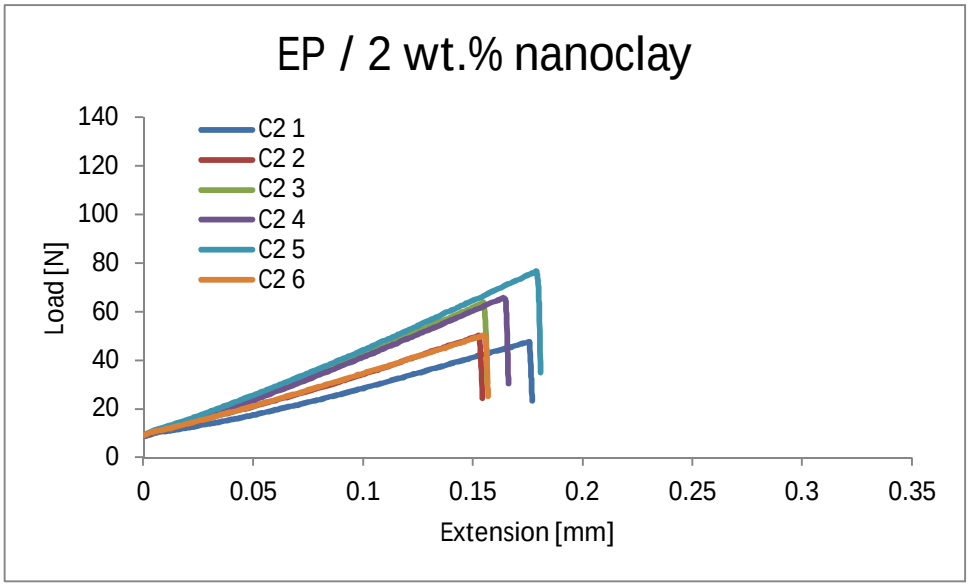
EP / 2 wt.% nanoclay
Load [N]
Extension [mm]
C2 1
C2 2
C2 3
C2 4
C2 5
C2 6
0
20
40
60
80
100
120
140
0
0.05
0.1
0.15
0.2
0.25
0.3
0.35

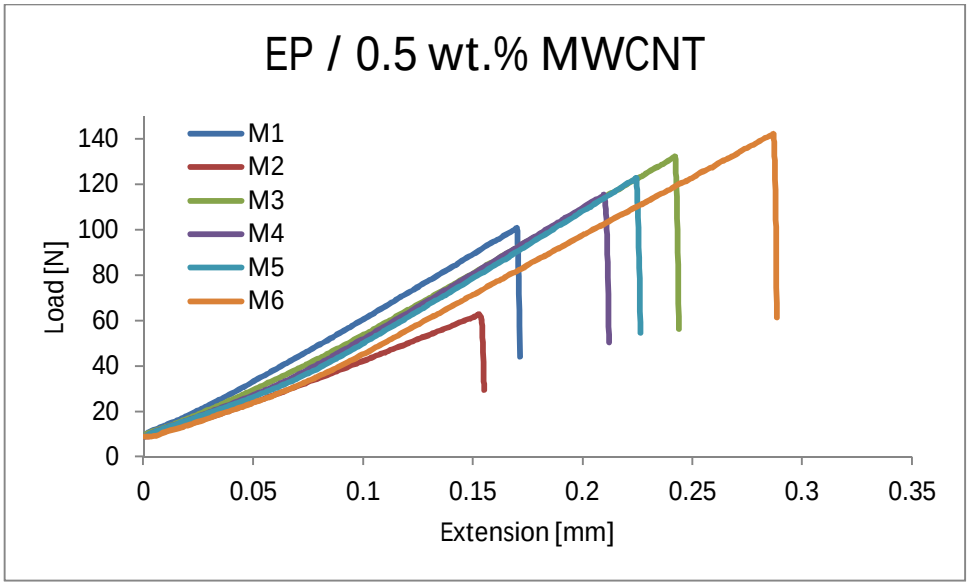
EP / 0.5 wt.% MWCNT
Load [N]
Extension [mm]
M1
M2
M3
M4
M5
M6
0
20
40
60
80
100
120
140
0
0.05
0.1
0.15
0.2
0.25
0.3
0.35

APPENDIX 3: SEM IMAGES

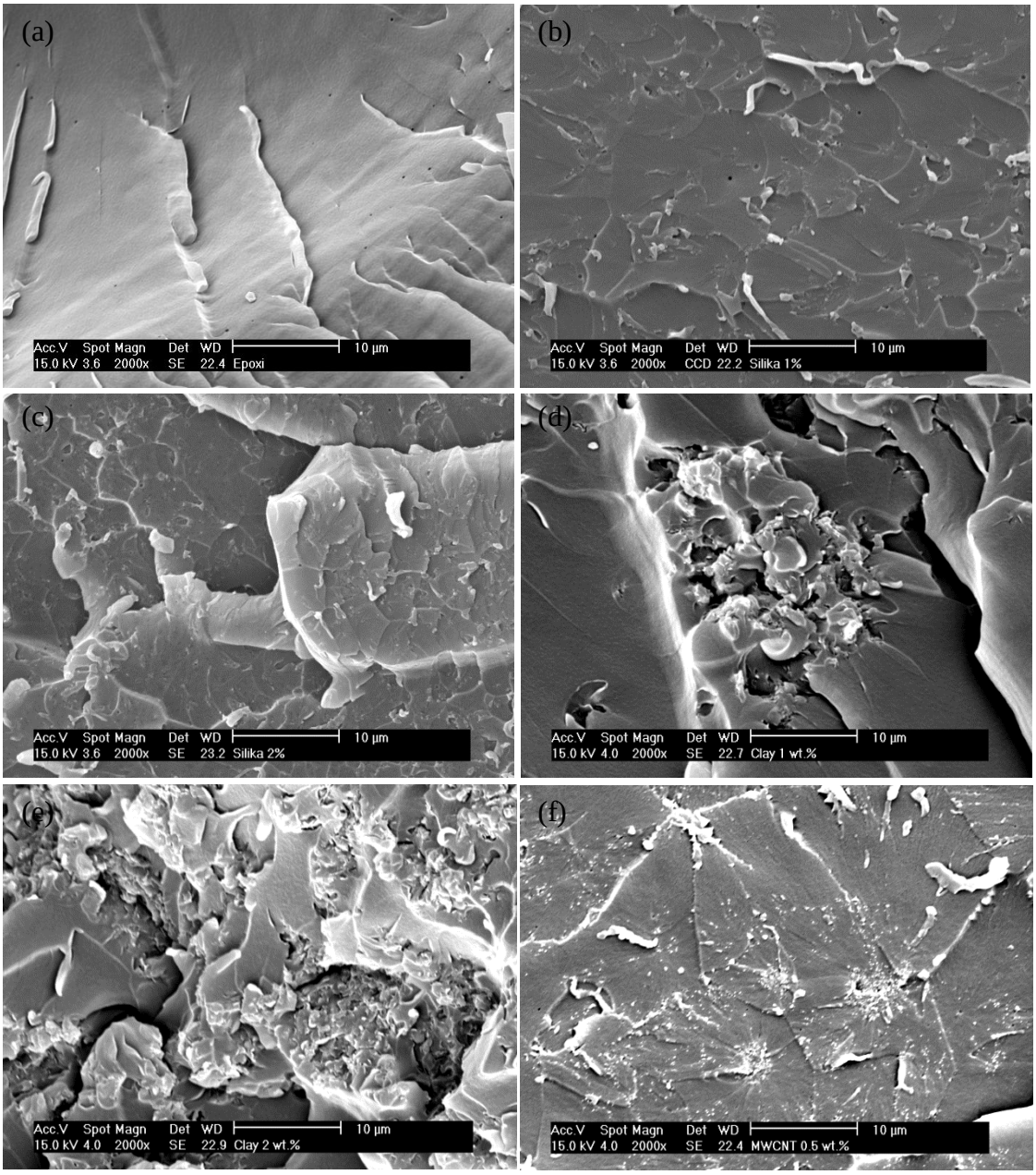

SEM images of (a) pure epoxy (b) EP / 1 wt.% SiO_2 (c) EP / 2 wt.% SiO_2 (d) EP / 1 wt.% nanoclay (e) EP / 2 wt.% nanoclay and (f) EP / 0.5 wt.% MWCNT (magnification of 2000)

APPENDIX 4: FESEM IMAGES

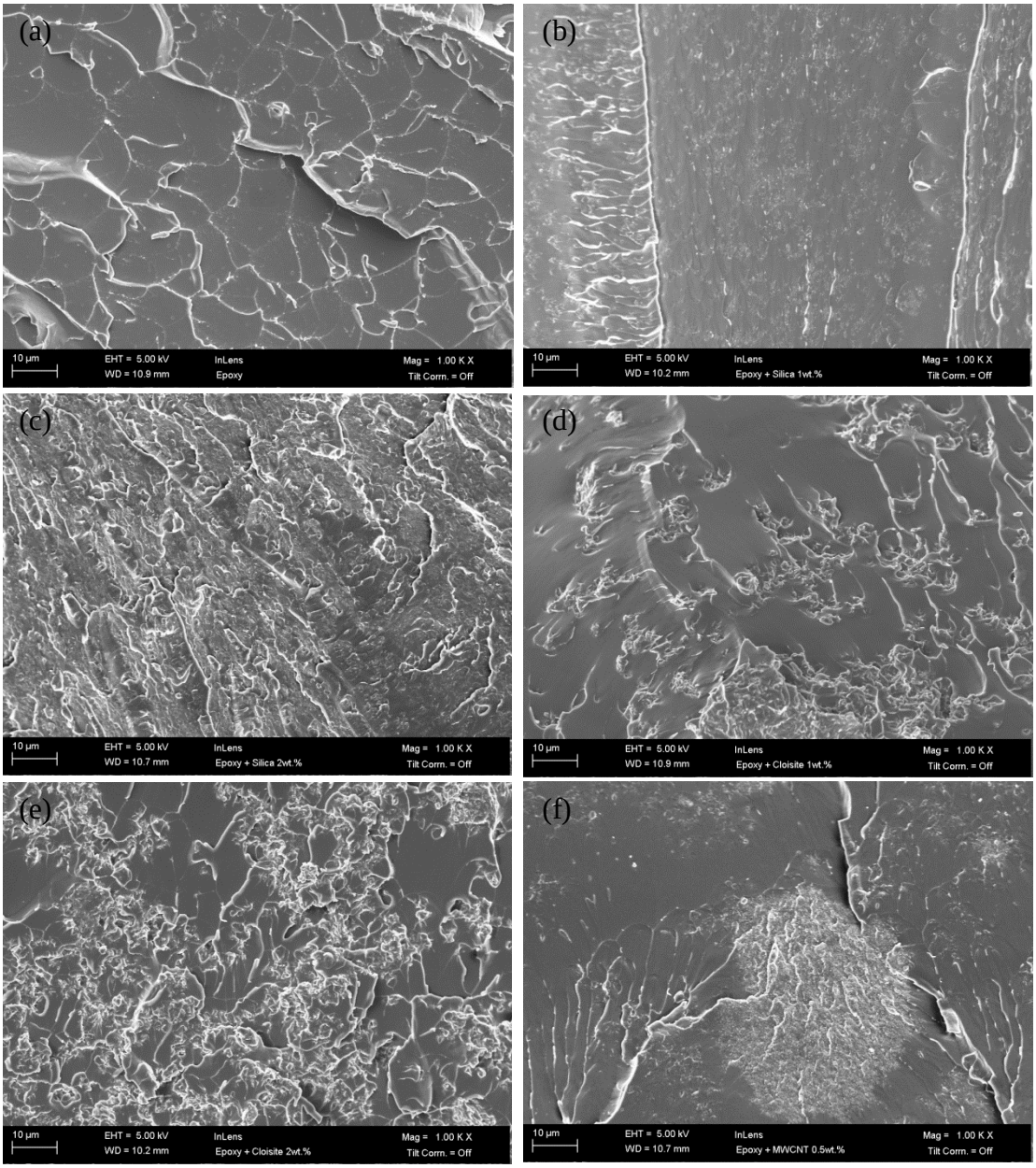

FESEM images of (a) pure epoxy (b) EP / 1 wt.% SiO_2 (c) EP / 2 wt.% SiO_2 (d) EP / 1 wt.% nanoclay (e) EP / 2 wt.% nanoclay and (f) EP / 0.5 wt.% MWCNT (magnification of 1000)

APPENDIX 5: FESEM IMAGES

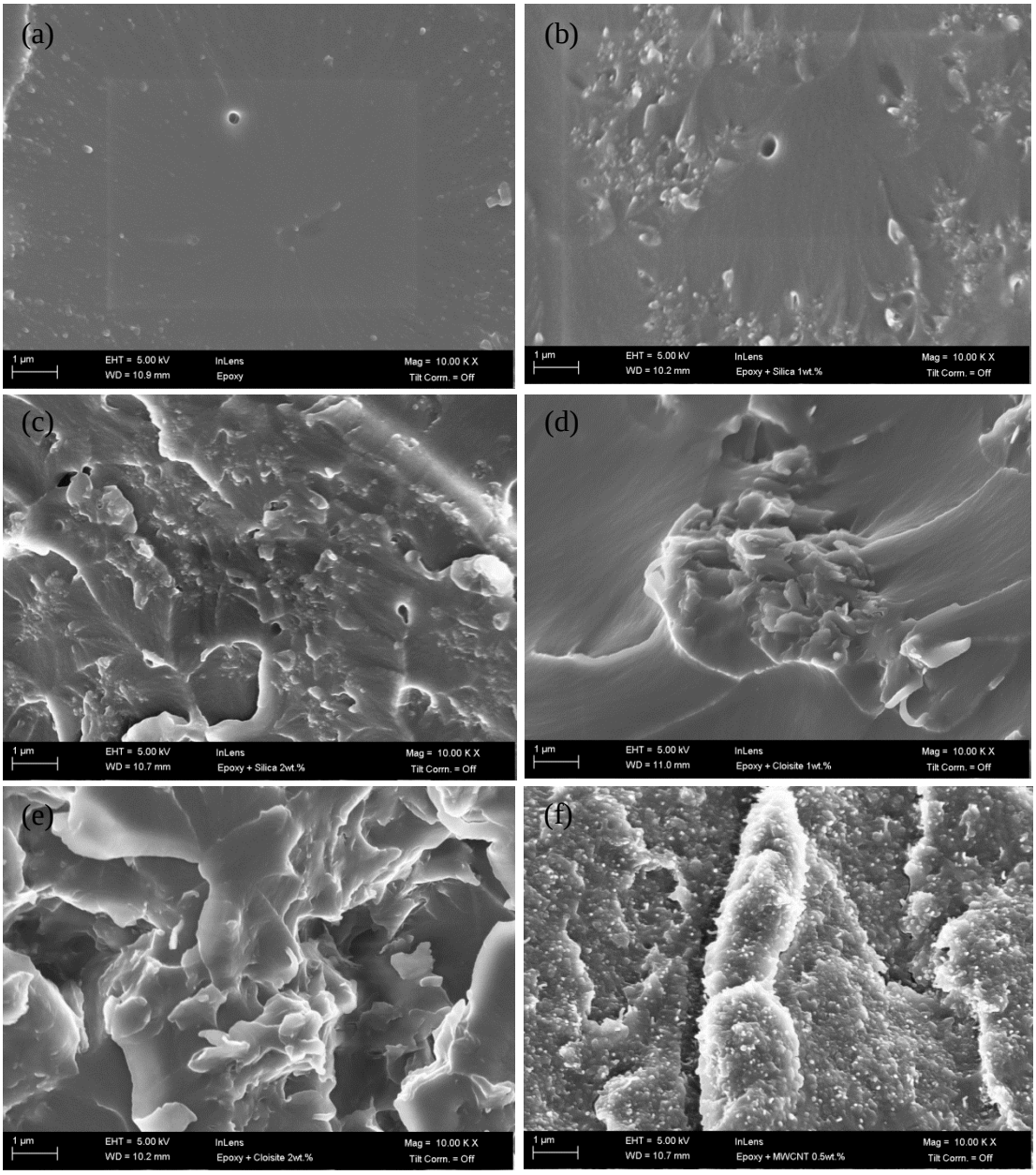

FESEM images of (a) pure epoxy (b) EP / 1 wt.% SiO_2 (c) EP / 2 wt.% SiO_2 (d) EP / 1 wt.% nanoclay (e) EP / 2 wt.% nanoclay and (f) EP / 0.5 wt.% MWCNT (magnification of 10 000)